Encapsulation of Indigoid Dyes

Sabine Maria Elfriede Barbara Weidlich

St Edmund Hall

University of Oxford

A thesis submitted for the degree of

Doctor of Philosophy

Michaelmas 2018

Encapsulation of Indigoid Dyes

D.Phil Thesis, Michaelmas 2018

Sabine Maria Elfriede Barbara Weidlich, St. Edmund Hall, University of Oxford

This thesis describes approaches towards the synthesis of encapsulated indigo-based systems. The chemistry and application of indigo has been widely investigated, but its use as an emitter is restricted by its low fluorescence, which is caused by the ultrafast proton transfer in the excited state. Substitution of the *N*-positions prevents this process, making indigo accessible for photonic applications. This thesis focuses on the synthesis and properties of indigo-derived materials. The aim is to make new encapsulated indigo-derived materials for photonic applications (*e.g.* OLEDs). Encapsulation is a common tool to prevent interactions (*e.g.* π-stacking) between molecules which can lead to a decreased emission in the solid state. Focus is set on two encapsulation methods, *i.e.* self-encapsulation by a metathesis reaction, and encapsulation under formation of hydrogen bonds between a tetralactam macrocycle (hydrogen bond donor) and several guest systems (hydrogen bond acceptor). The concept of increasing binding strengths in hydrogen bonding systems by electrochemically reducing the guest (hydrogen bond acceptor) has also been introduced and investigated.

Chapter 1 reviews encapsulation as a tool to enhance the emissive properties of host-guest systems. Focus is mainly on self-encapsulation and encapsulation with hydrogen bonding macrocycles. Additionally, the chemistry of indigo and its use in devices is explained.

Chapter 2 explores the *N*-substitution and the bay-annulation of indigo including a study of their photophysical properties. Analysis of several crystal structures shows the impact of substitution resulting in increased emissive properties.

Chapter 3 describes the synthesis of a self-encapsulated bay-annulated indigo derivative and its photophysical properties in solution and solid state.

Chapter 4 focuses on the binding between tetralactam macrocycles and hydrogen bond acceptors. Also, binding enhancement with electrochemical methods is investigated. Simulations of the binding processes are shown and their results compared to the common tools for calculating the binding constants in the reduced state.

Chapter 5 summarises the results in this thesis and contains proposals for future work in this research area.

Acknowledgements

First of all, I would like to thank Professor Harry L. Anderson for trusting me with this project; his support and encouragement during my DPhil in Oxford in the past three years helped me make this work successful. I am very grateful for the experience of working in such an exceptional group.

In the beginning of my time in Oxford, Dr. Ibrahim Bulut was helping me to set up this project, gave me a lot of scientific input, and ended up being a friend and excellent lab mate, thank you for that. Further on, I would like to thank Dr. Bart Limburg for his supportive role in this last year of my DPhil. I would also like to thank Yaoyao Xiong for the analysis of my crystal structures and the past three years in the G1 gang.

I would also like to thank the Amazing Andersons. For most of the time I have been part of G1 and would like to acknowledge the tidiness, great music, and fun times in this lab. Especially I would like to thank Michel, Pernille, Keith, Andrew, Wenjun, Bart, Yaoyao, Virginia, Lara, Renee, Przemek, Alistair, Lorel, Steffen, Isabell, Michael, Will, James, Andreas, Johannes, Nuntaporn, Cecile, Dan, Jonathan, Huawei, and Martin.

A very special thank you deserves Dr. Virginia Wycisk for reading my thesis and being a good friend in the past months. I would also like to thank Dr. Keith Andrews and Dr. Andrew Frawley for their input and thorough corrections. Dr. Bart Limburg also dedicated a lot of time reading through my thesis and giving valuable scientific input, thank you.

Finally, I would like to thank my family and friends for their endless love and support. I would not be where I am right now without you. Naomi, our friendship of already 18 years makes me eternally grateful and I am fortunate to have you in my life. Anne, thank you for being such an amazing friend, I am so glad I met you during my time in Oxford. Mama,

Papa thank you for always challenging me to be my best self, Reinhard and Christoph for being the best brothers I could wish for and the rest of my family for always being supportive.

At last, a very special thank you to Dr. Michael Kaye and his support throughout this DPhil. I am extremely grateful to have you in my life; you made the past years unforgettable, and I cannot wait for the upcoming ones.

Supplement to Statement of Authorship

In Chapter 2, the UV-vis and fluorescence measurements of the bay-annulated indigo dye and their blends were measured in conjunction with Alexandros Rapidis under the supervision of Prof. F. Cacialli at UCL.

In Chapter 4, simulations of the binding constants over our fitting model were performed by Dr. Bart Limburg.

Contents

List of Abbreviations

Å	Ångströms
Aq	Aqueous
Ar	Aryl
BQ	Benzoquinone
Bu	Butyl
CCDC	Cambridge Crystallographic Data Centre
CD	Cyclodextrin
cm	Centimetre
COSY	Correlation spectroscopy
CSD	Cambridge Structural Database
CV	Cyclic Voltammetry
δ	Chemical Shift
d	*doublet*
dba	Dibenzylideneacetone
DFT	Density Functional Theory
DMF	Dimethylformamide
DMSO	Dimethylsulfoxide
DNA	Desoxyribonucleic Acid
ε	Molar Absorption Coefficient

EI	Electron Impact Mass Spectrometry
e.g.	exemplum gratia
eq	Equivalents
ESI	Electronspray Ionisation
EtOAc	Ethyl acetate
F8BT	Poly(9,9-dioctylfluorene-alt-benzothiadiazole
g	Grams
h	Hours
HCl	Hydrochloric Acid
HRMS	High Resolution Mass Spectrometry
HOMO	Highest Occupied Molecular Orbital
Hz	Hertz
i	Iso
IC	Internal Conversion
ISC	Intersystem Crossing
J	Coupling Constant
λ	Wavelength
L	Litre
LUMO	Lowest Unoccupied Molecular Orbital
m	*multiplet*

M	Molar
MALDI	Matrix-Assisted Laser Desorption/Ionisation
Me	Methyl
mg	Milligram
MHz	Megahertz
MM	Molecular Mechanics
MOPAC	Molecular Orbital Package
MS	Mass Spectrometry
n-BuLi	*n*-Butyllithium
NMR	Nuclear Magnetic Resonance
nm	Nanometre
NOESY	Nuclear Overhauser Effect Spectroscopy
ns	Nanosecond
OFET	Organic Field-Effect Transistor
OLED	Organic Light-Emitting Diode
OPV	Organic Photovoltaics
p	Para
Ph	Phenyl
PL	Photoluminescence
PMMA	Polymethylmetacrylate

ppm	Parts per Million
q	quartet
R_f	Retention Factor
s	*singlet*
SWV	Square Wave Voltammetry
t	*triplet*
t-BOC	*tert*-butyloxycarbonyl
TCSPC	Time Correlated Single Photon Counting
TFA	Trifluoroacetic acid
THF	Tetrahydrofuran
TLC	Thin Layer Chromatography
TLM	Tetralactam Macrocycle
TMS	Trimethylsilane
TOF	Time of Flight
UV-vis-NIR	Ultra-Violet, Visible, Near Infrared

1

Introduction

1.1 Outline

This thesis explores the synthesis and analysis of acylated indigo dyes and their encapsulation into macrocycles to provide new fluorescent materials for incorporation into OLEDs. In this introductory chapter, a literature review on common encapsulation methods of host-guest systems is provided. This includes the synthesis of host and guest molecules and the improvement of their photophysical properties by encapsulation.

1.2 Fluorescence

Fluorescent molecules show radiative decay from the lowest vibrational state of the singlet state (S_1) to their electronic ground state (S_0). This appears after a photon was absorbed into a vibrational state of a singlet excited state by absorption of light or electromagnetic radiation. Figure 1 illustrates the general relaxation pathways for excitons in different electronic states in form of a Jabłoński diagram. Over the shown non-radiative or radiative relaxation pathways the molecule can revert to its ground state. While excitation usually occurs to higher vibrational levels, relaxation starts by non-radiative decay to the lowest vibrational state of the electronic level. Internal conversion occurs by non-radiative relaxation between excited states of the same spin multiplicity. The only way to occupy the triplet state (T_1) in this process is by intersystem crossing for which the spin-multiplicity is changed. It appears mainly in molecules with heavy atoms where spin-orbit coupling is more favourable. The non-radiative relaxation from the excited states (T_1 or S_1) in form of thermal energy (*e.g.* fluorescence quenching, energy transfer to non-fluorescent species or vibrations in the solid state) mostly occurs in parallel to radiative relaxation. Spin-allowed radiative emission happens between the singlet excited state, S_1, and the singlet ground state, S_0, in form of fluorescence and has shorter lifetimes than the spin-forbidden radiative

relaxation from the excited triplet state, T_1, to the singlet ground state S_0 in form of phosphorescence.[1]

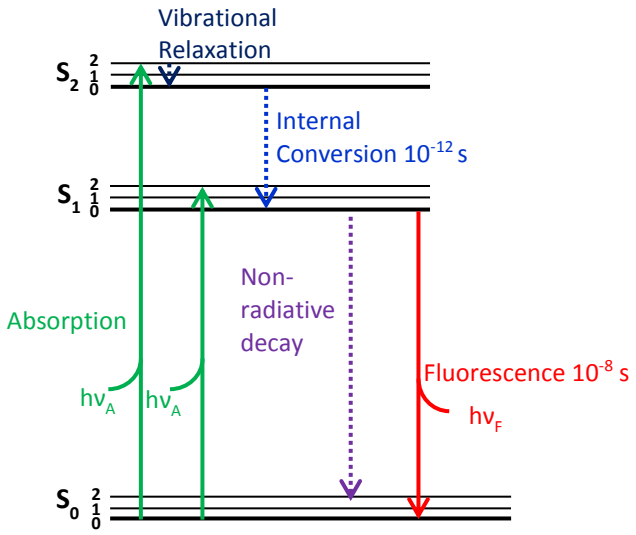

Figure 1: Jabłoński diagram to illustrate the electronic states of a molecule involved in luminescence.[1]

Fluorescence can appear in the gas, liquid, or solid phase. This is the absorption of photons to an excited state followed by the emission of light under radiative decay to the electronic ground state. The emission usually has a longer wavelength than the absorption, and their difference is known as the Stokes shift. This difference is caused by the energy differences of the ground and the excited state. Vertical transition of a photon from the lowest vibrational level of the ground state into the S_1 excited state, commonly leads to absorption into a higher vibrational level of the excited state. Relaxation in its lowest vibrational level leads to the Stokes shift, leading to a decay into a higher vibrational level of the ground state. Depending on the energy differences between the ground and excited state, the Stokes shift can be smaller or larger. In case of an Anti-Stokes shift the emitted photon has more energy than the absorbed photon and therefore leads to a blue shifted emission. The difference between absorption and emission is generally strongly influenced by the structure of the fluorophore.[1]

The lifetime of the electronic excited state is dependent on the fluorescence time τ by which the excited-state population converts to the ground state. The exponential decay of the excited-state population can be measured by the decrease in fluorescence intensity as a function of time, which is proportional to the population. This first-order process can be expressed as:

$$I(t) = I_0 \times e^{(-t/\tau)} \quad (1)$$

for which $I(t)$ is the time-dependent intensity, I_0 the intensity at time zero, t the time, and τ the fluorescence lifetime. Experimentally, the excited molecules relax to their ground state with emission of light. Usually the radiative decay from the excited state competes with non-radiative decay. Therefore, the lifetime is dependent on the radiative decay rate constants k_F and the non-radiative rate constants k_{NR} resulting in the following definition of τ:

$$\tau = 1/(k_F + k_{NR}) \quad (2)$$

The fluorescence lifetime is also related to the fluorescence quantum yield (Φ_F), which is the ratio of the number of emitted photons to the number of absorbed photons with a possible maximum value of 1. A value less than 1 is caused by non-radiative processes competing with the fluorescence. Therefore, the quantum yield can be defined in terms of the rate constants k_F and k_{NR} as:

$$\Phi_F = \frac{\text{number of emitted photons}}{\text{number of absorbed photons}} = \frac{k_F}{k_F + \Sigma k_{NR}} \quad (3)$$

Molecules with rigid structures usually show an increased fluorescence quantum yield compared to more flexible molecules, caused by the inhibition of internal conversion and vibrational motion. The fluorescence quantum yield can also be influenced by the

introduction of substituents on the fluorophore, as well as environmental conditions such as temperature, solvent, and pH.[1],[2]

Various processes can reduce the fluorescence quantum yields, which are collectively known as quenching. The most common types are static and dynamic quenching and both require contact between the fluorophore and the quencher. In static quenching, the fluorophore and quencher form a non-fluorescent complex. The intensity of the fluorescence, I_0, is highest in the absence of the quencher and is decreased in its presence to I. The Stern-Volmer equation allows the calculation of a static quenching constant, K_s, as follows:

$$1 + K_S[Q] = \frac{[I]_0}{[I]} \tag{4}$$

where $[I_0]/[I]$ is the ratio of intensity decrease due to the presence of a quencher and [Q] the concentration of the quencher.

Dynamic quenching of an excited fluorophore with a quencher results in the reduction of both the fluorophore lifetime and the fluorescence quantum yield. The excited fluorophore transfers its energy to the quencher and does not emit a photon while returning to the ground state. The intensity of the fluorescence corresponds to the lifetime and leads to the Stern-Volmer equation with dependency on the lifetime of the fluorophore, τ_0, and the reduced lifetime in presence of the quencher, τ, giving the following equation:

$$1 + K_D[Q] = \frac{\tau_0}{\tau} \tag{5}$$

Energy transfer can also occur between an excited atom or molecule (donor) and an acceptor atom or molecule during the excitation lifetime of the donor (Figure 2). A possible pathway is that the excited donor returns to its ground state while emitting a photon which

is reabsorbed by the acceptor (A to A*). The efficiency of this process is determined by the spectral overlap of the emission of the donor and the absorption of the acceptor.

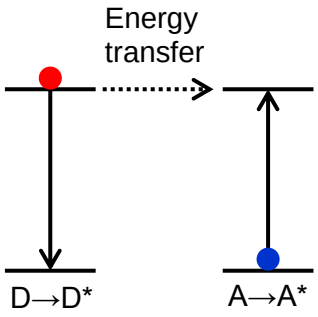

Figure 2: Energy transfer from a donor (D) to an acceptor (A) atom or molecule.

Non-radiative energy-transfer can occur by two major mechanisms, FRET[3] (Förster Resonance Energy Transfer) or Dexter charge transfer[4]. In FRET, non-radiative energy transfer can occur by dipole-dipole coupling between the donor and acceptor (up to 100 Å distance) if there is spectral overlap of the donor (D) emission and acceptor (A) absorption. However, if the energy difference between donor and acceptor is small (see Figure 2 right scheme) phonon-assisted energy transfer is possible. Alternatively, Dexter energy transfer requires contact between donor and acceptor and appears within a D-A distance of <5 Å.[1],[2]

Small-molecule chromophores can self-assemble in solution, at solid-liquid interfaces and in the solid state due to strong intermolecular van der Waals-like attractive interactions. This aggregation phenomenon leads to changes in the absorption spectra. An aggregation-induced bathochromic shift creates a *J*-band for *J*-aggregates and a hypsochromic shift forms an *H*-band for H-aggregates. Such shifts are induced by the coupling of dipole moments of neighbouring dye molecules (Figure 3). Excitation of the ground state molecules is coupled with the direction of their transition dipoles (red arrows in Figure 3) resulting in parallel or head-to-tail aggregates. The formation of these aggregates can

impact the energies of the excited states and the oscillator strengths of the $S_0 \rightarrow S_{1/2}$ transitions. Hence, the absorption and emission spectra are altered.[5]–[7]

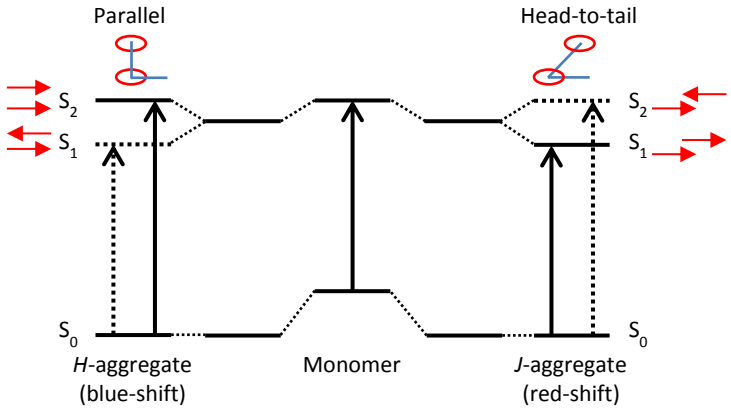

Figure 3: Schematic representation of *H*-and *J*-aggregate formation.

In terms of emission of *H*-aggregates, the low fluorescence is caused by the forbidden transition to the molecular ground state from the lowest excited state. As a result, most of the energy loss is non-radiative in the form of heat, giving low fluorescence quantum yields. In *J*-aggregates, transition into low excited states is allowed and leads to small Stokes shifts with larger fluorescence quantum yields resulting in aggregation induced emission.

Another very common form of quenching is the formation of excimers and exciplexes, yielding non-fluorescent excited species.[8],[9] An excimer (excited dimer) is a short-lived dimer of two electronically excited species that would not form in its electronical ground state. Exciplexes (excited complexes) show the same behaviour as excimers but are formed by more than two excited molecules. Exciplexes generally incorporate charge-transfer character and are able to form bonds with their unpaired electrons resulting in the formation of non-fluorescent excited complexes which non-radiatively relax to their ground state. This phenomenon appears often in the solid state due to stacking and other near-range interactions between molecules, especially when the lifetime of the excitons is long enough to allow their recombination under formation of excimers and exciplexes.

1.3 Supramolecular Encapsulation

To prevent loss of fluorescence due to aggregation, the structural encapsulation of a molecular subunit in the cavity of a larger molecule through intermolecular interactions can be performed. A conjugated molecule can be shielded from surrounding molecules by incorporation into a larger molecule (*e.g.* macrocycle). Threading of conjugated π-systems has different advantages; the greater distance between the molecules leads to less intermolecular interactions, therefore the quenching of the fluorescence can be prevented to achieve higher luminescence efficiencies and higher quantum yields in solid-state. Also the transport properties and the chemical stability are enhanced.[10]–[13] These mechanically interlocked molecules (MIMs), like rotaxanes (dumbbell shaped molecule threaded through a macrocycle), catenanes (two or more interlocked macrocycles which cannot be separated without breakage of covalent bonds), and knots (mechanically interlocked molecule analogous to a macroscopic knot) (Figure 4), have been investigated in the past 50 years for their use in molecular devices and their enhanced photophysical properties.[14] Especially, the encapsulation of conjugated molecules has resulted in tremendous changes in the photophysical properties by increasing the fluorescence quantum yields in solid state compared to the unthreaded species.[15],[16]

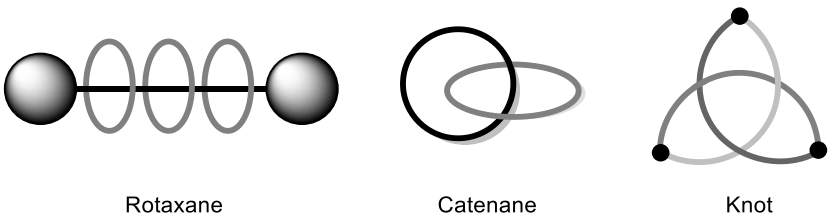

Figure 4: Schematic structures of rotaxanes, catenanes, and knots.

The synthesis of MIMs requires one of five typical strategies of encapsulation (Figure 5). In the capping method (1), the macrocycle first binds the thread to form a pseudorotaxane. The rotaxane is then built by attaching larger stopper groups to the ends to prevent the macrocycles from slipping off the thread.[17] It is also possible for a macrocycle to bind a thread with a bulky end group (semirotaxane) (2) which is followed by the connection of

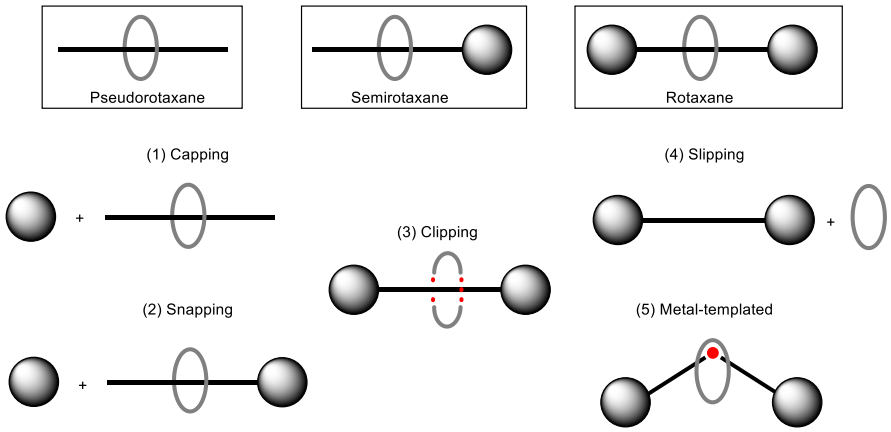

Figure 5: Strategies for the formation of rotaxanes.

the second stopper, allowing the synthesis of asymmetric rotaxanes.[18] For systems in which the macrocycles are not held in place during the rotaxane formation, the clipping method (3) can be used. The macrocycle forms around a dumbbell subunit.[19] In some cases, heating a mixture of dumbbell and macrocycle can give rotaxanes by slipping of the macrocyles over the stopper group (4).[20] The last common strategy is the template-directed rotaxane formation (5), in which the metal atom positions two half dumbbells and then the macrocycle promotes the covalent bond formation between the dumbbell subunits.[21],[22]

During rotaxane formation, the template methods between the MIMs can range from hydrogen bonding,[23] hydrophilic-hydrophobic[24] or metal-ligand interactions,[25] π-π stacking,[26],[27] (photo-induced) charge transfer,[28] and others (Figure 6).[29]

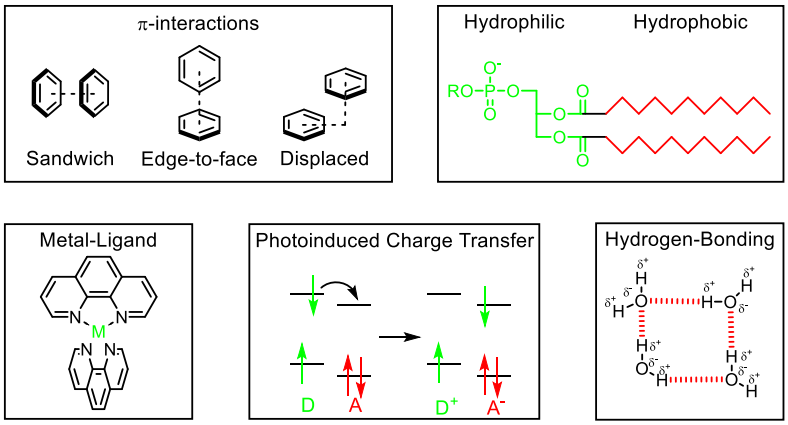

Figure 6: Various interaction patterns exploited in rotaxane synthesis.

The various binding patterns can be achieved by introduction of different macrocycles. The most commonly used macrocycles to encapsulate guests to form interlocked molecules are crown ethers, cyclodextrins, cucurbiturils, calixarenes, pillararenes, tetracationic cyclophanes, metal-ligand based macrocycles, and tetralactam macrocycles (Figure 7).[14]

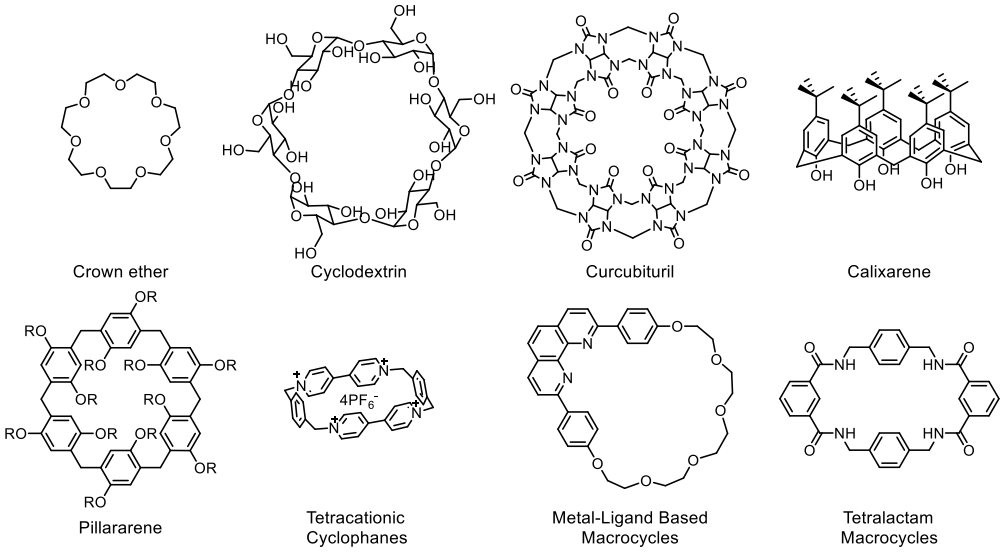

Figure 7: Commonly used macrocycles for the formation of rotaxanes.

1.3.1 Encapsulation with Hydrogen Bonds

For rotaxanes with hydrogen bonds between molecular wires and tetralactam macrocycles, stopper groups are also crucial, but binding is promoted by the formation of strong hydrogen bonds that help to keep the macrocycles in place.[30]–[33] Tetralactam macrocycles (TLMs) were first been reported by Vögtle[34] and Hunter,[35] who investigated their ability to form catenanes (Figure 8). The molecules are interlocked in a well-defined conformation due to hydrogen-bonds and π-π interactions, giving the catenane in a yield of 34% for Hunter's strategy, whereas Vögtle reached a yield of 8.4%.

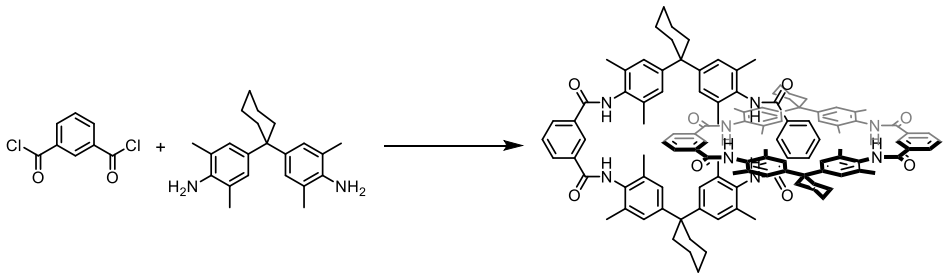

Figure 8: Tetralactam macrocycles interlocked with each other forming a catenane.[34],[35]

Although the reactions were performed at high dilution, further side products were formed, which were identified as the cyclic tetramer and the TLM (Figure 9).[36] Larger tetra- and octalactam macrocycles and their versatility as supramolecular building blocks have been further investigated by C. Schalley.[37],[38]

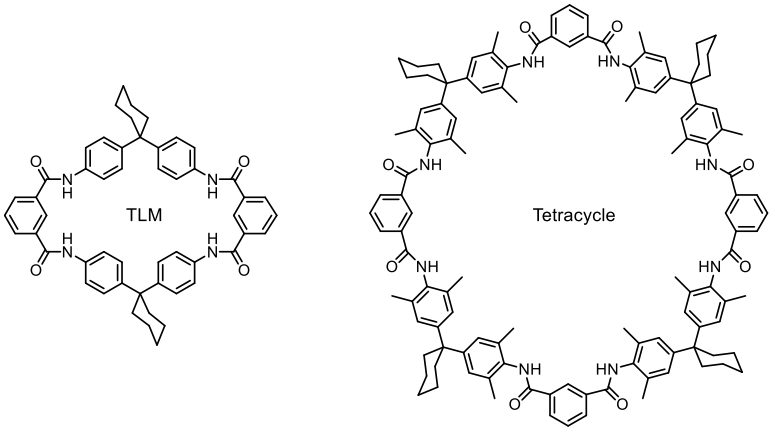

Figure 9: Structures of side products appearing during the catenane formation.[34],[35]

One of the first examples for the synthesis of rotaxanes with TLMs is the capping strategy of Vögtle, reported in 1995.[39] The macrocycle interacted with the half-dumbbell by forming hydrogen bonds between the NH-moieties of the macrocycle and the carbonyl-groups of the thread. Further on, bulky stopper groups were added (Figure 10).[40]

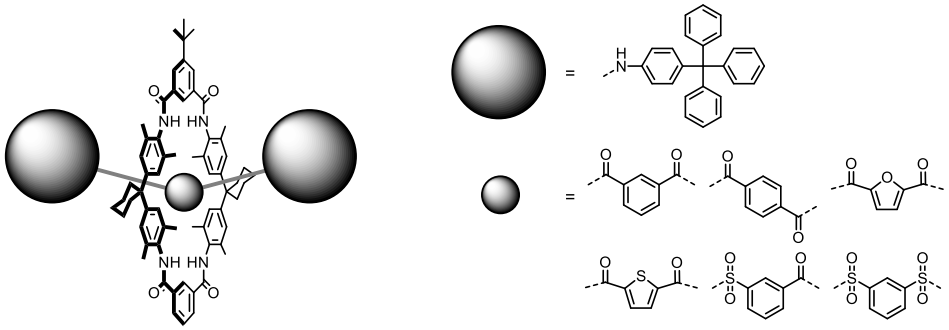

Figure 10: Rotaxanes with TLMs.[40]

The Vögtle-type macrocycles as shown above (Figure 9) exhibit a relatively large cavity for binding guest molecules. Leigh and co-workers made a smaller TLM with *p*-benzyl groups as wall units. With the same synthetic strategy as for the formation of the catenane, TLM, and octalactam macrocycle by Hunter and Vögtle (Figure 8), only the catenane was isolated.[41] The structure of this amide-based catenane was further investigated by X-ray crystallography, revealing inter- and intramolecular hydrogen bonds with π-stacking from aromatic rings. It is also worthwhile to note that the macrocycles adopt a chair-like

conformation and their carbonyl-groups are not all arranged in the *exo*-formation (Figure 11).

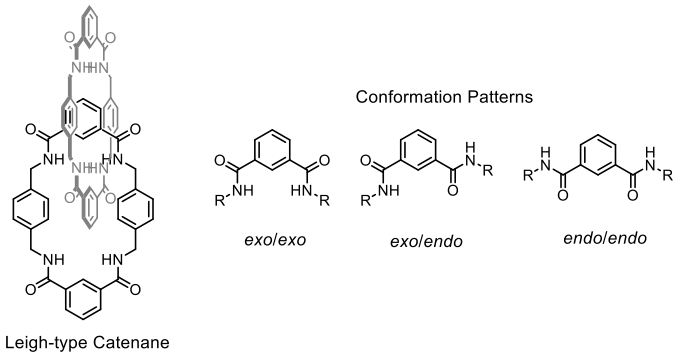

Figure 11: Leigh-type macrocycle in form of a catenane and the possible conformations of the amide units.[41]

These conformational changes were explored by Hunter and co-workers.[42],[43] At first, the synthesis of the monomacrocycle was improved by addition of another step to the reaction. Building a half-cycle at high concentrations, followed by capping of the macrocycle under high dilution led to an increased yield. Additionally, pyridine head groups were introduced instead of phenyl rings to improve the conformational properties of the macrocycle. The pyridine units are able to form intramolecular hydrogen bonds with the amide-NH groups. Calculations showed that the most favourable conformation is *exo*/*exo* with energy differences of 25 kJ/mol to *exo*/*endo* and 112 kJ/mol to *endo*/*endo*. In case of phenyl groups, the most favourable conformation is *exo*/*endo* with energy differences of 22 to 24 kJ/mol (Figure 12).

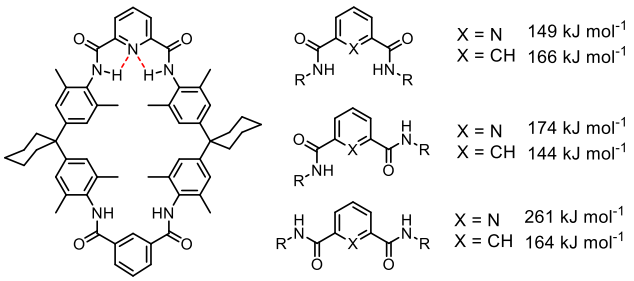

Figure 12: Conformational preferences of the individual subunits in TLMs.[42],[43]

To overcome the synthetic challenges for the formation of the smaller Leigh-type TLMs, the synthesis had to be template directed. A linear molecule with carbonyl functional groups acted as a template by forming hydrogen bonds with the half-cycle (Figure 13). Addition of the head group led to the final rotaxane.[44],[45] Leigh and co-workers made use of these macrocycles in molecular machines, in which the macrocycles can shuttle between different binding units depending on external stimuli.[46]

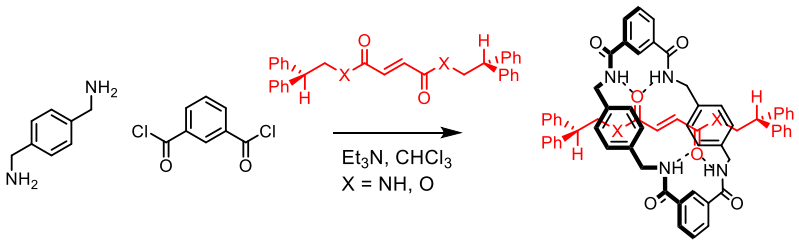

Figure 13: Template-directed rotaxane formation with a smaller TLM.[44],[45]

An alternative template strategy for anion binding has been explored by Beer and co-workers.[47],[48] Lactam-containing macrocycles were used for anion templating. Incorporation of an anion in the macrocycle was performed by binding to the isophthalamide sub unit and the pyridinium ion-pair of the guest molecule (Figure 14). Binding was further promoted by π-π stacking of the pyridinium cation and the hydroquinone groups of the macrocycle. Several pseudorotaxanes have been made via this strategy.[49],[50]

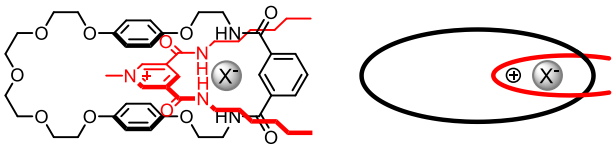

Figure 14: Anion-templated pseudorotaxane formation.[49],[50]

For the synthesis of anion-templated rotaxanes, introduction of sterically demanding stopper groups was required which were usually attached by ring-closing metathesis. With

a chloride atom as the template, the dumbbell and the open macrocycle bind the anion, and in a clipping reaction (ring-closing metathesis) the rotaxane is formed (Figure 15). However, this reaction only worked for chlorine atoms. Bromide, iodide, and hexafluorophosphate templates were unsuccessfully tested.[51]

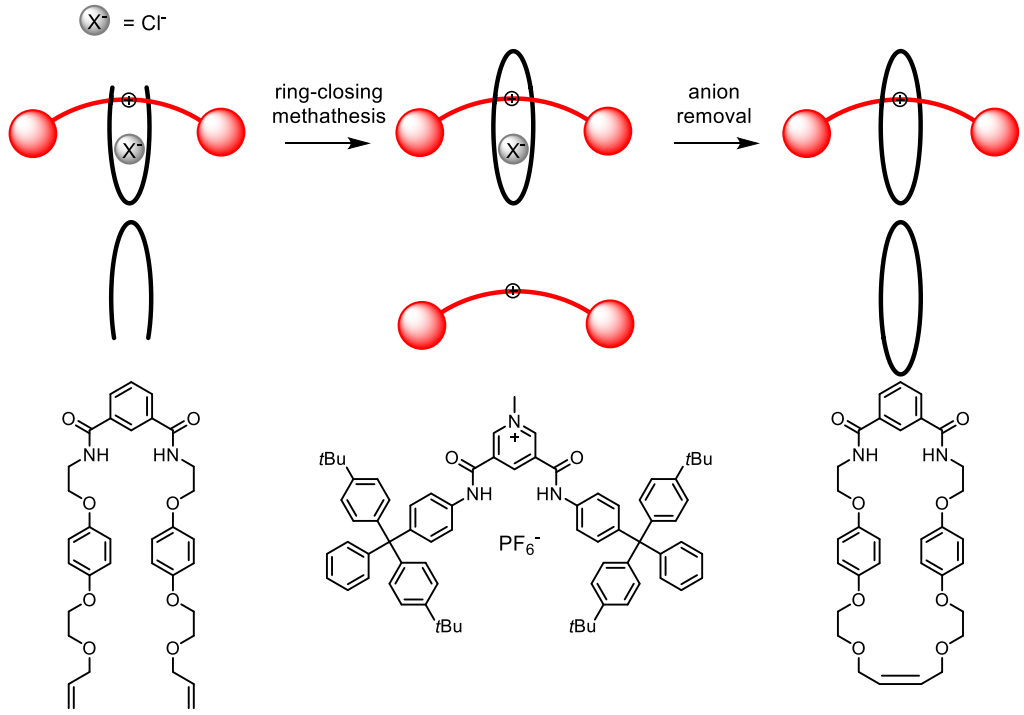

Figure 15: Anion-templated rotaxane formation by Beer *et al.*[51]

These examples of host-guest systems interacting by hydrogen bonding show impressive results in terms of chemical variety, but the macrocycles are still able to move by shuttling or slipping off the dumbbell. In order to encapsulate an emissive species, a strategy is required where the macrocycle is fixed in its position.

1.3.2 Self-Encapsulation with Covalent Bonds

Another method of encapsulation is the formation of covalently bound macrocycles threading around the molecule.[52],[53] Strapping of chromophores has been reported for iron-porphyrins by Baldwin *et al.* in 1976, with the aim to prevent the formation of irreversible μ-oxo-iron(III) dimers.[54] However, the steric hindrance of the strap was too

low to prevent ligand attack. This strapping and capping strategy was further pursued with different strapping groups to result in steric hindrance, preventing attack from other ligands.[55]–[61]

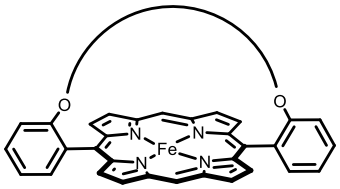

Figure 16: Schematic representation of a strapped porphyrin.[54]

Under the same aim, Würthner and co-workers presented another example for a covalently interlocked structure, *i.e.* the half-encapsulated perylene bisimide (PBI) in 2011. A glycol chain was introduced on perpendicularly located resorcinol derivatives.[62] Crystal structures revealed that π-stacking was still promoted for the 'free' side of the molecule, whereas it was prevented on the encapsulated one (Figure 17), leading to the formation of dimers.

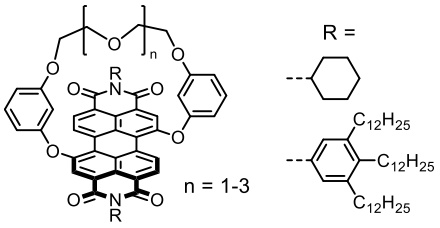

Figure 17: Half-threaded PBI, preventing π-interactions on the encapsulated side of the molecule.[62]

In 2010, Sugiyasu *et al.* first reported a fully insulated molecular wire based on polythiophene prepared using a metathesis reaction.[52],[53] Usually, interlocked rotaxanes are connected by hydrogen-bonds, hydrophilic-hydrophobic interactions, π-interactions, or metal-ligand interactions. In this case, however, the macrocycle and the thread are covalently connected. Alkyl side chains are introduced to two resorcinol units subsequently which undergo double ring-closing metathesis (Figure 18). The encapsulation prevents the

π-π interactions between adjacent polymers leading to an increased fluorescence quantum yield by 20% for the encapsulated species with a Stokes-shift of 790 cm^{-1}, compared to 4970 cm^{-1} for the unthreaded molecule.[52]

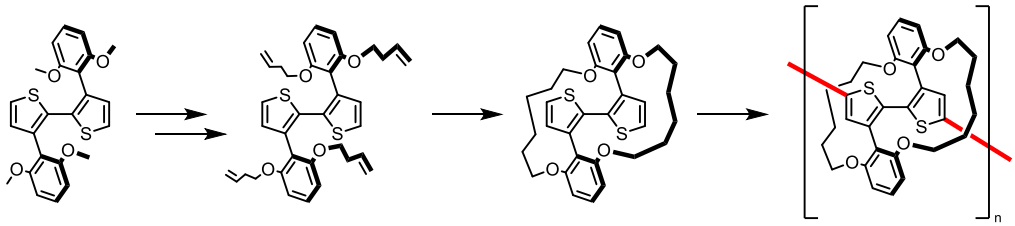

Figure 18: Sugiyasu's synthetic strategy for a self-threading polythiophene.[52],[53]

These insulated polythiophenes were used for the formation of charge carriers.[63] To allow charge transport, p-doping of the molecule was crucial. The insulated bis-thiophene units were polymerised with 3,4-ethylenedioxythienyl (EDOT) moieties through Stille-coupling (Figure 19). Upon controlled electrochemical oxidation, charge carriage was generated.

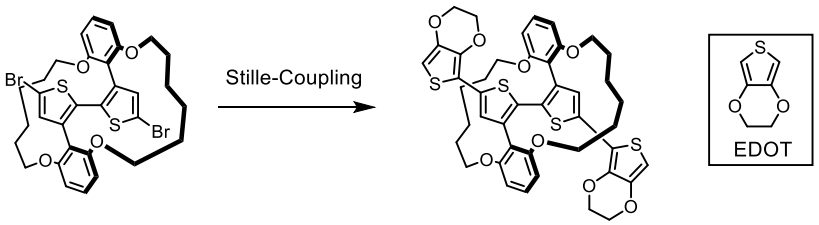

Figure 19: Sugiyasu's synthetic strategy for a p-doped self-threaded polythiophene.[63]

Takeuchi and his co-workers pursued this work further by self-threading a phenyl-ring with the same strategy. These were polymerised with thiophene, but also with thiophene and EDOT units (Figure 20).[64],[65] Both polymeric structures showed an impressive enhancement of the electro- and photoluminescence.

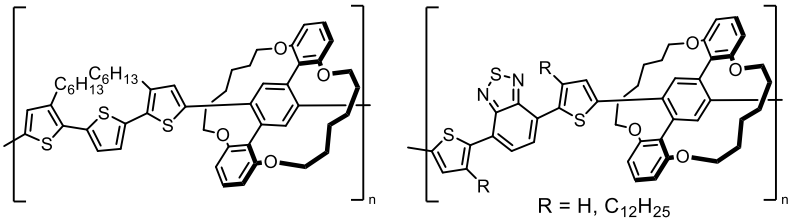

Figure 20: Self-threaded polymers by Sugiyasu *et al.*[64],[65]

In early 2018, Bronstein and co-workers published another example for a self-encapsulated polymer based on diketopyrollopyrrole (DPP).[8] Using the same strategy as shown by Sugiyasu *et al.*,[52] DPP was substituted with a dimethoxybenzene derivative, leading to the encapsulated species over 4 steps (Figure 21). Successful encapsulation was demonstrated by X-ray crystallography. The self-threaded monomer was polymerised with different spacers, giving DPPF, DPPP, and DPPT. The encapsulated species were photophysically compared to the 'naked' polymers, showing a strong increase in fluorescence quantum yields in the solid state, with values for solid state fluorescence of up to 28%.

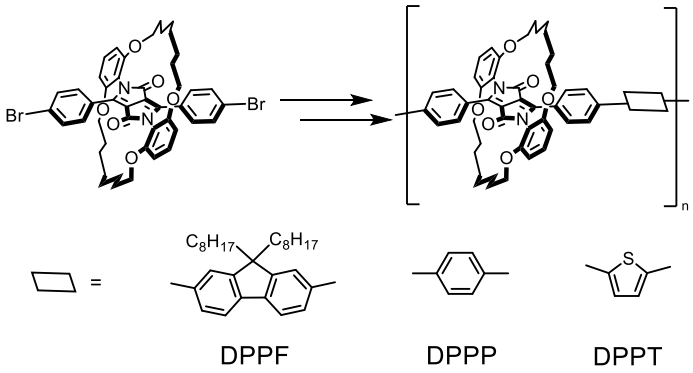

Polymer	Φ_F (solution) [%]	Φ_F (film) [%]
E-DPPF	95	20
E-DPPP	74	23
E-DPPT	74	28
N-DPPF	-	-
N-DPPP	19	8.0
N-DPPT	18	5.6

Figure 21: Self-threaded DPP polymers and their fluorescence quantum yields in solution and solid state by Bronstein *et al.*[8]

1.4 Indigo

A classic example of a hydrogen bonding pigment is indigo. It is one of the oldest natural, nontoxic products, and the most widely produced organic dye.[66] The hydrogen bonds and π-π stacking lead to strong inter- and intramolecular interactions and high crystal lattice energies.[67]–[69] The intramolecular hydrogen-bonding results in ultrafast proton transfer in the excited state, leading to quenching of the luminescence.[70],[71] Moreover, these hydrogen-bonds are useful to control self-assembly which is particularly important in aqueous media.[72]–[74]

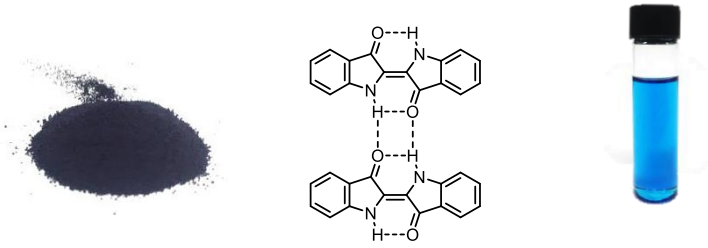

Figure 22: Indigo as a coarse material, molecular structure, and in DMSO-solution.

Indigo has unique properties, in particular, the origin of its absorption wavelength (~ 600 nm) is uncommon for such a small molecule and is not yet fully understood. Explanations include, for example, that the high aggregation in the solid/crystalline state due to the hydrogen bonds causes a bathochromic shift.[75] Alternatively, it is possible that the relatively low-lying excited state of indigo results in a small ΔE value compared to the ground state, leading to the observed long-wavelength absorption. Theoretical approaches employ MO (molecular orbital) theory and localise the structural subunit that determines the colour; in this context, the cross-conjugated π-system over the two central 5-membered rings seems to be important in determining the redshift in absorption compared to other small molecules.[75]

Saricifci and co-workers have previously reported the use of indigo in electronic devices. Incorporation of indigo in organic field-effect transistors (OFETs) demonstrated ambipolar transport properties with electron mobility ranging from 0.01-0.4 $cm^2 \cdot V^{-1} \cdot s^{-1}$ with excellent air stability.[76]–[79] Substitution of the *N*-moieties of indigo requires the break-up of its inter- and intramolecular hydrogen bonds, but increases the solubility of the derivatives.[80] Additionally, the ultrafast proton transfer in the excited state is prohibited, revealing fluorescent structures based on indigo. Yang *et al.* made use of this substitution method by introducing *t*-BOC groups on indigo. This derivative shows red emission in crystalline form. Replacing the *t*-BOC groups with acetyl moieties, led to a change in the fluorescence properties showing strong emission in the non-aggregated state but only moderate emission in the crystalline state.[81] Głowacki *et al.* implemented a *N*-disubstituted 6,6'-dithienylindigo into organic semiconductors (Figure 23). The thermolabile *t*-BOC groups were introduced for electropolymerisation giving a soluble poly-thienylindigo and were removed by heating the polymer.[82] This resulted in the formation of intermolecular hydrogen bonds in indigo, preserving its planarity.[83],[84]

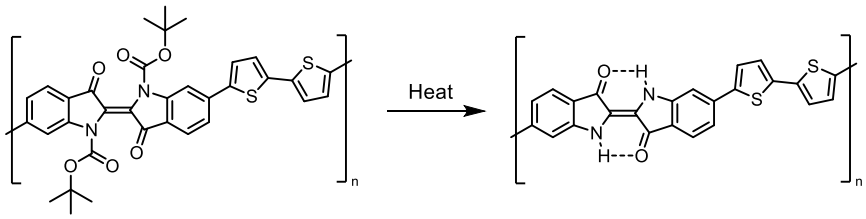

Figure 23: *t*-BOC substituted indigo polymers with thienyl subunits, giving a transistor by removal of the thermolabile *N*-substitutents.[82]

A similar polymer has been used by Li and co-workers to make a donor-acceptor polymer to be implemented in organic photovoltaics (OPVs).[85] To increase the solubility of the polymers, acyl groups were attached to the *N*-moieties. Tightly packed adjacent polymer chains in the solid state strengthened the intermolecular interactions,[86] resulting in a

shorter π-π stacking distance allowing charge carrier hopping between the polymer chains.[87] This strong intermolecular charge transfer led to relatively small HOMO/LUMO band gaps of ~1.7 eV.

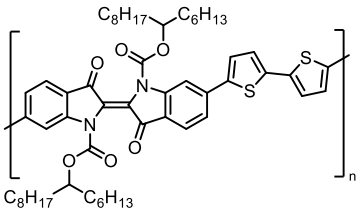

Figure 24: Substituted indigo polymer with thienyl subunits used in OPVs.[85]

Another phenomenon arising from the substitution of the indigo-*N*-positions is the isomerisation around the central double bond. *Cis*-*trans* isomerisation has not been observed in indigo due to the intermolecular hydrogen bonds,[88] but alkyl substitution allows photoconversion between both isomers (Figure 25).[89]–[91] Hicks and co-workers further investigated this behaviour on indigo and thioanalogues.[92],[93] Protonated salts of indigo derivatives were shown to form stable compounds in which the central double bond isomerises to the *cis*-configuration; deprotonation led to the formation of the *trans*-isomer. Compared to the former studies, the photoisomerisation requires the presence of acid, but is also possible for unsubstituted indigo.

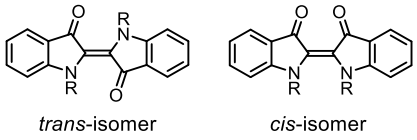

Figure 25: *Trans*- and *cis*-isomer structures of indigo.

To prevent *cis*/*trans* isomerisation in substituted, fluorescent indigo based derivatives, Engi first reported the synthesis of a bridged indigo dye '*Cibalackrot*' by condensation of indigo and phenylacetyl chloride (Figure 26).[94] This process is known as the bay-annulation of indigo. The conjugated, rigid structure shows an impressive fluorescence quantum yield of

93% in methylcyclohexane and a fluorescence life time of 6.9 ns.[95] De Melo *et al.* further investigated the photophysical behaviour of the dye.[96] The absorption and emission of the bridged species are blue-shifted over 60 nm relative to native indigo with a small Stokes shift of 23 nm. The spectra are narrower and display fine structure. Liu and co-workers used the approach of rigidifying the indigo-core to make high performance organic semiconductors.[97] Heating the indigo with thienylacetyl chloride gave the bridged species, which was further substituted by bromination and Stille-coupling (Figure 26). These donor-acceptor polymers showed hole and electron mobility of 1.5 and 0.41 $cm^2 \cdot V^{-1} \cdot s^{-1}$, respectively.

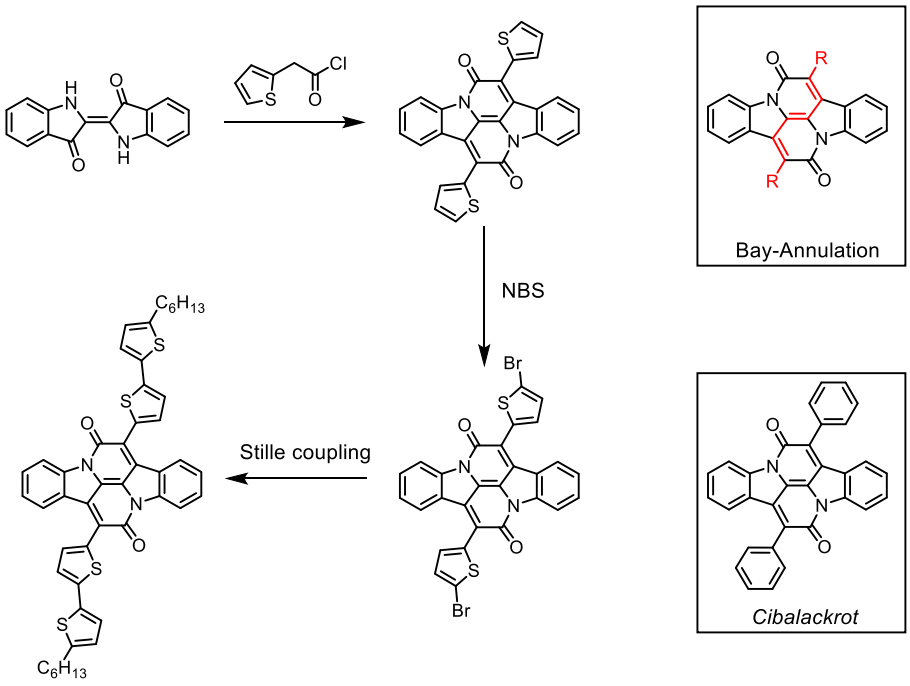

Figure 26: Bay-annulation of indigo with its oldest derivative *Cibalackrot*, and its functionalisation to give a high performance semiconductor.[94],[97]

This approach was further pursued by Bronstein and co-workers in 2015,[98] where a soluble bay-annulated indigo derivative was used in conjugated polymers. This highly crystalline polymer with a narrow bandgap was implemented into OFET devices showing high

ambipolar transport. The OPV efficiencies gave values of up to 2.35% with a photocurrent generated up to 950 nm showing its potential use in near-IR devices.

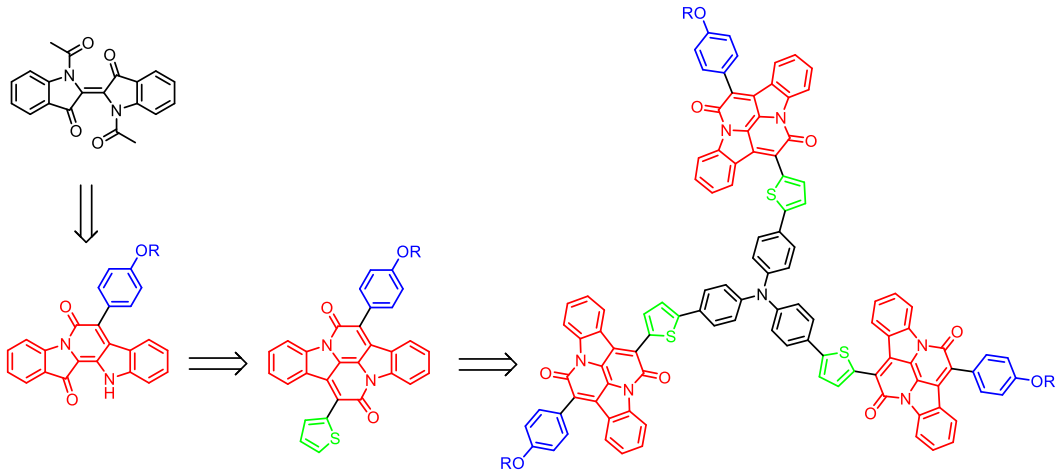

Figure 27: A stepwise bay-annulated indigo.[99]

In 2016, Kolaczkowksi *et al.* presented the stepwise bay-annulation of indigo yielding unsymmetrical bay-annulated subunits.[99] Synthesis of the soluble diacetyl indigo allowed the formation of mono-bridged indigos which then underwent a second bay-annulation (Figure 27). This allowed the construction of highly fluorescent donor-acceptor dendrimers with controllable electronic properties.

1.5 OLEDs

A common application for fluorescent materials is their incorporation into organic light-emitting diodes (OLEDs). OLEDs consist of organic layers between an anode and a cathode which are deposited on a substrate material.[100] Delocalisation of the π-electrons due to conjugation in the organic molecules makes them conductive. Classification of conductors, insulators, and semiconductors is determined by the number of electrons in their conducting and valence bands (Figure 28). If all states in a band are occupied, no movement of

electrons is possible; the same accounts for unoccupied bands. In metals, the conducting and the valence bands overlap and allow facile electron transport. The conducting and valence bands in insulators on the other hand, do not overlap and require a large amount of energy to transfer charges from the fully occupied valence band into the empty conducting band. Semiconductors are known for their small energy gap allowing movement of electrons from the valence band to the conducting band. Addition of a small number of different atoms (doping) of semiconductors leads to the formation of *n*-type and *p*-type semiconductors. Electron-rich doping materials produce *n*-type materials by contribution of more electrons, whereas doping with electron-poor materials creates holes, giving electron deficient *p*-type semiconductors. The energy needed to promote an electron in the conducting band is lowered during the doping process to a level comparable to thermal energy (205 cm^{-1} at room temperature).[101]

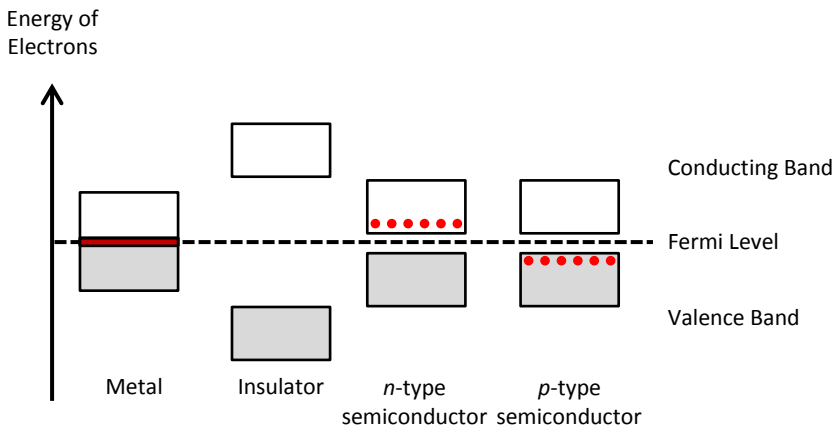

Figure 28: Conduction in metals, insulators, and semiconductors. Doping is shown by red dots in the conducting or valence band.

In OLEDs, electrons and holes are inserted from the electrodes into the organic layers, where a charge recombination leads to the formation of an exciton which emits light during relaxation. In general, OLEDs are fabricated on glass substrates where the organic layers lie between the anode and cathode (Figure 29). The emitting layer (EML) is composed of

a host material and a dopant with high quantum yield and carrier mobility. The EML is located between the hole-transporting layer (HTL) and the electron-transporting layer (ETL). These bring in the carriers for charge recombination. Further on, hole- and electron-injection layers (HIL and EIL) transport the charges from the conductors to the organic layers. The anode and cathode supply holes and electrons which are transferred to the EML for exciton formation leading to emission of light.[102]

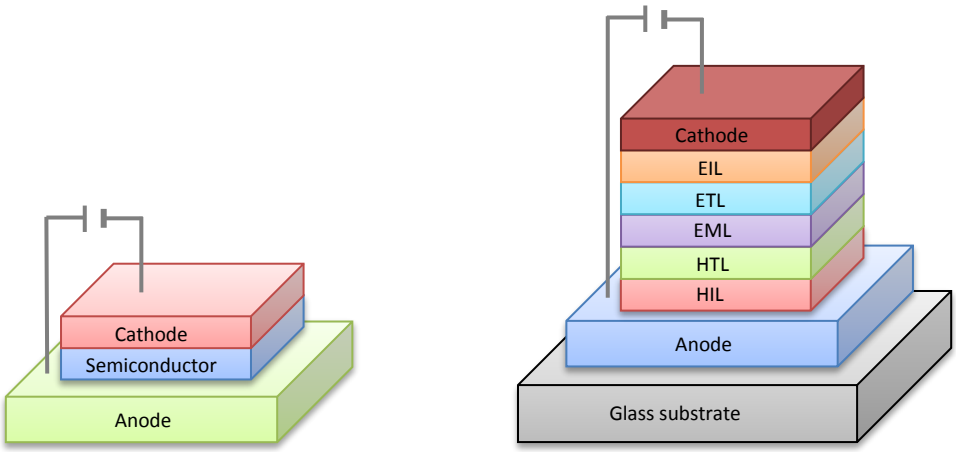

Figure 29: Schematic diagram of an OLED device. (Left) Basic structure of an OLED. (Right) Multi-layer structure in current OLEDs. On a glass substrate, the anode is placed, followed by a hole-injection layer (HIL), a hole-transporting layer (HTL), an emitting layer (EML), an electron-transporting layer (ETL), an electron-injection layer (EIL), and the cathode.

Generally, OLEDs are not made purely from fluorescent compounds. This is caused by the distribution of singlet and triplet states in the excited state of these solid materials. As soon as photons of a fluorophore are absorbed into their excited state, the excited singlet and triplet levels are occupied in a 1 to 3 ratio, allowing a maximal physically possible fluorescence quantum yield of 25%. If reversed intersystem crossing between the triplet and singlet state is suppressed due to large energy differences, the quantum yield is not high enough to build efficient OLEDs. To avoid this phenomenon, fluorescent molecules are used as dopants in phosphorescent substances to fine tune the emissive properties of the OLED while maintaining high efficiency.

Several fluorescent, encapsulated materials have been tested in OLEDs and were compared to their 'naked' materials. In a former project in the Anderson group, a strategy for the incorporation of organic polymeric materials into cyclodextrin macrocycles over a capping reaction has been established, leading to an increase of solid state fluorescence quantum yields from 4 to 17% for the encapsulated species (Figure 30). However, this binding relies completely on the incorporation of sterically demanding stopper groups to prevent slipping of the macrocycles off the molecular wire (MW).[15],[16]

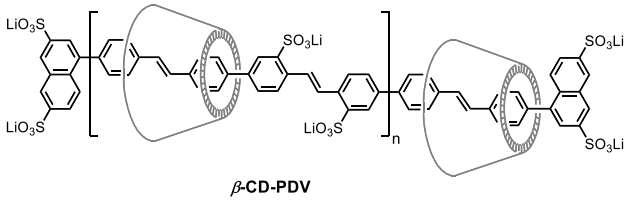

Figure 30: PDV-rotaxane from the Anderson group.[15],[16]

These encapsulated polyrotaxanes with cyclodextrins were implemented in OLEDs showing better efficiencies compared to the unthreaded counterpart. Up to two orders-of-magnitude increase in the electroluminescence quantum yield was observed, but also a greater operational robustness. All of the different threaded derivatives showed increased fluorescence and higher efficiencies in OLEDs when compared to their unthreaded analogues.[12],[13],[16],[103]–[105] The same behaviour has also been reported for self-encapsulated derivatives.[8],[65],[106],[107] The self-encapsulated DPP-polymer from Bronstein and co-workers showed that the performance of the OLEDs incorporating the encapsulated species was strongly increased. The enhanced structural order resulting from encapsulation also leads to an increase in the spectral purity of the devices.[8] Similar results have also been published by Sugiyasu *et al.* for devices made from their molecular wires based on self-encapsulated phenyl rings and the bisthiophene derivatives.[65],[106],[107]

1.6 Prospective

This thesis aims to report new materials based on indigo which can be encapsulated and tested in organic light-emitting diodes. It has already been proven that encapsulation leads to better device efficiencies.[8],[12],[13],[16],[65],[103]–[107] However, new doping materials are still sought after. The cheap and readily available dye, indigo, which emits in the visible part of the spectrum when functionalised, presents a suitable opportunity for synthesis of new materials for OLEDs. We explored the chemistry of indigo and its encapsulation to build up mechanically interlocked molecules. By substitution of indigo with different sterically demanding groups and further on their bay-annulation, we aimed to synthesise materials with enhanced fluorescence in the solid state, providing new materials for OLEDs.

In Chapter 2, the substitution of indigo and its synthetic challenges are investigated. We showed that *N*-substitution enhances the photophysical properties and that rigidification and extension of the π-system gave a highly fluorescent bay-annulated dye.

Chapter 3 investigates the self-encapsulation of the highly fluorescent bay-annulated indigos. The synthetic challenges are laid out and discussed. A thorough photophysical and structural examination of the target structures is described at the end of the chapter.

Chapter 4 analyses the hydrogen bonding between tetralactam macrocycles (TLMs) and indigo structures as another form of encapsulation. The binding behaviour was analysed for neutral complexes, but also for reduced species which enhance the binding strengths. Binding constants for the neutral and reduced species were analysed and compared.

Chapter 5 comprises a summary of this thesis and an outlook for possible further projects.

1.7 References

[1] Lakowicz, J. R. *Principles of Fluorescence Spectroscopy*; Lakowicz, J. R., Ed.; Springer US: Boston, MA, 2006.

[2] Lindon, J. . C.; Tranter, G. . E.; Koppenaal, D. *Encyclopedia of Spectroscopy and Spectrometry*, 3rd ed.; Elsevier Science, 2010.

[3] Főrster, T. *Discuss. Faraday Soc.* **1959**, *27*, 7–17.

[4] Dexter, D. L. *J. Chem. Phys.* **1953**, *21*, 836–850.

[5] Franck, J.; Teller, E. *J. Chem. Phys.* **1938**, *6*, 861–872.

[6] Jelley, E. E. *Nature* **1936**, *138*, 1009–1010.

[7] Würthner, F.; Kaiser, T. E.; Saha-Möller, C. R. *Angew. Chem. Int. Ed.* **2011**, *50*, 3376–3410.

[8] Leventis, A.; Royakkers, J.; Rapidis, A. G.; Goodeal, N.; Corpinot, M. K.; Frost, J. M.; Bučar, D. K.; Blunt, M. O.; Cacialli, F.; Bronstein, H. *J. Am. Chem. Soc.* **2018**, *140*, 1622–1626.

[9] Liang, J.; Nguyen, Q. L.; Matsika, S. *Photochem. Photobiol. Sci.* **2013**.

[10] Michels, J. J.; O'Connell, M. J.; Taylor, P. N.; Wilson, J. S.; Cacialli, F.; Anderson, H. L. *Chem. Eur. J.* **2003**, *9*, 6167–6176.

[11] Taylor, P. N.; Hagan, A. J.; Anderson, H. L. *Org. Biomol. Chem.* **2003**, *1*, 3851–3856.

[12] Cacialli, F.; Wilson, J. S.; Michels, J. J.; Daniel, C.; Silva, C.; Friend, R. H.; Severin, N.; Samorì, P.; Rabe, J. P.; O'Connell, M. J.; Taylor, P. N.; Anderson, H. L. *Nat.*

Mater. **2002**, *1*, 160–164.

[13] Brovelli, S.; Meinardi, F.; Winroth, G.; Fenwick, O.; Sforazzini, G.; Frampton, M. J.; Zalewski, L.; Levitt, J. a.; Marinello, F.; Schiavuta, P.; Suhling, K.; Anderson, H. L.; Cacialli, F. *Adv. Funct. Mater.* **2010**, *20*, 272–280.

[14] Xue, M.; Yang, Y.; Chi, X.; Yan, X.; Huang, F. *Chem. Rev.* **2015**, *115*, 7398–7501.

[15] Frampton, M. J.; Anderson, H. L. *Angew. Chem.- Int. Ed.* **2007**, *46*, 1028–1064.

[16] Frampton, M. J.; Sforazzini, G.; Brovelli, S.; Latini, G.; Townsend, E.; Williams, C. C.; Charas, A.; Zalewski, L.; Kaka, N. S.; Sirish, M.; Parrott, L. J.; Wilson, J. S.; Cacialli, F.; Anderson, H. L. *Adv. Funct. Mater.* **2008**, *18*, 3367–3376.

[17] Reuter, C.; Wienand, W.; Hübner, G. M.; Seel, C.; Vögtle, F. *Chem. Eur. J.* **1999**, *5*, 2692–2697.

[18] Isnin, R.; Kaifer, A. E. *J. Am. Chem. Soc.* **1991**, *113*, 8188–8190.

[19] Yin, J.; Dasgupta, S.; Wu, J. *Org. Lett.* **2010**, *12*, 1712–1715.

[20] Affeld, A.; Hübner, G. M.; Seel, C.; Schalley, C. A. *European J. Org. Chem.* **2001**, *2001*, 2877.

[21] Leigh, D. a.; Venturini, A.; Wilson, A. J.; Wong, J. K. Y.; Zerbetto, F. *Chem. Eur. J.* **2004**, *10*, 4960–4969.

[22] Beves, J. E.; Blight, B. A.; Campbell, C. J.; Leigh, D. A.; McBurney, R. T. *Angew. Chem. Int. Ed.* **2011**, *50*, 9260–9327.

[23] Seel, C.; Parham, A. H.; Safarowsky, O.; Hübner, G. M.; Vögtle, F. *J. Org. Chem.* **1999**, *64*, 7236–7242.

[24] Nepogodiev, S. A.; Stoddart, J. F. *Chem. Rev.* **1998**, *98*, 1959–1976.

[25] Chambron, J. C.; Heitz, V.; Sauvage, J. P. *J. Am. Chem. Soc.* **1993**, *115*, 12378–12384.

[26] Asakawa, M.; Ashton, P. R.; Ballardini, R.; Balzani, V.; Bělohradský, M.; Gandolfi, M. T.; Kocian, O.; Prodi, L.; Raymo, F. M.; Stoddart, J. F.; Venturi, M. *J. Am. Chem. Soc.* **1997**, *119*, 302–310.

[27] Hunter, C. A.; Sanders, J. K. M. *J. Am. Chem. Soc.* **1990**, *112*, 5525–5534.

[28] Sambrook, M. R.; Beer, P. D.; Lankshear, M. D.; Ludlow, R. F.; Wisner, J. A. *Org. Biomol. Chem.* **2006**, *4*, 1529.

[29] Amabilino, D. B.; Stoddart, J. F. *Chem. Rev.* **1995**, *95*, 2725–2828.

[30] Gibson, H. W.; Wang, H.; Niu, Z.; Slebodnick, C.; Zhakharov, L. N.; Rheingold, A. L. *Macromolecules* **2012**, *45*, 1270–1280.

[31] Kirchner, B.; Spickermann, C.; Reckien, W.; Schalley, C. *J. Am. Chem. Soc.* **2010**, *132*, 484–494.

[32] Gassensmith, J. J.; Barr, L.; Baumes, J. M.; Paek, A.; Nguyen, A.; Smith, B. D. *Org. Lett.* **2008**, *10*, 3343–3346.

[33] Gassensmith, J. J.; Baumes, J. M.; Smith, B. D. *Chem. Commun. (Camb).* **2009**, 6329–6338.

[34] Vögtle, F.; Meier, S.; Hoss, R. *Angew. Chem. Int. Ed. English* **1992**, *31*, 1619–1622.

[35] Hunter, C. A. *J. Am. Chem. Soc.* **1992**, *114*, 5303–5311.

[36] Hunter, C. A. *J. Chem. Soc. Chem. Commun.* **1991**, 749–751.

[37] Li, X.; Illigen, J.; Nieger, M.; Michel, S.; Schalley, C. A. *Chem. Eur. J.* **2003**, *9*, 1332–1347.

[38] Kaufmann, L.; Dzyuba, E. V.; Malberg, F.; Löw, N. L.; Groschke, M.; Brusilowskij, B.; Huuskonen, J.; Rissanen, K.; Kirchner, B.; Schalley, C. a. *Org. Biomol. Chem.* **2012**, *10*, 5954.

[39] Vögtle, Fritz; Händel, Mirko; Meier, Stephan; Ottens-Hildebrandt, Stephan; Ott, Frank; Schmidt, T. *Liebigs Ann.* **1995**, 739–743.

[40] Dünnwald, T.; Jäger, R.; Vögtle, F. *Chem. Eur. J.* **1997**, *3*, 2043–2051.

[41] Johnston, A. G.; Leigh, D. A.; Pritchard, R. J.; Deegan, M. D. *Angew. Chem. Int. Ed.* **1995**, *34*, 1209–1212.

[42] Hunter, C. A.; Purvis, D. H. *Angew. Chem. Int. Ed.* **1992**, *31*, 792–795.

[43] Carver, F. J.; Hunter, C. A.; Shannon, R. J. *J. Chem. Soc. Chem. Commun.* **1994**, 1277.

[44] Leigh, D. a; Murphy, A.; Smart, J. P.; Slawin, A. M. Z. *Angew. Chem. Int. Ed.* **1997**, *36*, 728–732.

[45] Gatti, F. G.; Leigh, D. A.; Nepogodiev, S. A.; Slawin, A. M. Z.; Teat, S. J.; Wong, J. K. Y. *J. Am. Chem. Soc.* **2001**, *123*, 5983–5989.

[46] Kay, E. R.; Leigh, D. A.; Zerbetto, F. *Angew. Chem. Int. Ed.* **2007**, *46*, 72–191.

[47] Wisner, J. A.; Beer, P. D.; Drew, M. G. B. *Angew. Chem. Int. Ed.* **2001**, *40*, 3606.

[48] Lankshear, M. D.; Beer, P. D. *Acc. Chem. Res.* **2007**, *40*, 657–668.

[49] Sambrook, M. R.; Beer, P. D.; Wisner, J. A.; Paul, R. L.; Cowley, A. R.; Szemes,

F.; Drew, M. G. B. *J. Am. Chem. Soc.* **2005**, *127*, 2292–2302.

[50] Wisner, J. A.; Beer, P. D.; Berry, N. G.; Tomapatanaget, B. *Proc. Natl. Acad. Sci.* **2002**, *99*, 4983–4986.

[51] Wisner, J. A.; Beer, P. D.; Drew, M. G. B.; Sambrook, M. R. *J. Am. Chem. Soc.* **2002**, *124*, 12469–12476.

[52] Sugiyasu, K.; Honsho, Y.; Harrison, R. M.; Sato, A.; Yasuda, T.; Seki, S.; Takeuchi, M. *J. Am. Chem. Soc.* **2010**, *132*, 14754–14756.

[53] Ouchi, Y.; Sugiyasu, K.; Ogi, S.; Sato, A.; Takeuchi, M. *Chem. - An Asian J.* **2012**, *7*, 75–84.

[54] Baldwin, J. E.; Klose, T.; Peters, M. *J. Chem. Soc., Chem. Commun.* **1976**, 881–883.

[55] Gunter, M. J.; Mander, L. N. *J. Org. Chem.* **1981**, *46*, 4792–4795.

[56] Baldwin, J. E.; Crossley, M. J.; Klose, T.; O'Rear, E. A.; Peters, M. K. *Tetrahedron* **1982**, *38*, 27–39.

[57] Momenteau, M.; Mispelter, J.; Loock, B.; Bisagni, E. *J. Chem. Soc. Perkin Trans. 1* **1983**, 189.

[58] Boitrel, B.; Lecas, A.; Renko, Z.; Rose, E. *J. Chem. Soc., Chem. Commun.* **1985**, 1820–1821.

[59] Wytko, J. A.; Graf, E.; Weiss, J. *J. Org. Chem.* **1992**, *57*, 1015–1018.

[60] Collman, J. P.; Zhang, X.; Herrmann, P. C.; Uffelman, E. S.; Boitrel, B.; Straumanis, A.; Brauman, J. I. *J. Am. Chem. Soc.* **1994**, *116*, 2681–2682.

[61] Urbani, M.; Torres, T. *Chem. Eur. J.* **2014**, *20*, 16337–16349.

[62] Safont-Sempere, M. M.; Osswald, P.; Stolte, M.; Grüne, M.; Renz, M.; Kaupp, M.; Radacki, K.; Braunschweig, H.; Würthner, F. *J. Am. Chem. Soc.* **2011**, *133*, 9580–9591.

[63] Shomura, R.; Sugiyasu, K.; Yasuda, T.; Sato, A.; Takeuchi, M. *Macromolecules* **2012**, *45*, 3759–3771.

[64] Kushida, S.; Braam, D.; Pan, C.; Dao, T. D.; Tabata, K.; Sugiyasu, K.; Takeuchi, M.; Ishii, S.; Nagao, T.; Lorke, A.; Yamamoto, Y. *Macromolecules* **2015**, *48*, 3928–3933.

[65] Méhes, G.; Pan, C.; Bencheikh, F.; Zhao, L.; Sugiyasu, K.; Takeuchi, M.; Ribierre, J.-C.; Adachi, C. *ACS Macro Lett.* **2016**, *5*, 781–785.

[66] Seefelder, M. *Indigo in culture, science and technology*, 2nd ed.; ecomed: Landsberg, Germany, 1994.

[67] Zollinger, H. *Color chemistry: syntheses, properties, and applications of organic dyes and pigments*; VCH: Weinheim ; New York, 1991.

[68] Faulkner, E. B.; Schwartz, R. J. *High Performance Pigments*, 2nd ed.; Wiley-VCH Verlag GmbH & Co. KGaA, Weinheim, 2009.

[69] Herbst, W.; Hunger, K.; Wilker, G.; Ohleier, H.; Winter, R. *Industrial Organic Pigments*; Wiley-VCH Verlag GmbH & Co. KGaA: Weinheim, FRG, 2004.

[70] Yamazaki, S.; Sobolewski, A. L.; Domcke, W. *Phys. Chem. Chem. Phys.* **2011**, *13*, 1618–1628.

[71] Pina, J.; Sarmento, D.; Accoto, M.; Gentili, P. L.; Vaccaro, L.; Galvão, A.; Seixas de Melo, J. S. *J. Phys. Chem. B* **2017**, *121*, 2308–2318.

[72] De Luca, G.; Pisula, W.; Credgington, D.; Treossi, E.; Fenwick, O.; Lazzerini, G. M.; Dabirian, R.; Orgiu, E.; Liscio, A.; Palermo, V.; Müllen, K.; Cacialli, F.; Samorì, P. *Adv. Funct. Mater.* **2011**, *21*, 1206–1206.

[73] Görl, D.; Zhang, X.; Würthner, F. *Angew. Chem. Int. Ed.* **2012**, *51*, 6328–6348.

[74] Rondão, R.; de Melo, J. S.; Schaberle, F. A.; Voss, G. *Phys. Chem. Chem. Phys.* **2012**, *14*, 1778–1783.

[75] Christie, R. *Biotech. Histochem.* **2007**, *82*, 51–56. Serrano-Andres L, Roos BO.

Chem. Eur. J. **1997**; *3*, 717–725. Klessinger M. *Dyes Pigments* **1982**; *3*, 235–241. Griffiths J. *Dyes Pigments* **1982**; *3*,: 211–233.

[76] Irimia-Vladu, M.; Głowacki, E. D.; Troshin, P. A.; Schwabegger, G.; Leonat, L.; Susarova, D. K.; Krystal, O.; Ullah, M.; Kanbur, Y.; Bodea, M. A.; Razumov, V. F.; Sitter, H.; Bauer, S.; Sariciftci, N. S. *Adv. Mater.* **2012**, *24*, 375–380.

[77] Głowacki, E. D.; Voss, G.; Sariciftci, N. S. *Adv. Mater.* **2013**, *25*, 6783–6800.

[78] Głowacki, E. D.; Leonat, L.; Voss, G.; Bodea, M.-A.; Bozkurt, Z.; Ramil, A. M.; Irimia-Vladu, M.; Bauer, S.; Sariciftci, N. S. *AIP Adv.* **2011**, *1*, 042132.

[79] Głowacki, E. D.; Irimia-Vladu, M.; Bauer, S.; Sariciftci, N. S. *J. Mater. Chem. B* **2013**, *1*, 3742.

[80] Porada, J. H.; Neudörfl, J.-M.; Blunk, D. *New J. Chem.* **2015**, *39*, 8291–8301.

[81] Yang, C.; Trinh, Q. T.; Wang, X.; Tang, Y.; Wang, K.; Huang, S.; Chen, X.; Mushrif, S. H.; Wang, M. *Chem. Commun.* **2015**, *51*, 3375–3378.

[82] Głowacki, E. D.; Voss, G.; Demirak, K.; Havlicek, M.; Sünger, N.; Okur, A. C.;

Monkowius, U.; Gąsiorowski, J.; Leonat, L.; Sariciftci, N. S. *Chem. Commun.* **2013**, *49*, 6063.

[83] Głowacki, E. D.; Apaydin, D. H.; Bozkurt, Z.; Monkowius, U.; Demirak, K.; Tordin, E.; Himmelsbach, M.; Schwarzinger, C.; Burian, M.; Lechner, R. T.; Demitri, N.; Voss, G.; Sariciftci, N. S. *J. Mater. Chem. C* **2014**, *2*, 8089–8097.

[84] Liu, C.; Xu, W.; Xue, Q.; Cai, P.; Ying, L.; Huang, F.; Cao, Y. *Dye. Pigment.* **2016**, *125*, 54–63.

[85] Guo, C.; Sun, B.; Quinn, J.; Yan, Z.; Li, Y. *J. Mater. Chem. C* **2014**, *2*, 4289–4296.

[86] Osaka, I.; Sauvé, G.; Zhang, R.; Kowalewski, T.; McCullough, R. D. *Adv. Mater.* **2007**, *19*, 4160–4165.

[87] Li, Y.; Sonar, P.; Murphy, L.; Hong, W. *Energy Environ. Sci.* **2013**, *6*, 1684.

[88] Brode, W. R.; Pearson, E. G.; Wyman, G. M. *J. Am. Chem. Soc.* **1954**, *76*, 1034–1036.

[89] Weinstein, J.; Wyman, G. M. *J. Am. Chem. Soc.* **1956**, *78*, 2387–2390.

[90] Pummerer, R.; Marondel, G. *Justus Liebigs Ann. Chem.* **1957**, *602*, 228–232.

[91] Giuliano, C. R.; Hess, L. D.; Margerum, J. D. *J. Am. Chem. Soc.* **1967**, *90*, 587–594.

[92] Nicholls-Allison, E. C.; Nawn, G.; Patrick, B. O.; Hicks, R. G. *Chem. Commun.* **2015**, *51*, 12482–12485.

[93] Hajjar, L.; Hicks, R. G.; Zeng, T. *J. Phys. Chem. A* **2016**, *120*, 7569–7576.

[94] Engi, G. *Zeitschrift für Angew. Chem.* **1914**, *27*, 144–148.

[95] Haucke, G.; Paetzold, R. *J. für Prakt. Chemie* **1979**, *917*, 978–986.

[96] Seixas de Melo, J.; Rondão, R.; Burrows, H. D.; Melo, M. J.; Navaratnam, S.; Edge, R.; Voss, G. *J. Phys. Chem. A* **2006**, *110*, 13653–13661.

[97] He, B.; Pun, A. B.; Zherebetskyy, D.; Liu, Y.; Liu, F.; Klivansky, L. M.; McGough, A. M.; Zhang, B. A.; Lo, K.; Russell, T. P.; Wang, L.; Liu, Y. *J. Am. Chem. Soc.* **2014**, *136*, 15093–15101.

[98] Fallon, K. J.; Wijeyasinghe, N.; Yaacobi-Gross, N.; Ashraf, R. S.; Freeman, D. M. E.; Palgrave, R. G.; Al-Hashimi, M.; Marks, T. J.; McCulloch, I.; Anthopoulos, T. D.; Bronstein, H. *Macromolecules* **2015**, *48*, 5148–5154.

[99] Kolaczkowski, M. A.; He, B.; Liu, Y. *Org. Lett.* **2016**, *18*, 5224–5227.

[100] Tang, C. W.; VanSlyke, S. A. *Appl. Phys. Lett.* **1987**, *51*, 913–915.

[101] Klauk, H. *Organic Electronics: Materials, Manufacturing, and Applications*; Wiley, 2006.

[102] Chen, H.-W.; Lee, J.-H.; Lin, B.-Y.; Chen, S.; Wu, S.-T. *Light Sci. Appl.* **2018**, *7*, 17168.

[103] Wilson, J. S.; Frampton, M. J.; Michels, J. J.; Sardone, L.; Marletta, G.; Friend, R. H.; Samorì, P.; Anderson, H. L.; Cacialli, F. *Adv. Mater.* **2005**, *17*, 2659–2663.

[104] Brovelli, S.; Latini, G.; Frampton, M. J.; McDonnell, S. O.; Oddy, F. E.; Fenwick, O.; Anderson, H. L.; Cacialli, F. *Nano Lett.* **2008**, *8*, 4546–4551.

[105] Petrozza, A.; Brovelli, S.; Michels, J. J.; Anderson, H. L.; Friend, R. H.; Silva, C.; Cacialli, F. *Adv. Mater.* **2008**, *20*, 3218–3223.

[106] Sun, C.; Mróz, M. M.; Castro Smirnov, J. R.; Lüer, L.; Hermida-Merino, D.; Zhao, C.; Takeuchi, M.; Sugiyasu, K.; Cabanillas-González, J. *J. Mater. Chem. C* **2018**, *6*,

6591–6596.

[107] Pan, C.; Sugiyasu, K.; Wakayama, Y.; Sato, A.; Takeuchi, M. *Angew. Chem. Int. Ed.* **2013**, *52*, 10775–10779.

2

Acylation of Indigo

2.1 Introduction

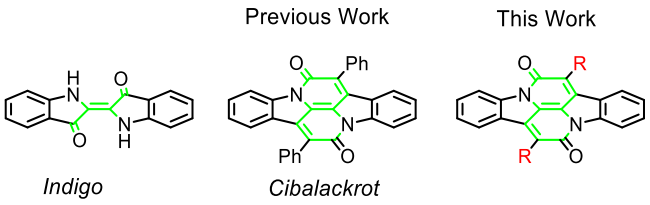

Figure 31: Molecular structures of indigo and *Cibalackrot* showing the extended conjugation in the main body.

The synthesis of the indigo-based, bay-annulated red emitter, *Cibalackrot* (Figure 31) was first reported in 1914; indigo and phenylacetyl chloride react in a simple condensation reaction yielding the red fluorescent solid.[1] Compared to indigo, this rigid bay-annulated form has an extended, conjugated structure, revealing enhanced photophysical properties. Further studies in 1974 by Paetzold *et al.* revealed that *Cibalackrot* has a high fluorescence quantum yield of 93% in methylcyclohexane and a fluorescence lifetime of 6.9 ns.[2] This made the molecule particularly attractive for its use in photonic applications. However, the insolubility of *Cibalackrot* hindered further investigation. More recently, derivatives with thienyl groups were made.[3],[4] Kolaczkowski *et al.* used the soluble starting material *N,N'*-diacetyl indigo (**2.3a**) for the stepwise bay-annulation of indigo to introduce different substituents on the nitrogen atoms, allowing the formation of unsymmetrical bay-annulated derivatives.[5]

Our aim was the formation of new bay-annulated indigo derivatives for their application in OLEDs. In this chapter we describe the investigation of the *N*-acylation of indigo and the resulting changes in structure and photophysical properties to achieve new indigo-based compounds with fluorescent properties, leading to the formation of new bay-annulated derivatives (Figure 32). Different acid chlorides were chosen based on variation of their steric impact. We were able to show that nucleophilic addition on the NH-moieties with acid chlorides increased the solubility and resulted in changes of the photophysical behaviour (*e.g.* higher fluorescence quantum yields, blue-shift of the absorption). Also, an organic soluble bay-annulated indigo derivative **2.4d** with a fluorescence quantum yield of

90% in CH_2Cl_2 was formed. Several compounds were crystallised and their structural properties were compared to those of indigo.[6]–[8]

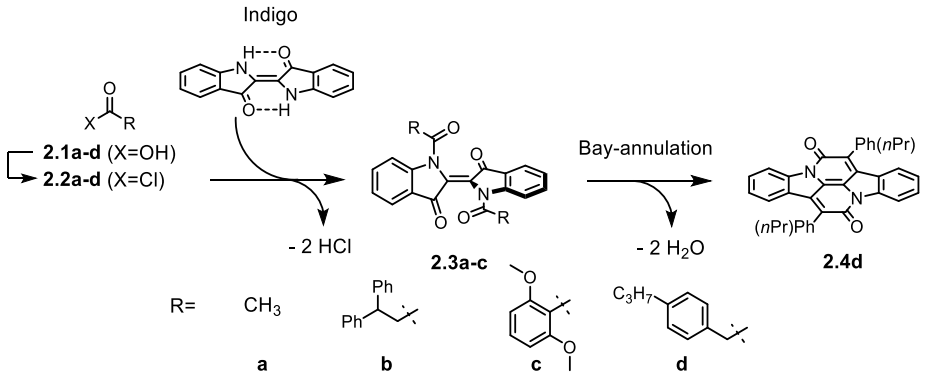

Figure 32: Synthetic pathway for the *N*-acylation and bay-annulation of indigo.

2.2 Synthesis

2.2.1 Synthesis of Acid Chlorides

The acylation of indigo is mostly accomplished by reaction of indigo with acid chlorides at high temperatures.[5] Chlorination of carboxylic acids is usually performed by treating the respective acid with thionyl chloride,[9] phosphorus trichloride,[10] or phosphorus pentachloride.[11] During the reaction of thionyl chloride with a carboxylic acid, SO_2 and HCl are generated, which leave the reaction as gases, and drive the reaction forward.[12] We chose the several acid chlorides as model compounds for the bay-annulation of indigo. It was tested whether other substituents than the known examples are tolerated. Two of the acid chlorides are commercially available (*i.e.* **2.2a** and **2.2c**); the others (**2.2b** and **2.2d**) were bought as carboxylic acids and converted to the acyl chlorides with $SOCl_2$ (Figure 32). The carboxylic acids **2.1a** and **2.1d** were each dissolved in an excess of thionyl chloride (>10 eq.) and heated to reflux (75 °C) for 2-3 h.[13] The remaining thionyl chloride was removed using distillation, and the residue was dried under high vacuum for several hours.

The reactions gave yields of 99%. Acid chlorides are generally moisture-sensitive, so, we decided to use the freshly prepared derivatives without further purification.

2.2.2 Reactions of Indigo with Acid Chlorides

For the acylation of indigo, different sterically-demanding groups were introduced on the *N,N'*-moieties of indigo to monitor their structural influence on the indigo main core and the change in the photophysical properties. The indigo was dissolved in a high boiling solvent to allow high reaction temperatures followed by addition of the respective acid chloride.[5],[14],[15] Some of the reactions were performed in the presence of Brønsted bases to catalyse the product formation. For the synthesis of **2.3a**, indigo was heated with acetyl chloride (**2.1a**) in acetic anhydride, yielding 70% of the product, under conditions known in the literature.[5]

To form the bay-annulated indigo derivative with two bulky phenyl groups, 3,3-diphenylpropionyl chloride (**2.2b**) reacted with commercially-available indigo according to a published procedure.[16] The mixture was heated in toluene for up to 48 h yielding *N,N'*-bis(3,3'-diphenylpropionyl) indigo (**2.3b**) in only 12% yield, but no bay-annulated dye **2.4b**. Nevertheless, it was possible to enhance the yields from 12 to 90% for **2.3b**. Interestingly, during optimisation of the reaction conditions, three different derivatives were formed as summarised in Figure 33. Use of DMF as solvent with an excess of pyridine gave **2.3b** almost quantitatively, but no bay-annulation emerged during the reaction. Addition of K_2CO_3 instead of pyridine gave a half bay-annulated version **2.3b-II**, which was used to further undergo reaction with **2.2b**, but no reaction occurred. Using the method from Kolaczkowski *et al*, heating soluble *N,N'*-diacetyl indigo (**2.3a**) with the acyl chloride **2.2b**, gave the mono-substituted indigo derivative **2.3b-III**. The synthesis of the fully bay-annulated species **2.4b** was attempted from the *N,N'*-bissubstituted derivative **2.3b** (Figure

33). Compound **2.3b** was heated in toluene, DMF, or acetic anhydride, but no reaction occurred. Additionally, heating **2.3b** in DMF with a Brønsted base (K_2CO_3) or in toluene with a dehydrating agent (P_2O_5) resulted in decomposition. None of the tested reaction conditions led to the formation of **2.4b**. The reason for this can be explained by the decreased acidity of the α-protons of the amide group compared to those in phenylacetic acids.[3]–[5] The sterically demanding phenyl-substituents could also have hindered the double bay-annulation.

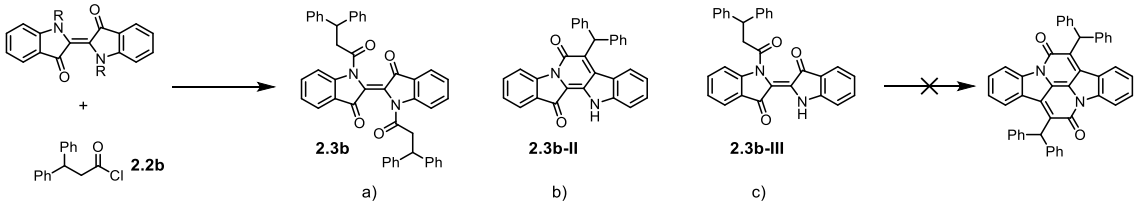

Figure 33: Reaction conditions for 3,3'-diphenylpropionyl *N*-substituted and *N,N'*-disubstituted indigo derivatives. (a) Indigo, DMF, pyridine (10 eq), 130 °C, 15 min, 90%; (b) Indigo, DMF, K_2CO_3 (2 eq), 130 °C, 15 min, 10%; (c) 2.3a, DMF, pyridine (10 eq), 130 °C, 2 h, 12%.

The synthesis of **2.3c** was attempted to see whether *ortho*-substitutents on the acyl chloride are tolerated during reaction with indigo and was used as a model compound for an *ortho*-substituted bay-annulated derivative. During the reaction of indigo with **2.2c** in DMF and pyridine, the desired product **2.3c** was obtained in a yield of 10%. Purity of the species was indicated by MS, but the ^{1}H NMR spectrum at room temperature showed extensive broadening of the signals (Figure 34). It is likely that the molecule aggregates over intermolecular interactions (*e.g.* π-interactions) which can be proven by VT-NMR-measurements.

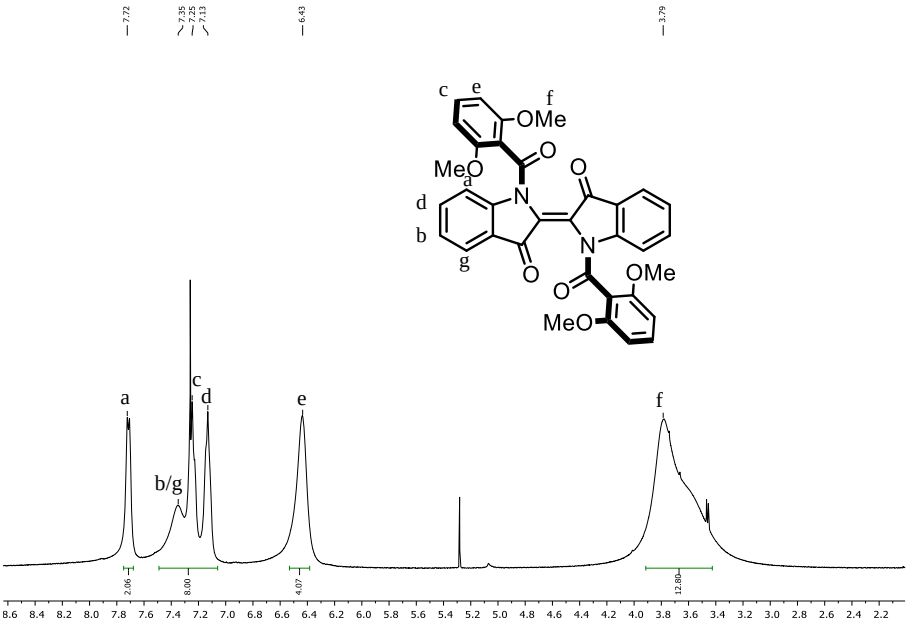

Figure 34: ^{1}H NMR spectrum (400.2 MHz, $CDCl_3$) of 2.3c at room temperature.

Increasing the temperature to 100 °C gave sharper signals either due to a large increase of the kinetic energy in the system, breaking up the aggregation (Figure 35). The sharpening of the signals can already be seen at 80 °C, but improves further by measuring at 100 °C.

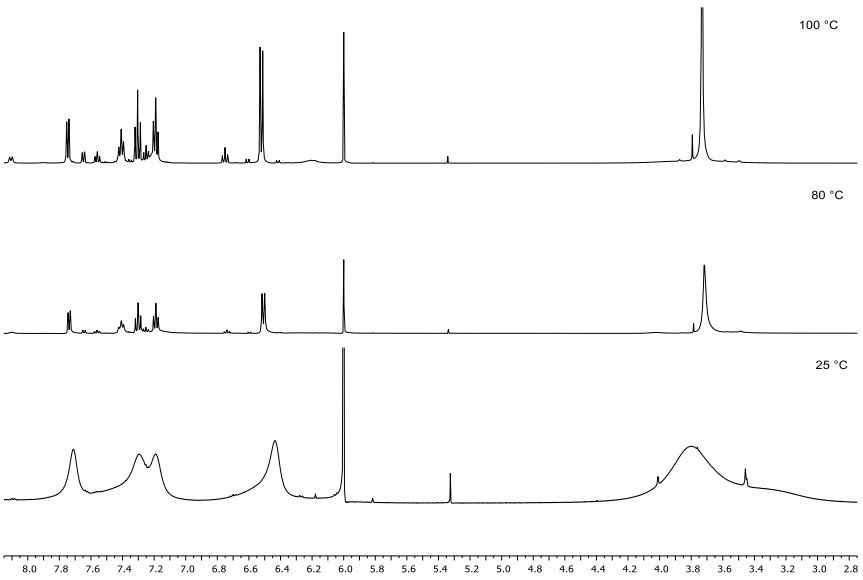

Figure 35: ^{1}H-NMR spectra (500.5 MHz, $C_2D_2Cl_4$) of 2.3c at different temperatures.

For the synthesis of an organic soluble bay-annulated indigo derivative **2.4d** and to investigate the reaction conditions known from the literature,[1],[2],[5] indigo was reacted

with 4-propylphenylacetic chloride (**2.2d**) in toluene to give the luminescent compound **2.4d**. Firstly, the known reaction conditions from de Melo *et al.*[17] to give **2.4d** in xylenes were performed, however, product formation was not observed after 30 h. It could be that the reaction took longer than 30 h to be successful. Nevertheless, the conditions were changed to a solvent with a lower boiling point, toluene, to prevent decomposition due to the high temperatures which appeared during the reaction in xylenes. After 30 h, TLC showed complete consumption of the starting material and the reaction was stopped. Column chromatography and crystallisation from CH_2Cl_2/MeOH yielded the desired product **2.4d** in 5%. In a later experiment, the reaction time was increased to 68 h yielding the bay-annulated dye **2.4d** in 30%. The solubility of indigo in common organic solvents, especially in m-xylene and toluene, is very poor. Introduction of mesityl groups in the 6,6'-positions improved the solubility in organic solvents. The preparation of this indigo derivative is described in Chapter 3. Under the same reaction conditions as for **2.4d**, we were able to prepare **2.4d-mes** in a yield of 18% (Figure 36), indicating that solubility is not the issue leading to low yields during product formation.

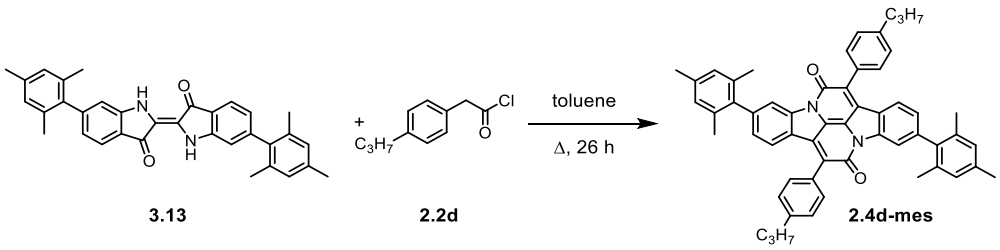

Figure 36: Synthesis of the bay annulated 6,6'-mesityl indigoid dye 2.4d-mes.

2.3 X-Ray Crystallography Analysis

From the synthesised indigoid dyes **2.3a**, **2.3b**, and **2.3c** crystals were obtained from CH_2Cl_2 by slow evaporation of the solvent and measured by Yaoyao Xiong. These were investigated to determine their structural parameters compared to unsubstituted indigo and how the conformational changes lead to alteration of the chemical properties (*e.g.* increased solubility in organic solvents compared to indigo) (Figure 37).[7],[18] The structure of **2.3a** was previously reported, but is shown here for comparison.[19] All parameters of the single crystals can be found in the Appendix (Table 6).

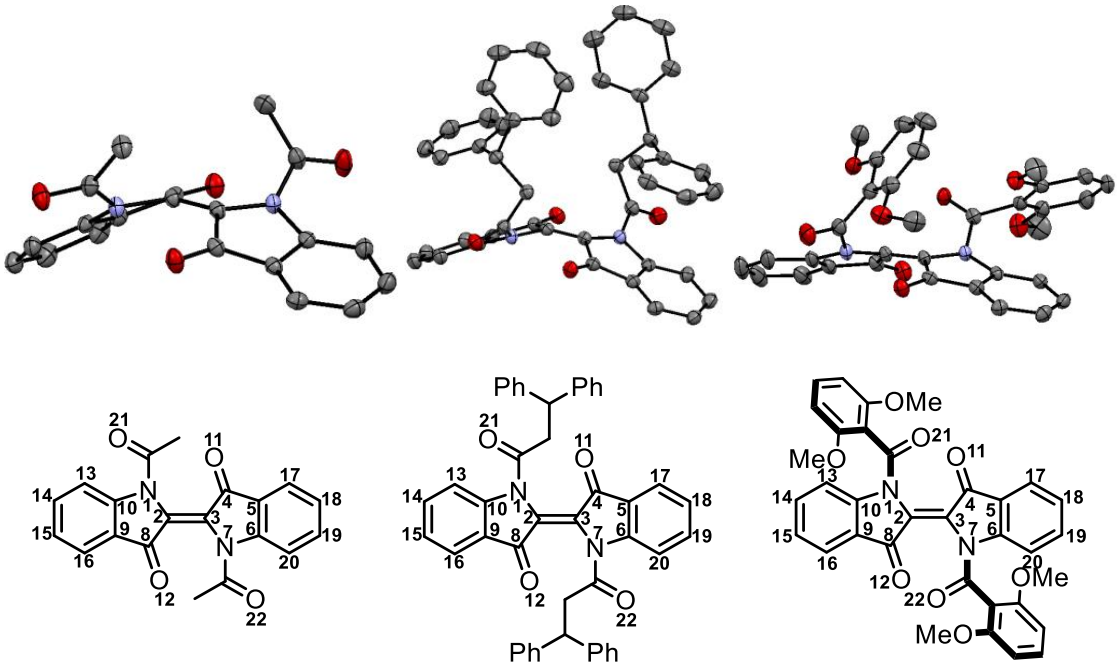

Figure 37: Three crystallised indigoid dyes 2.3a, 2.3b, and 2.3c (from left to right) and a general numbering scheme for the crystal structure analysis.

As seen in indigo,[20] derivatives **2.3a-c** crystallised in their *trans* conformation. In the solid state of indigo, inter- and intramolecular hydrogen bonds between the amine and carbonyl groups assure that the molecule is planar and allow for a high symmetry in the crystal lattice. The deviations in bond lengths and bond angles of indigo compared to the crystallised structures are negligible (<0.01 Å, <1°). However, the *N,N'*-substitution in the

derivatives **2.3a**, **2.3b**, and **2.3c** introduces a twist between the indoline planes. The analysis of torsion angles gives further information about the twist in **2.3a**, **2.3b**, and **2.3c** compared to indigo (Table 1). The carbonyl groups of the indigo main body and the *N,N'*-disubstituted derivatives would sterically clash if the structures were planar. Compound **2.3b** reveals an especially large degree of rotational freedom regarding the two phenyl groups which are bound via an acetylic moiety to indigo. In indigo, the N(1)-C(2)-C(3)-N(7) torsion angle of 180° is still similar for these structures with values ranging between 4°-12° deviation. However, looking at the torsion of the C(4)-C(3)-C(2)-C(8) angle, large differences with a deviation of 45° from the indigo angle of 180° can be observed. The twist is particularly strong for **2.3a** and **2.3b**. Compound **2.3c** with its dimethoxyphenyl groups is structurally more similar to indigo than **2.3a** and **2.3b**.

Table 1: Several torsion angles of the crystallised compounds 2.3a, 2.3b, 2.3c, and indigo

	Bond	**2.3a**	**2.3b**	**2.3c**	**Indigo**
Torsion Angles (°)	N(1)-C(2)-C(3)-N(7)	177	171	169	180
	C(4)-C(3)-C(2)-C(8)	42	144	136	180
	O(12)-C(2)-C(3)-O(11)	24	163	144	180
	C(14)-C(2)-C(3)-C(18)	35	8	143	167
	C(10)-C(2)-C(3)-C(6)	103	97	41	180
	C(14)-C(2)-C(3)-C(19)	69	62	77	180

More information about the angle between the indoline planes in each molecule was retrieved by simulating planes through each of the indoline units and measurement of the angle in between the planes (Table 2 and Figure 38). As expected, indigo is planar with an angle of 0°. Compound **2.3a** with the diacetyl groups reveals the largest

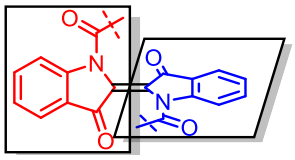

Figure 38: Illustration of the simulated planes in the indoline subunits.

deviation to indigo with a plane angle of 52°, whereas compounds **2.3b** and **2.3c** show angles of 38° and 46°, respectively.

Table 2: Angles between indoline planes of the crystallised compounds 2.3a, 2.3b, 2.3c, and indigo

	Planes	**2.3b**	**2.3c**	**2.3a**	**Indigo**
Plane Angles (°)	N(1)-C(2)-C(8)-C(9)-C(10)-C(13)-C(14)-C(15)-C(16)/ C(3)-C(4)-C(5)-C(6)-N(7)-C(17)-C(18)-C(19)-C(10)	46	38	52	0

The packing patterns of **2.3a**, **2.3b**, and **2.3c** are represented in Figure 39. **2.3a** does not show any π-π interaction inter- or intramolecularly in the crystal lattice. The only π interaction emerged between methyl-hydrogen atoms and the indoline unit with a distance of 2.87 Å being well within the range of H-π interactions.[21],[22] For the structures **2.3b** and **2.3c** on the other hand, π-π interactions are present. An attractive interaction in the form of π-stacking between the phenyl units and the indoline subunit with a distance of 3.93 Å is represented in **2.3b**. Additionally, some degree of long-range order appears between two 3,3'-diphenyl units with 5.39 Å. The intramolecular distance of 3.75 Å between the two indoline units indicates interaction within the crystal lattice. Molecule **2.3c** shows intermolecular π-π interactions between the dimethoxyphenyl and indoline subunits with a distance of 3.523 Å which contributes to the twisted crystal pattern. These interactions might also have an impact on the photophysical properties which are discussed in Section 2.4.

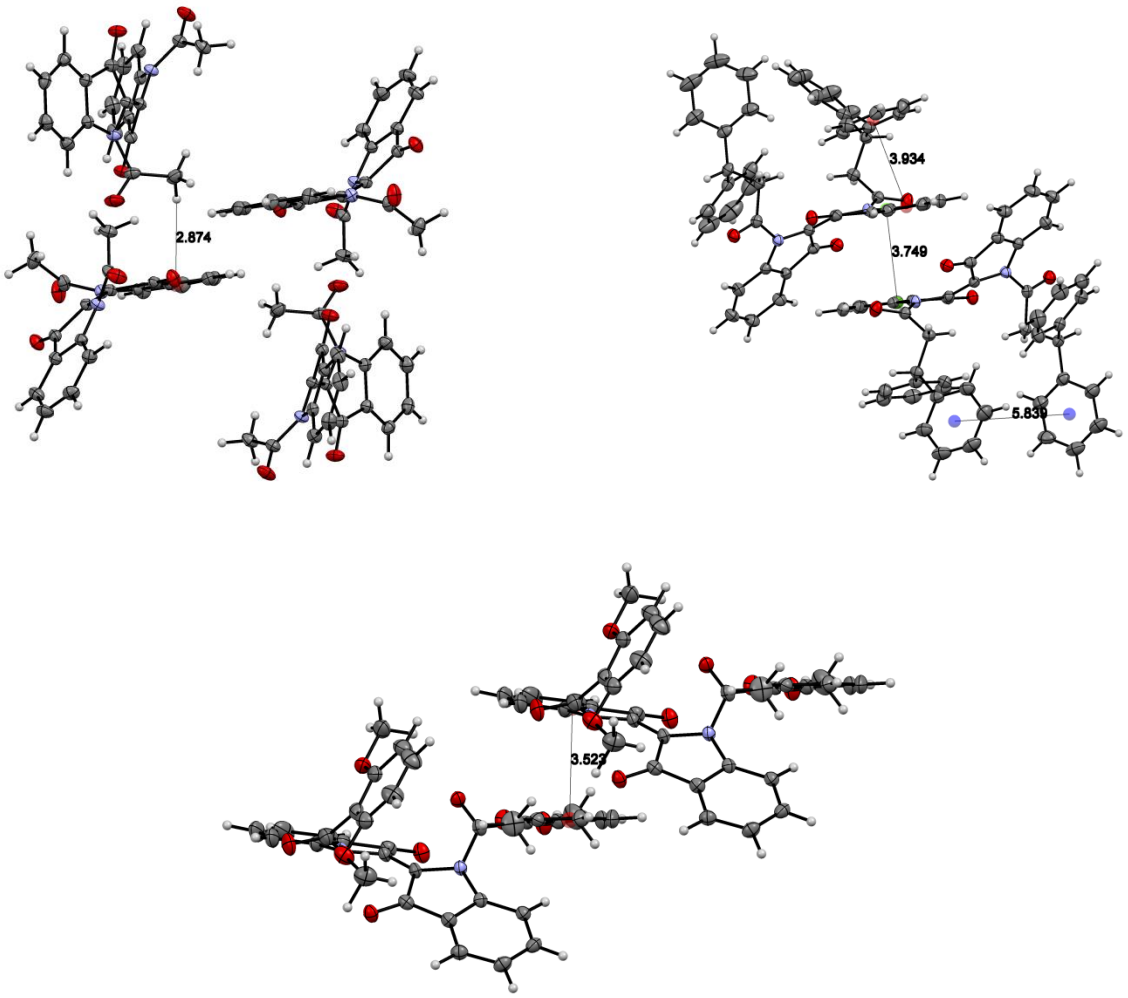

Figure 39: Packing patterns of 2.3a (top left), 2.3b (top right), and 2.3c (bottom). π-π interactions have been highlighted in the graphics.

2.4 Photophysical Properties

The photophysical properties of the compounds **2.3a**, **2.3b**, **2.3b-II**, **2.3c, 2.4d,** and **2.4d-mes** were investigated and are presented here. Unsubstituted indigo dissolved in DMF shows a broad absorption band at 610 nm (not shown).[17] The absorption spectra of the compounds are blue-shifted compared to indigo and the broad bands range from 561-619 nm. The methoxy-substituted derivative **2.3c** reveals the largest blue shift with an absorption maximum at 540 nm. Moreover, the spectra of substituted indigos exhibit sharper peaks and the presence of a blue-shifted shoulder due to their rigid structure. This can be observed especially for **2.3b-II** for which a more distinct shoulder appears.[23] Compound **2.3c** has the broadest spectrum with an emission maximum at 557 nm.

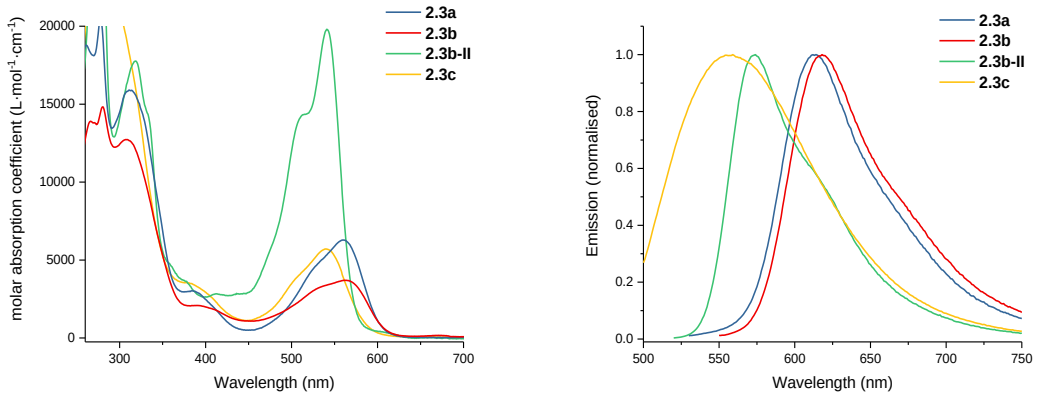

Figure 40: Absorption and normalised emission spectra of 2.3a, 2.3b, 2.3b-II, and 2.3c in CH_2Cl_2.

In Table 3, a summary of the data is presented. The fluorescence quantum yield of 0.1% for **2.3c** is probably caused by its distorted conformation. The emission spectra of **2.3a** and **2.3b** indicate shoulder formation at around 675 nm and give quantum yields of 4%. These values are not very high, but show a large increase compared to unsubstituted indigo (QY = 0.0023%).[17] The molar absorption coefficients for the materials are relatively low compared to the mono-bay-annulated derivative **2.3b-II** which revealed ε values of up to 20000 $L \cdot mol^{-1} \cdot cm^{-1}$. The brighter colour and the larger fluorescence quantum yield also

lead to a prolonged fluorescence lifetime of 7.20 ns for **2.3b-II**, compared to values of around 3 ns for the other derivatives **2.3a-c** with fluorescence quantum yields of 0.1-4%. In Figure 41 the fluorescence lifetimes are presented on a logarithmic scale showing the monoexponential decays. However, it is not clear why the lifetime of **2.3b-II** is so much longer compared to the other compounds. It indicates that non-radiative decays must be slower than the fluorescence leading to the high quantum yield.

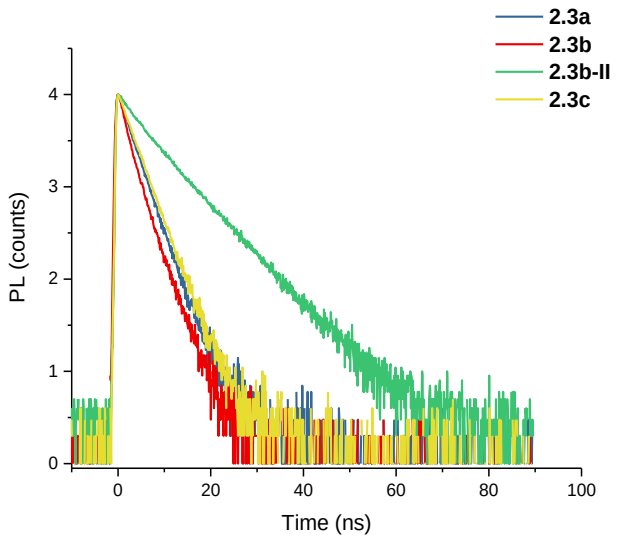

Figure 41: Fluorescence lifetime decays of 2.3a, 2.3b, 2.3b-II, and 2.3c in CH_2Cl_2.

Photophysical measurements of indigo in DMF showed a broad absorption spectrum with a maximum at 610 nm and an emission wavelength of 653 nm.[17] Our data show that disruption of the hydrogen bonds in indigo leads to a blue-shift in absorption and emission, as well as to an increase in fluorescence quantum yields, depending on the substituent. Extension of the π-system of the dye by bay-annulation improves the fluorescence properties by one order of magnitude due to an enhanced conjugation and rigidification of the system.[23].

Table 3: Absorption and emission parameters of 2.3a, 2.3b, 2.3b-II, and 2.3c in CH_2Cl_2.

Molecule	ε [L·mol^{-1}·cm^{-1}]	λ_{abs} [nm]	λ_{em} [nm]	Stokes shift [nm]	QY [%]	τ [ns]
2.3a	6282	561	614	53	4	2.93
2.3b	3700	563	619	56	4	2.15
2.3b-II	19807	541	573	32	43	7.20
2.3c	5712	540	557	17	0.1	3.00
2.4d	37015	545	565	20	93	4.45
2.4d-mes	20517	545	565	20	50	-

The photophysical properties of the bay-annulated indigo **2.4d** were investigated during a secondment at University College London in collaboration with the group of Franco Cacialli. The behaviour of the dye in solution and the solid state was tested to evaluate its potential use in OLEDs. Figure 42 shows the absorption (red curve) and emission (blue curve) spectra in solution (CH_2Cl_2) and the absorption in solid state (black curve). The absorption spectrum in solid state does not correspond to the structure of the solution spectrum. In the solid state, the absorption of the shoulders is increased indicating stacking between the monomers, revealing a hypsochromic shift as seen in H-aggregates.

A 1 mM solution of **2.4d** in toluene was used to spin-coat the material on glass plates (1 min at 1000 rpm). The slide was then baked on a hot plate at 60 °C for 5 min. Photophysical measurements of the sample revealed that films of the pure dye did not form, rather microcrystallisation on the glass plates occurred which made the measurement of absorption and emission spectra difficult. Blending the dye in different concentrations with a polymer material like F8BT (poly(9,9-dioctylfluorene-alt-benzothiadiazole) led to good films. 1 mM stock solutions of the dye **2.4d** and F8BT in toluene were mixed in different

ratios. The films were fabricated as described for pure **2.4d**. The emission spectra of these can be seen in Figure 42 (right). The black curve shows F8BT as a pure film. The addition of **2.4d** led to a red shift of the spectra and with increasing concentration a red shift to the NIR region can be observed. This results in lower fluorescence quantum yields compared to pure F8BT (Table 4); the dye quenches the fluorescence of F8BT which has a solid state fluorescence quantum yield of about 50% in pure films. To determine the fluorescence quantum yield of **2.4d**, rhodamine 101 was used as an external standard. The standard sample (rhodamine 101) has a fixed and known fluorescence quantum yield in the same region as the dye **2.4d**. The value of the quantum yield was consistent with the result recorded in the integrating sphere.

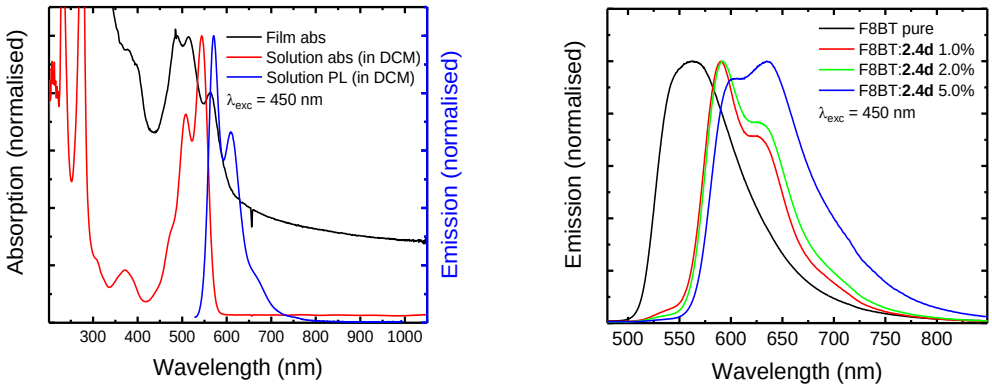

Figure 42: Absorption and emission spectra of the dye 2.4d in solution (CH_2Cl_2) as well as the absorption in solid state (black curve); the second graphic shows the emission of blends with the dye and F8BT in different concentrations

Table 4: PL efficiencies of 2.4d in solution and blends

Sample	Quantum Yield (%)
2.4d in $CHCl_3$ solution with an integrating sphere	93 ± 7
2.4d in CH_2Cl_2 solution vs. rhodamine 101	87
F8BT pure	50
F8BT:2.4d 1.0%	43
F8BT:2.4d 2.0%	36
F8BT:2.4d 5.0%	17

The fluorescence lifetimes of the dye **2.4d** in solution and in blends are shown in Table 5. The radiative decay of the dye **2.4d** in solution is mono exponential whereas the blends show two different τ-values in the host-guest measurements. The shortening of the lifetime is caused by quenching of the fluorescence of F8BT by **2.4d**. Also, depending on the amount of dye **2.4d** being present in the film, different contributions of each lifetime are shown. Another interesting outcome is the red-shifted emission spectrum in the 5% host-guest film which indicates intermolecular interactions between the host and guest molecules leading to a bathochromic shift, as seen in J-aggregates.

Table 5: τ-values of 2.4d in solution and blends.

	τ_1 [ns]	τ_2 [ns]	λ collection
2.4d in $CHCl_3$	4.45	-	570 nm
F8BT:2.4d 1.0%	2.50 (20 %)	5.29 (80 %)	600 nm
F8BT:2.4d 2.0%	2.50 (50 %)	5.29 (50 %)	600 nm

The photophysical properties of **2.4d-mes** were also obtained and are in the same range as the values for compound **2.4d**. The wavelengths for absorption and emission are the same; however, the presence of mesityl groups on the bay-annulated dye led to a decrease in fluorescence quantum yield in solution from 90% to 50% caused by these structural changes.

2.5 Conclusion

In conclusion, we were able to successfully synthesise three *N,N'*-substituted derivatives of indigo and fine-tune the reaction conditions for the bay-annulation.

The comparison of the crystal structures of some derivatives revealed the influence of *N,N'*-substitution on the indigo moiety. The missing inter- and intramolecular hydrogen bonds lead to a twist in the indoline sub units. Long-range ordering over hydrogen bonds and extended π-stacking is therefore prevented. Investigation of the packing patterns showed inter- and intramolecular long-range orders influencing the structural twisting of the molecules.

Acylation of indigo increased the fluorescence quantum yield from 0.5% up to 5% and blue-shifted signals in the absorption spectra in CH_2Cl_2. Mono-bay-annulation even gave a fluorescence quantum yield of 40% in solution. Furthermore, bis-bay-annulation of indigo revealed structures with optimised fluorescence quantum yields of up to 90% in solution. Solution processing of **2.4d** led to uneven film formation on the glass plates. Blended, homogenous films with F8BT were prepared and investigated, showing quenching of F8BT by the bay-annulated species, and therefore a reduction of the fluorescence quantum yields from 43 to 17% depending on the weight percentage (1.0-5.0%) of dye added to F8BT.

2.6 Experimental Details

General Procedures

All reagents were purchased from commercial sources and used as received. Solvents were bought from Honeywell, formerly Sigma Aldrich. Column chromatography was carried out using SiO_2 60 (particle size 40-63 μm, Merck, UK) as stationary phase. NMR spectra were acquired on a Bruker AVII400, AVIII400, or AVII500 instrument. ^{1}H NMR chemical shifts are reported in ppm and were referenced internally to residual protons in the solvent (δ = 7.26 for $CDCl_3$; 2.50 for DMSO). $^{13}C\{^{1}H\}$ NMR chemical shifts are reported in ppm and were referenced internally with respect to the solvent signal (δ = 77.2 for $CDCl_3$; 39.52 for DMSO). Standard abbreviations indicating multiplicity were used as follows: s = *singlet*, d = *doublet*, dd = *doublet* of *doublets*, t = *triplet*, q = *quartet*, m = *multiplet*, br = broad signal. High-resolution mass spectra (HRMS) were obtained on a Bruker μTOF instrument or a Waters GCT.

Stock solutions for the photophysical measurements of all compounds were prepared at concentrations in the range 0.3–2.2 mM and stored at –20 °C, and thawed before each experiment. Spectroscopic measurements were recorded in HPLC grade solvents. The UV-vis absorption spectra were recorded on a Perkin Elmer Lambda 20 spectrometer using quartz cuvettes from Starna (10 mm path length), and temperature was controlled by a PTP-1 Peltier unit from Perkin Elmer. For characterisation of photophysical and photochemical properties, the sample concentration was adjusted to have absorbance at the excitation wavelength below 0.1 to avoid the inner filter effect. The emission spectra were acquired on a FS5 fluorescence spectrophotometer (Edinburgh Instruments). OriginLab software was used for data analysis. The fluorescence lifetime was determined by time correlated single photon counting (TCSPC) using the FS5-TCSPC unit (Edinburgh Instruments) with

a picosecond pulsed diode laser (473.4 nm ± 0.5 nm). Once the time-resolved fluorescence decay and the instrumental response function were measured, a reconvolution fit analysis was carried out using the software Fluoracle (Edinburgh Instruments) by fitting in a mono-exponential function: Fit $= A + Be^{\left(-\frac{t}{\tau}\right)}$, where A is the calculated background, B is the calculated pre-exponential factor, and the goodness of fit is given as χ^2. The absolute fluorescence quantum yields were measured using a SC-30 integrating sphere module (Edinburgh Instruments) and the re-absorption effect was corrected when possible.

3,3-Diphenylpropionyl chloride **2.2b**

The synthesis of the target molecule has already been reported by Zhang *et al.*[24]

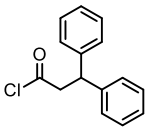

In a two-neck flask, 3,3-diphenylpropionic acid (3.12 g, 13.8 mmol) and $SOCl_2$ (16.4 g, 138 mmol) were heated to reflux for 2 h. The remaining $SOCl_2$ was removed in vacuo and the product **2.2b** dried under high vacuum for 2 h yielding a yellow oil in quantitative yield. The compound was used without further purification or characterisation.

4-Propylphenylacetic chloride **2.4b**

The reaction conditions for the formation of **2.2b** reported by Zhang *et al.* have been adapted for the synthesis of **2.4b**.[24]

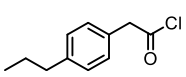

4-Propylphenylacetic acid (2.50 g, 14.0 mmol) and thionyl chloride (10.0 mL, 137 mmol) were heated for 2 h under argon. After cooling of the mixture and evaporation of the remaining $SOCl_2$, **2.4** was dried under high vacuum for 2 h yielding a yellow oil in quantitative yield. The compound was used without further purification or characterisation.

N,N'-Diacetyl indigo **2.3a**

The synthesis of the target molecule has already been reported by Kolczkowski *et al.*[5]

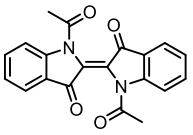

In a two-neck flask, indigo (1.31 g, 5.00 mmol, 1 eq.) and acetyl chloride (1.78 mL, 25.0 mmol, 5 eq.) were dissolved in acetic anhydride (20 mL) and heated to reflux overnight. The mixture was concentrated in vacuo and the product precipitated from Et_2O/hexanes (1:2) yielding **2.3a** as a red solid (1.21 g, 3.49 mmol, 70%).

^{1}H NMR ($CDCl_3$, 400.2 MHz): δ 8.26 (m, 2H), 7.78 (ddd, *J* = 8.5, 7.3, 1.4 Hz, 2H), 7.66 (ddd, *J* = 8.5, 7.3, 1.4 Hz, 2H), 7.27 (m, 2H), 2.56 (s, 6H). ^{13}C NMR (100.1 MHz, $CDCl_3$): δ 184.3, 170.2, 149.3, 137.0, 126.4, 125.4, 124.5, 122.0, 117.4, 24.1. MS (ESI +ve in methanol) *m/z*: 369.0 ($[M+Na]^+$, $C_{20}H_{14}N_2O_4$ requires 369.34)

N,N'-Bis(3,3-diphenylpropionyl) indigo **2.3b**

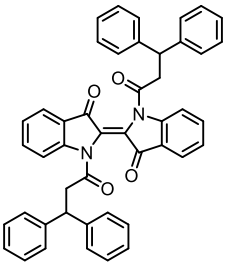

In a two-neck flask, indigo (360 mg, 1.37 mmol, 1 eq.) and pyridine (1.14 mL, 14.2 mmol, 10 eq.) were diluted in dry DMF (10 mL) and heated for 2 h to 130 °C to dissolve indigo. 3,3-Diphenylpropionyl chloride **2.2b** (2.32 g, 9.48 mmol, 7 eq.) was added and the suspension heated for 15 min until the starting material was consumed as observed by TLC. After cooling, the mixture was diluted with EtOAc (250 mL) and the mixture washed with water (4 × 100 mL). The organic phase was dried over Na_2SO_4. After evaporation of the solvent the solid was redissolved in CH_2Cl_2 and methanol was added to crystallise the product in the freezer overnight (447 mg). The remaining solution was evaporated and separated via column chromatography (EtOAc 3:7 PE; 386 mg) yielding **2.3b** in the same purity as from crystallisaton. The products were combined and gave **2.3b** in form of a purple powder (833 mg, 1.23 mmol, 90%).

^{1}H NMR ($CDCl_3$, 400.2 MHz): δ 7.87 (d, *J* = 8.4 Hz, 2H), 7.57 (ddd, *J* = 8.4, 7.3, 1.4 Hz, 2H), 7.44 (ddd, *J* = 8.4, 7.3, 1.4 Hz, 2H), 7.12 (dd, *J* = 7.5, 0.9 Hz, 2H), 7.03 (m, 20H), 4.74 (t, *J* = 8.4 Hz, 2H), 3.57 (d, *J* = 8.1 Hz, 4H). ^{13}C NMR ($CDCl_3$, 100.6 MHz): δ 184.6, 172.5, 149.4, 136.78, 128.5, 127.8, 126.8, 125.6, 124.8, 124.0, 120.9, 116.6, 100.1, 49.1, 43.4. MS (ESI +ve in methanol) *m*/*z*: 701.4 ($[M+Na]^+$, $C_{46}H_{34}N_2O_4Na$ requires 701.79).

7-Benzhydryl-6H-pyrido[1,2-a:3,4-b']diindole-6,13(12H)-dione **2.3b-II**

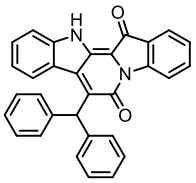

In a two-neck flask, indigo (360 mg, 1.37 mmol, 1 eq.) and K_2CO_3 (1.97 g, 14.2 mmol, 10 eq.) were dissolved in dry DMF (10 mL) and heated to 130 °C until indigo was mostly dissolved. 3,3-Diphenylpropionyl chloride **2.2b** (3.00 mL, 14.22 mmol, 10 eq.) was added and the mixture was allowed to cool to 20 °C over 30 mins. EtOAc (250 mL) was added to the solution and the mixture washed with water (2 × 200 mL). The organic phase was dried over Na_2SO_4. After evaporation of the solvent, the solid was diluted in CH_2Cl_2 and methanol was added to crystallise the product **2.3b-II** in the freezer overnight in form of a red crystalline material (87.0 mg, 0.19 mmol, 14%).

^{1}H NMR (DMSO-d_6, 400.2 MHz): δ 11.79 (br, 1H, NH), 8.51 (d, *J* = 8.2 Hz, 1H), 7.81 (d, *J* = 7.8 Hz, 2H), 7.67 (dd, *J* = 9.9, 7.8 Hz, 4H), 7.43–7.23 (m, 12H), 6.94 (t, *J* = 7.8 Hz, 1H), 6.51 (s, 1H). ^{13}C NMR ($CDCl_3$, DMSO-d_6): δ 179.9, 156.6, 147.6, 145.9, 140.9, 138.9, 137.7, 135.4, 131.5, 129.3, 128.8, 128.3, 126.5, 126.3, 126.2, 125.0, 123.6, 120.9, 119.4, 117.8, 114.4, 112.4, 49.0. MS (ESI +ve in methanol) *m*/*z*: = 453.16 ($C_{31}H_{11}N_2O_2$, requires 453.16)

N-3,3-Diphenylpropionyl indigo **2.6-monosubstituted**

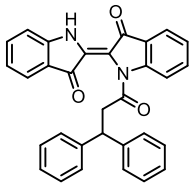

In a two-neck flask, diacetylindigo **2.3a** (474 mg, 1.37 mmol, 1 eq.) and pyridine (1.14 mL, 14.2 mmol, 10 eq.) were dissolved in dry DMF (10 mL) and heated for 2 h to reflux. 3,3-Diphenylpropionyl chloride **2.2b** (1.50 mL, 7.11 mmol, 5 eq.) was added and the suspension heated for 15 min until the starting material was consumed as observed by TLC. EtOAc (500 mL) was added to the solution and the mixture washed with water (5 × 100 mL). The organic phase was dried over Na_2SO_4 and concentrated. The mixture was separated via column chromatography (PE 7:3 EtOAc) yielding the main compound **2.3b-III** as a purple powder (75 mg, 0.16 mmol, 12%).

^{1}H NMR ($CDCl_3$, 400.2 MHz): δ 8.36 (br, 1H, NH), 8.19 (m, 1H), 8.02 (d, *J* = 8.1 Hz, 1H), 7.75 (d, *J* = 7.4 Hz, 1H), 7.66 (d, *J* = 7.4 Hz, 1H), 7.58 (d, *J* = 7.4 Hz, 1H), 7.51 (t, *J* = 8.1 Hz, 1H), 7.21–7.08 (m, 13H), 4.69 (t, *J* = 7.8 Hz, 1H), 3.53 (s, 2H). ^{13}C NMR ($CDCl_3$, 100.6 MHz): δ 137.0, 136.6, 128.6, 127.8, 126.8, 125.2, 124.9, 124.5, 124.1, 121.2, 116.8, 49.4, 42.6. MS (ESI +ve in methanol) *m/z*: 471.2 ($[M+H]^+$, $C_{31}H_{23}N_2O_3$ requires 471.53)

N,N'-Bis(dimethoxybenzoyl) indigo **2.3c**

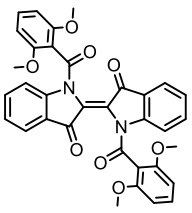

In a two-neck flask, indigo (360 mg, 1.37 mmol, 1 eq.) and pyridine (2.00 mL, 24.9 mmol, 20 eq.) were dissolved in dry DMF (10 mL) and heated for 2 h to reflux. 2,6-Dimethoxybenzoyl chloride **2.3b** (2.50 g, 12.5 mmol, 10 eq.) was added and the suspension heated to reflux for about 20 min until the starting material was consumed as observed by TLC. EtOAc (250 mL) was added to the solution and the mixture extracted with water (4×100 mL). The organic phase was dried over Na_2SO_4 and concentrated. The product was separated via column chromatography (PE

1:1 CH_2Cl_2) and further recrystallised from CH_2Cl_2 and methanol yielding pure compound **2.3c** as a red solid (76.0 mg, 0.13 mmol, 10%).

^{1}H NMR ($CDCl_3$, 400.2 MHz): δ 7.72 (m, 2H), 7.35 (m, 2H), 7.26 (m, 2H), 7.14 (m, 2H, Ind-H), 6.44 (m, 4H), 3.80 (s, 12H). ^{13}C NMR ($CDCl_3$, 100.1 MHz): δ 158.3, 149.6, 135.1, 132.1, 124.5, 123.7, 116.6, 103.9, 56.2. MS (ESI +ve in methanol) *m*/*z*: 613.2 ($[M+Na]^+$, $C_{34}H_{26}N_2O_8Na$ requires 613.59)

7,14-Bis(4-propylphenyl)diindolo[3,2,1-de:3',2',1'-ij][1,5]naphthyridine-6,13-dione **2.4d**

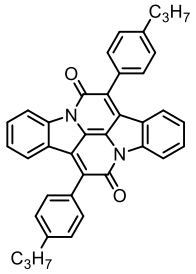

In dry m-xylene (10 mL), indigo (360 mg, 1.37 mmol) and 4-propylphenylacetylchloride **2.4b** (2.70 g, 13.4 mmol) were heated for 30 h under reflux. After cooling down the mixture was separated via column chromatography in CH_2Cl_2 (R_f = 0.5) yielding the desired product in a crude yield of 65% (450 mg). The crude product was then precipitated from CH_2Cl_2 with MeOH and put in the freezer overnight yielding **2.4d** as a red solid (241 mg, 439 µmol, 32%).

^{1}H NMR (400 MHz, $CDCl_3$): δ 8.49 (dt, *J* = 8.1, 0.9 Hz, 2H), 7.64 (m, 6H), 7.55 (m, 2H), 7.40 (m, 4H), 7.22 (td, *J* = 7.7, 1.1 Hz, 2H), 2.72 (dd, *J* = 8.1, 7.7 Hz, 4H), 1.75 (m, 4H), 1.03 (t, *J* = 7.7 Hz, 6H). ^{13}C NMR (100 MHz, $CDCl_3$) δ 184.6, 159.8, 144.8, 144.2, 132.1, 131.9, 130.9, 130.2, 128.8, 126.1, 126.0, 125.8, 122.2, 117.7, 38.3, 24.6, 14.1. MS (MALDI, TOF LD+) m/z: 564.23 (100.0%), 547.23 (41.1%), 548.24 (8.2%); found: 547.06). UV/Vis (CH_2Cl_2): λ_{max}^{abs} = 545 (37015), 509 (26586), 476 nm; λ_{max}^{em} (excitation λ = 509 nm): 565, 602 nm.

3,10-Dimesityl-7,14-bis(4-propylphenyl)diindolo[3,2,1-de:3',2',1'-ij][1,5]naphthyridine-6,13-dione **2.4d-mes**

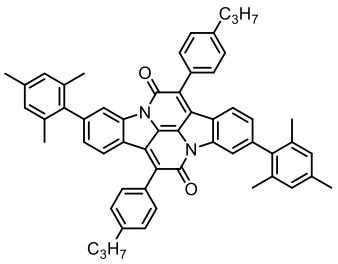

6,6'-Bismesityl indigo **3.13** (150 mg, 0.30 mmol, 1 eq) and 4-*n*-propylphenylacetyl chloride **2.4b** (355 mg, 1.80 mmol, 6 eq) were heated to reflux in toluene (4 mL) for 68 h until the starting material was consumed as observed by TLC. The solvent was evaporated and the product separated by column chromatography (PE/ CH_2Cl_2 1:1, R_f = 0.3). The product was recrystallised from a CH_2Cl_2/MeOH mixture yielding the desired product **2.4d-mes** as a red solid (42.9 mg, 0.05 mmol, 18%).

^{1}H NMR ($CDCl_3$, 400.2 MHz): δ 8.36 (m, 2H), 7.71 (m, 2H), 7.67 (m, 4H), 7.40 (m, 4H), 7.03 (m, 2H), 6.93 (s, 4H), 2.71 (m, 4H), 2.23 (s, 6H), 2.04 (s, 12H), 1.73 (m, 4H), 1.01 (m, 6H). ^{13}C NMR ($CDCl_3$, 100.1 MHz): 135.6, 130.2, 128.7, 128.4, 127.5, 125.5, 118.9, 38.2, 24.6, 21.2, 20.9, 14.1. MS (MALDI, TOF LD+) m/z: 782.39 (100.0%), 783.39 (60.6%), 784.39 (18.0%), 785.40 (2.7%), found: 785.71) UV/Vis (CH_2Cl_2): λ_{max}^{abs} = 545 (20517), 509 (14736), 476 nm; λ_{max}^{em} (excitation λ = 509 nm): 565, 602 nm.

2.7 Appendix

Table 6: Crystal structure parameters of 2.3a, 2.3b, and 2.3c.

	2.3a	**2.3b**	**2.3c**
Empirical Formula	$C_{20}H_{14}N_2O_4$	$C_{46}H_{34}N_2O_4$	$C_{34}H_{26}N_2O_8$
Molecular Mass (g × mol^{-1})	346.34	678.79	590.59
Measurement Temperature [K]	150	150	150
Wavelength [Å]	1.54184	1.54184	1.54184
Crystal System	monoclinic	triclinic	triclinic
Space Group	$P2_1/n$	*P*-1	*P*-1
***a, b, c*[Å]**	13.5452(6), 8.4837(2), 14.7018(6)	12.9586(5), 15.6318(2), 18.0759(3)	9.2021(5), 9.2546(5), 17.6083(8)
***α, β, γ*[°]**	90, 112.359(5), 90	100.4943(6), 93.5769(6), 107.1674(7)	84.680(4), 80.201(4), 71.563(5)
V[Å^3]	1562.42(6)	3413.52(9)	1400.62(13)
Z	2	4	2
d_{cal}[g×cm^3]	1.472	1.321	1.400
F(000)	720	1424	616
Crystal Size [mm^3]	-	0.280×0.400×0.500	0.050×0.130×0.210
θ[°]	3.781 to 76.261	5.123 to 27.550	5.042 to 76.340
h, k, l	-14 to 16, -10 to 10, -18 to 18	-16 to16, -20 to 20, -23 to 23	-11 to 11, -11 to 11, -22 to 22
Measured reflexes	9739	29800	28068
Independent reflexes	3229	15578	5872

R_{int}	0.015	0.036	0.044
Absorption Correction	multi-scan	multi-scan	multi-scan
Structure Solving	Full-matrix least-squares on F^2	Full-matrix least-squares on F^2	Full-matrix least-squares on F^2
Refined Parameters	235	973	398
***R* (I≥2σ(I))**	R=0.0356; wR_2=0.0863	R=0.0560; wR_2=0.0967	R=0.0813; wR_2=0.2538
***R* (all data)**	R=0.0356; wR_2=0.0863	R=0.0990; wR_2=0.1288	R=0.0871; wR_2=0.2571
GooF on F^2	0.9981	0.5021	1.0136
Rest Electron Density [e×Å^{-3}]	-0.23, 0.25	-0.48, 0.49	-0.42, 2.08

2.8 References

[1] Engi, G. *Zeitschrift für Angew. Chem.* **1914**, *27*, 144–148.

[2] Haucke, G.; Paetzold, R. *J. für Prakt. Chemie* **1979**, *917*, 978–986.

[3] He, B.; Pun, A. B.; Zherebetskyy, D.; Liu, Y.; Liu, F.; Klivansky, L. M.; McGough, A. M.; Zhang, B. A.; Lo, K.; Russell, T. P.; Wang, L.; Liu, Y. *J. Am. Chem. Soc.* **2014**, *136*, 15093–15101.

[4] Fallon, K. J.; Wijeyasinghe, N.; Yaacobi-Gross, N.; Ashraf, R. S.; Freeman, D. M. E.; Palgrave, R. G.; Al-Hashimi, M.; Marks, T. J.; McCulloch, I.; Anthopoulos, T. D.; Bronstein, H. *Macromolecules* **2015**, *48*, 5148–5154.

[5] Kolaczkowski, M. A.; He, B.; Liu, Y. *Org. Lett.* **2016**, *18*, 5224–5227.

[6] Głowacki, E. D.; Voss, G.; Demirak, K.; Havlicek, M.; Sünger, N.; Okur, A. C.; Monkowius, U.; Gąsiorowski, J.; Leonat, L.; Sariciftci, N. S. *Chem. Commun.* **2013**, *49*, 6063–6065.

[7] Porada, J. H.; Neudörfl, J.-M.; Blunk, D. *New J. Chem.* **2015**, *39*, 8291–8301.

[8] Huang, C.-Y.; Bonasera, A.; Hristov, L.; Garmshausen, Y.; Schmidt, B. M.; Jacquemin, D.; Hecht, S. *J. Am. Chem. Soc.* **2017**, *139*, 15205–15211.

[9] Helferich, B.; Schaefer, W. *Org. Synth.* **1929**, *9*, 32.

[10] Allen, C. F. H.; Barker, W. E. *Org. Synth.* **1932**, *12*, 16.

[11] Adams, R. *Org. Synth.* **1923**, *3*, 75.

[12] Clayden, J.; Greeves, N.; Warren, S. *Organic Chemistry*; OUP Oxford, 2012.

[13] Chaudhary, S.; Naikade, N. K.; Tiwari, M. K.; Yadav, L.; Shyamlal, B. R. K.; Puri,

S. K. *Bioorg. Med. Chem. Lett.* **2016**, *26*, 1536–1541.

[14] Omote, Y.; Fujiki, K.; Awano, H.; Kubota, I.; Nishio, T.; Aoyama, H. *Bull. Chem. Soc. Jpn.* **1981**, *54*, 627–628.

[15] Posner, T. *Berichte der Dtsch. Chem. Gesellschaft (A B Ser.* **1926**, *59*, 1799–1827.

[16] He, B.; Pun, A. B.; Zherebetskyy, D.; Liu, Y.; Liu, F.; Klivansky, L. M.; McGough, A. M.; Zhang, B. A.; Lo, K.; Russell, T. P.; Wang, L.; Liu, Y. *J. Am. Chem. Soc.* **2014**, *136*, 15093–15101.

[17] Seixas de Melo, J.; Rondão, R.; Burrows, H. D.; Melo, M. J.; Navaratnam, S.; Edge, R.; Voss, G. *J. Phys. Chem. A* **2006**, *110*, 13653–13661.

[18] Abe, J.; Nagasawa, Y.; Takahashi, H. *J. Chem. Phys.* **1989**, *91*, 3431–3434.

[19] Grimme, G.; Boldt, P.; Grimme, S.; Jones, P. G. *Chem. Ber.* **1993**, *126*, 1015–1021.

[20] Kettner, F.; Hüter, L.; Schäfer, J.; Röder, K.; Purgahn, U.; Krautscheid, H. *Acta Crystallogr. Sect. E Struct. Reports Online* **2011**, *67*, o2867–o2867.

[21] Donnay, J. D. H.; Donnay, G. *J. Appl. Crystallogr.* **1970**, *3*, 423–423.

[22] Nishio, M. *CrystEngComm* **2004**, *6*, 130.

[23] Lakowicz, J. R. *Principles of Fluorescence Spectroscopy*; Lakowicz, J. R., Ed.; Springer US: Boston, MA, 2006.

[24] Zhang, W.; Haskins, C. W.; Yang, Y.; Dai, M. *Org. Biomol. Chem.* **2014**, *12*, 9109–9112.

3

Bay-Annulation and Self-Encapsulation of Indigo

3.1 Introduction

The bay-annulation of indigo, as described in Chapter 2, is a way to extend the indigo chromophore while maintaining planarity. The first reported derivative is *Cibalackrot*, for which indigo reacted with phenylacetyl chloride yielding a red fluorescent solid (Figure 43) which exhibited high fluorescence quantum yields in cyclohexane of 90%.[1],[2]

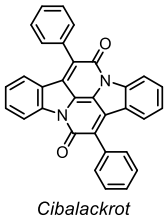

Cibalackrot

Figure 43: Molecular structure of *Cibalackrot*.

The properties of *Cibalackrot* were further investigated by Paetzold *et al.* in 1979.[3] The synthetic strategy for the bay-annulation has since been used by the groups of Bronstein, Liu, Voss, and Kolaczkowski to prepare different derivatives.[4]–[8] Mostly thienyl groups or *para*-substituted phenylacetyl chlorides were attached to indigo, yielding the bay-annulated species. Also, bay-annulated indigos synthesised over two steps with different acid chlorides are known,[7] but until now there have been no reports of dyes synthesised using *ortho*-substituted phenyl groups on the bay-annulated dye.

Many molecules with strong fluorescence in solution are known, but they often show a large decrease in their solid state fluorescence in which non-radiative decays like quenching of the fluorescent state are promoted due to intermolecular interactions (*e.g.* π-stacking). To prevent this long-range ordering, encapsulation of the molecules can be performed, separating the molecules from their surroundings, leading to increased fluorescence in the solid state.[9]–[11] For the example models from the literature **Thi$_2$**, **Ph**, and **DPP** a strong enhancement of their photophysical properties was shown (Figure 44). We therefore

proposed the synthesis of the bay-annulated derivative **3.1**. In this chapter, the synthetic pathway and the properties of a self-encapsulated, bay-annulated indigo are described, revealing quantum yields in solution and solid state of 45% and 25%, respectively.

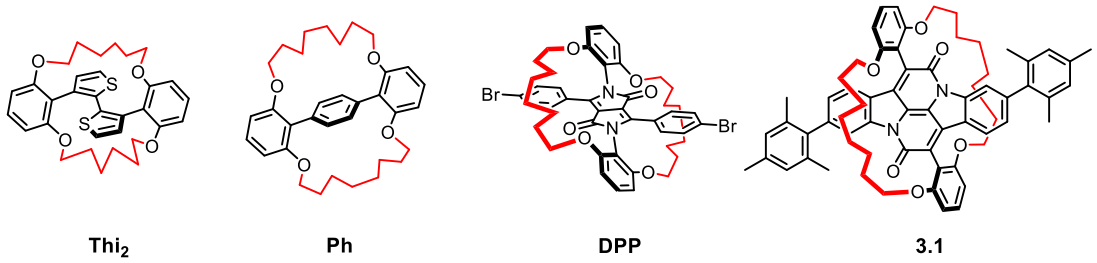

Figure 44: Known examples for the self-encapsulation of bis-thienyl (Thi_2), phenyl (Ph), and diketopyrrolopyrrol (DPP) derivatives, and the synthesised bay-annulated compound 3.1.[9]–[11]

3.2 Synthesis

3.2.1 Synthesis of Acid Chlorides

For the self-encapsulation of the bay-annulated indigo, we decided to follow the synthetic strategy shown by Sugiyasu and Bronstein *et al.*[9]–[11] The introduction of *ortho*-methoxy substituents on the core is crucial. Subsequent demethylation of these allows the introduction of long linkers which are able to covalently bind by wrapping around the molecule. Hence, the synthesis of the *ortho*-substituted methoxy- and alkoxy-derivatives was started from 1,3-dihmethoxybenzene derivatives or 1,3-dihydroxybenzene. In case of the dimethoxy derivative, different reaction conditions were tested. 2,6-Dimethoxybenzoic acid is commercially available, and homologation was required.

For the addition of a CH_2-group, we attempted to use TMS-substituted diazomethane to insert the methyl group between the phenyl and carbonyl moiety by an Arndt-Eistert reaction.[12] However, no product formation was visible by ^{1}H-NMR spectroscopy, which showed the hydrolysed starting material. Instead, we decided to pursue with a synthetic strategy which did not require the use of explosive compounds. Adaption of the reaction

conditions from Oestreich *et al*.,[13] gave the desired compound in an overall yield of 80% in three steps (Scheme 1).

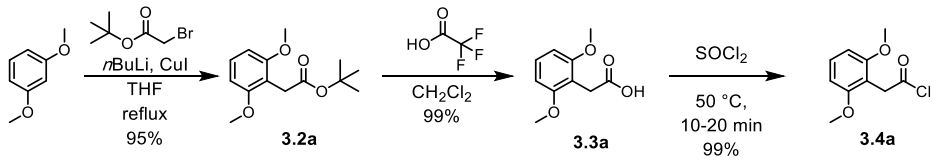

Scheme 1: Synthetic strategy for the formation of 2-(2,6-dimethoxyphenyl)acetyl chloride 3.3.

Chelation-promoted lithiation of 1,3-dimethoxybenzene at the 2-position[14],[15] was followed by addition of CuI to form the cuprate.[16] Cuprate formation softened the nucleophilic character and activated the C-Br bond leading to the desired species **3.2a**. Deprotection of *tert*-butyl ester **3.2a** with trifluoroacetic acid was straightforward and gave 2-(2,6-dimethoxyphenyl)acetic acid (**3.3a**) in quantitative yield. Using $SOCl_2$ in large excess at high temperatures (reflux at 80 °C) in the following reaction led to unexpected side product formation and mostly chlorination of the 2,6-methoxyphenyl moiety in the 3-position. To prevent chlorination of the phenyl moiety and to achieve clean product formation, the starting material was heated to no more than 50 °C for 10–20 mins to give 2-(2,6-dimethoxyphenyl)acetyl chloride (**3.4a**).

Under the same conditions as for **3.2-3.4a**, derivatives with alkoxy chains were synthesised. These were needed for the bay-annulation and encapsulation reaction of indigo. In Scheme 2, the general reaction pathway for the acid chloride formation is shown. It includes alkylation of 1,3-dihydroxybenzene derivatives, followed by lithiation, cuprate formation, and building of the *tert*-butyl acetate. Deprotection and conversion to the acid chloride then leads to the desired compounds (Scheme 2).

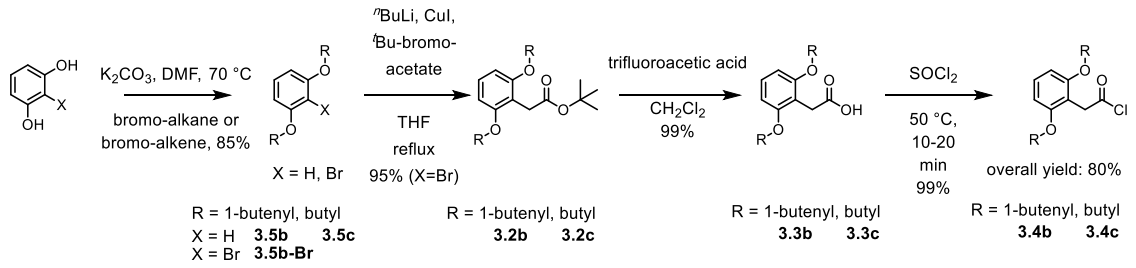

Scheme 2: Synthetic strategy for the synthesis of dialkoxyphenylacetyl and dialkenoxyphenylacetyl chlorides.

For the preparation of **3.5b**, 1,3-dihydroxybenzene was dissolved in DMF and heated with K_2CO_3.[17] Addition of 4-bromo-1-butene gave the alkenylated species **3.5b** in a yield of 40% with mono-substituted 1,3-dihydroxybenzene as the only side product. Increase of the amount of base and 4-bromo-1-butene to 15 eq. yielded the same mono- and bissubstitution ratio which could be separated by column chromatography. Further on, 1,3-bis(but-3-en-1-loxy)benzene (**3.5b**) underwent lithiation followed by cuprate formation unsuccessfully. Treatment of **3.5b** with *n*BuLi followed by DMF led to an introduction of an aldehyde in the 2-position in a yield of 30% indicating that the lithiation reaction was not completed. To improve the lithiation reaction, alkylated 1-bromo-2,6-dihydroxybenzene **3.5b-Br** was prepared. Hence, 1-bromo-2,6-dihydroxybenzene was substituted with 4-bromo-1-butene, yielding **3.5b-Br** in 85% yield. Lithiation followed by treatment with CuI and *tert*butyl bromoacetate was successful with a yield of 95% for **3.2b**. These successful conditions for the lithiation were applied to prepare **3.5c** by alkylation of 1-bromo-2,6-dihydroxybenzene leading to product formation in 90% yield. Treatment with *n*BuLi, CuI, and *tert*butylbromo actetate gave pure product **3.2c** in 50% yield.

Esters **3.2b** and **3.2c** were deprotected with trifluoroacetic acid, giving the carboxylic acids **3.3b** and **3.3c** quantitatively. Treatment with $SOCl_2$ gave the respective acid chlorides (**3.4b** and **3.4c**). These were subsequently used for the bay-annulation of indigo.

3.2.2 Synthesis of 6,6'-Bismesityl-Indigo

To increase the solubility of indigo, mesityl groups were attached to the 6 and 6' positions. The synthesis of 6,6'-substituted indigo **3.7** was performed over two steps (Figure 45). The mesityl groups were introduced in a Suzuki coupling reaction between mesityl-boronic acid and 4-bromo-2-nitrobenzaldehyde giving **3.6** in a yield of 65%.[18]

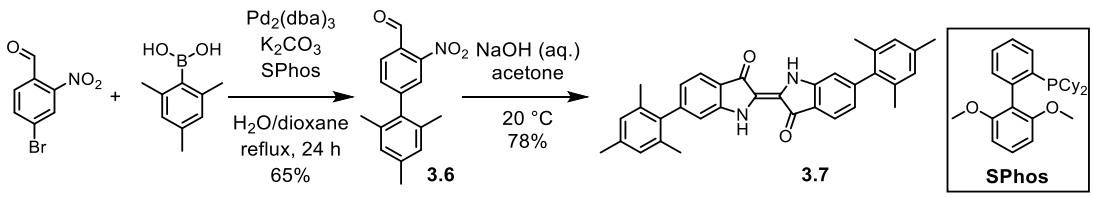

Figure 45: Synthetic strategy for the formation of 6,6'-bismesityl indigo (3.7)

The Suzuki coupling reaction was first tested with $Pd(PPh_3)_4$ as catalyst, Cs_2CO_3 as base, and a mixture of toluene, ethanol, and water as solvents. The reaction mixture was heated to 100 °C for 24 h, however, only homo-coupled nitro compound appeared in the ESI-MS spectrum. The reaction conditions for the Suzuki coupling were adapted, and instead of $Pd(PPh_3)_4$, $Pd_2(dba)_3$ was used. Addition of 2-dicyclohexylphosphino-2′,6′-dimethoxybiphenyl (**SPhos**), a phosphine ligand known to increase the activity of palladium complexes during Suzuki coupling reactions,[18] a change of base to K_2CO_3, and a solvent mixture of dioxane and water successfully gave product in a yield of up to 65%.

For the indigo formation, nitro-aldehyde **3.7** was dissolved in acetone and treated with aqueous NaOH. The reaction is known as the Baeyer-Drewson indigo synthesis and its mechanism is shown in Figure 46.[19] The reaction was followed by colour changes of the solution and after 12 h up to 78% yield was achieved. To remove side products, the dye was recrystallised from CH_2Cl_2 using petrol ether as a counter-solvent. Fine blue needles precipitated and their purity was verified by NMR spectroscopy.

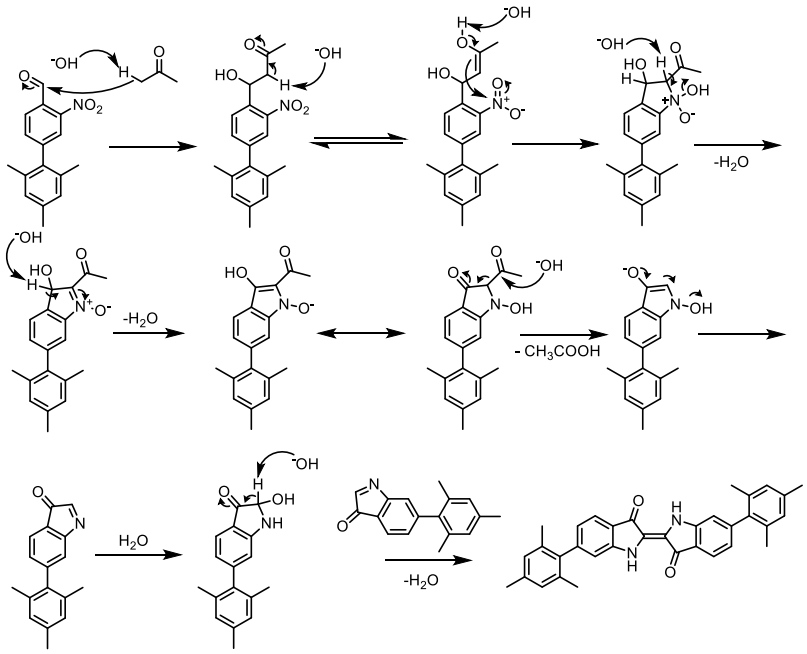

Figure 46: Reaction mechanism for the 6,6'-bismesityl indigo synthesis.

3.2.3 Synthesis of a Bay-Annulated 6,6'-Bismesityl Indigo

As described in Chapter 2, synthesis of **2.4d-Mes** was performed with the indigo compound and the respective acid chloride (Figure 47) yielding the bay-annulated species. To synthesise precursors for the self-encapsulation via a metathesis reaction, bay-annulated derivatives that can be functionalised had to be prepared. There is no straightforward synthetic protocol for the bay-annulation of indigoids.[7],[20],[21] In general, the solubility of indigo has an impact on the reaction outcome, but switching to more soluble indigoids (*e.g.* **3.7**) does not make the reaction more accessible. The reaction conditions were thoroughly screened for the mesityl derivative **3.8d** (Table 7) and the dimethoxy derivative **3.8a** (Table 8).

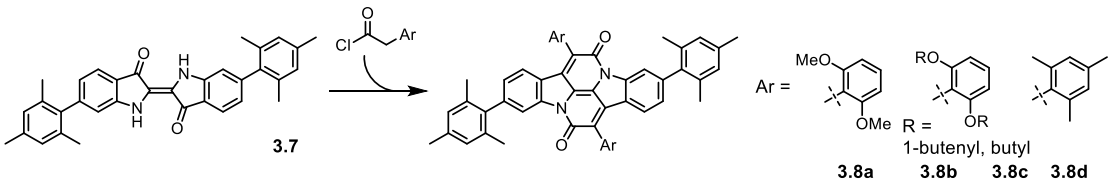

Figure 47: Synthetic strategy for the bay-annulation of 6,6'-bismesityl indigo (3.7) to form 3.8a, 3.8c, and 3.8d.

Table 7: Condition screening of the mesitylderivative (3.8d).

Entry	Acid Chloride (eq.)	Additive (eq.)	Solvent	Time	Temp. (°C)	Product
1	6	-	Cl_2-Benzene	2 d	160	Decomposition
2	6	Mol Sieves	Cl_2-Benzene	2 d	160	Decomposition
3	12	-	DMF	3 d	140	Decomposition
4	12	Pyridine (exc.)	DMF	14 d	140	Decomposition
5	12	-	Pyridine	3 d	120	Decomposition
6	6	-	m-xylene	3 d	140	Decomposition
7	6	Mol Sieves	m-xylene	3 d	140	Decomposition
8	10	$Ti(OiPr)_4$ (10)	m-xylene	1 d	140	Decomposition
9	10	BF_3 (10)	m-xylene	1 d	140	Decomposition
10	10	$Zn(OTf)_2$ (10)	m-xylene	1 d	140	Decomposition
11	13	Protonsponge (13)	m-xylene	7 d	140	Decomposition
12	12	DMAP (4)	m-xylene	1 d	140	Decomposition
13	12	Et_3N (exc.)	m-xylene	18 h	140	Decomposition
14	12	Pyridine (exc.)	m-xylene	5 d	140	Decomposition
15	10	Pyridine (2)	m-xylene	12 d	140	Decomposition
16	10	Pyridine (4)	m-xylene	12 d	140	Decomposition
17	10	Pyridine (10)	m-xylene	8 d	140	traces[a]
18	6	-	Toluene	9 d	120	traces[a]

[a] Traces of product were observed by MALDI-MS.

These small scale reactions were carried out in closed, dry vials under argon and heated to the temperatures shown in Table 7 and Table 8 respectively. Only in rare cases could product traces be observed by MALDI measurements. The use of strong Brønsted-acids or

DMF at high temperatures led to decomposition within hours (entries 1, 2, 3, 8-11, 15 in Table 7), whereas the other reaction conditions were milder giving decomposed species only after several days, making toluene and m-xylene more suitable solvents for these reactions. Still, heating for several days resulted in precipitation of a black insoluble solid and decomposition. Addition of weaker Brønsted-bases (*e.g.* pyridine) led to product traces (entry 15 in Table 7). Nevertheless, it also showed that addition of more than 2 eq. Brønsted base gave decomposed material. The synthesis of **3.8d** was unsuccessful and solely used as a model compound for testing whether *ortho*-substituted acid chlorides are tolerated during bay-annulation. Focus was on **3.8a** which was used as precursor for the self-encapsulation.

Table 8: Condition screening of the dimethoxyderivative (3.8a).

Entry	Acid Chloride (eq.)	Additive (eq.)	Solvent	Time	Temp. (°C)	Product
1	10	-	Benzonitrile	7 d	140	Decomposition
2	10.	-	Benzonitrile	5 d	140	Decomposition
3	10	-	Toluene	5 d	120	Decomposition
4	10	Pyridine (10)	Toluene	5 d	120	Decomposition
5	10	-	m-xylene	1 d	140	Decomposition
6	10	Proton sponge (10)	m-xylene	10 d	140	Decomposition
7	10	2,6-lutidine (10)	m-xylene	5 d	140	Decomposition
8	10	2,6-lutidine (17)	m-xylene	10 d	140	Decomposition
9	10	Pyridine (40)	m-xylene	10 d	140	Decomposition
10	20	Pyridine (20)	m-xylene	7 d	140	Decomposition
11	10	Pyridine (10)	m-xylene	4 d	140	Decomposition

12	10	Pyridine (10)	m-xylene	5 d	140	Decomposition
13	10	Pyridine (10)	m-xylene	10 d	60-140 in steps	Decomposition
14	10	Pyridine (10)	m-xylene	7 d	140	9%
15	10	Pyridine (2)	m-xylene	9 d	140	14%
16	10	Pyridine (1)	m-xylene	20 d	140	13-40%

As we believed oxidative decomposition by reaction with O_2 to be a contributing factor, experiments were performed with degassed solvents. Experiment outcomes under these reactions can be seen in Table 8 (entries 14-16), showing that addition of more than 1 equivalent of Brønsted-base lowered the yield. Heating the respective acid chloride with **3.7** and low stoichiometric amounts of pyridine (1 eq.) gave the desired product in up to almost 40% yield.

Precursors for the metathesis reaction require terminal alkene straps, therefore **3.7** underwent reaction with the acid chlorides **3.4b** and **3.4c** to give **3.8b** and **3.8c**. Similarly, as for the formation of the dimethoxy derivative **3.8a**, mainly decomposition of the reaction mixtures occurred. The reactions were monitored by MALDI-MS and TLC, however, formation of the desired product **3.8b** could not be achieved in any of the trial reactions. Mostly black solid and unidentifiable mixtures appeared during the reaction.

Table 9: Screening of conditions for the reaction of 6,6'-bismesityl indigo (3.7) with 2-(2,6-dibutenoxy)phenyl *tert*butyl acetate (3.4b) to build 3.8b.

Entry	Acid Chloride (eq.)	Additive (eq.)	Solvent	Time	Temp. (°C)	Product
1	15	-	Mesitylene	1 d	180	Decomposition
2	15	2,6-lutidine (1)	Mesitylene	1 d	180	Decomposition
3	10	-	m-xylene	2 d	140	Decomposition
4	10	Pyridine (1)	m-xylene	2 d	140	Decomposition
5	10	Pyridine (2)	m-xylene	2 d	140	Decomposition
6	10	Pyridine (10)	m-xylene	2 d	140	Decomposition
7	10	2,6-lutidine (1)	m-xylene	6 d	140	Decomposition
8	10	-	m-xylene (degassed)	7 d	140	Traces of side products
9	10	2,6-*tert*-butyl-pyridine (1)	m-xylene (degassed)	5 d	140	Decomposition
10	10	2,6-lutidine (1)	m-xylene (degassed)	5 d	140	Decomposition
11	10	2,6-lutidine (10)	m-xylene (degassed)	5 d	140	Decomposition

To prevent reaction with the terminal double bonds on the acid chloride **3.4b**, the indigo dye **3.7** was subjected to reaction with **3.4c** to yield **3.8c**. Product formation was possible, but in a yield of less than 1%. The positive reaction outcome was proven by MALDI-MS after separation of the reaction mixtures with column chromatography. Unfortunately, not enough material could be synthesised for NMR-spectroscopy. Apart from that, larger reaction yields would be needed to perform the self-encapsulation reaction of the bay-annulated indigo. It is likely that the bay-annulation reaction does not tolerate sterically

demanding groups in the *ortho*-position, therefore other reaction conditions had to be found.

We adapted the established reaction conditions from Sugiyasu *et al.*[9],[10] and Bronstein *et al.*[11] for their polythiophene and DPP derivatives, respectively, to our system (Figure 48).

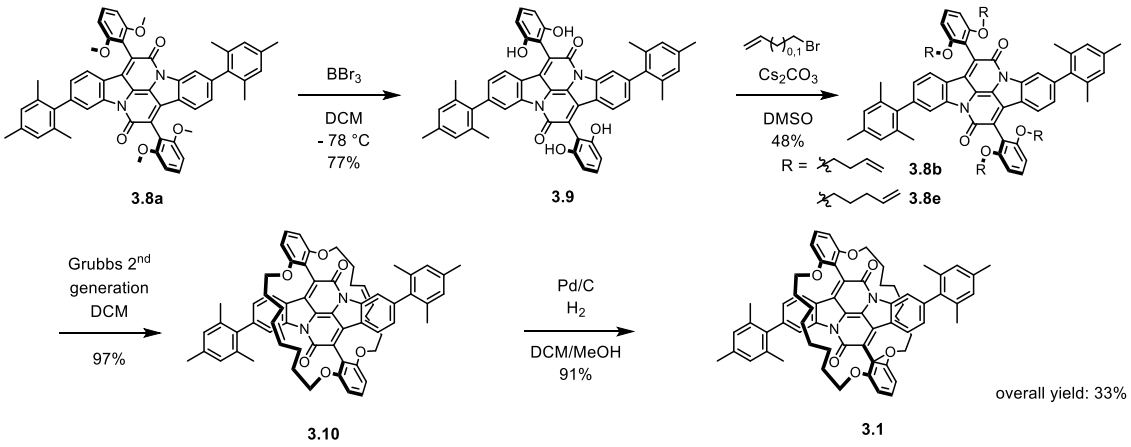

Figure 48: Reaction scheme for the self-encapsulation of the bay-annulated indigo 3.8a to yield the self-encapsulated species 3.1 by methoxy deprotection, Williamson ether synthesis, ring-closing metathesis and hydrogenation reactions.

Deprotection was performed by treating **3.8a** with BBr_3[22] or pyridinium hydrochloride[23] (Figure 48 first step). Addition of BBr_3 in aliquots, and following the reaction by MALDI-MS until completion, allowed access to **3.1** in 43% yield. More than 8 eq. of BBr_3 and slightly higher temperatures (20 °C instead of 0 °C) led to bromination in the *ortho*-position to the respective OH-moiety. These side products could be removed by column chromatography; however, the bromination could be prevented by leaving the reaction longer at 0 °C with a maximum of 8 eq. BBr_3 and quenching as no intermediate products (where some methyl groups are still present) were observed by MALDI-MS.

Deprotected species **3.9** was heated in DMSO to 100 °C in the presence of Cs_2CO_3 as base and 4-bromo-1-butene to provide the metathesis precursor **3.8b** (Figure 48 second step) and conversion was observed by TLC. After heating the mixture for 3 h complete conversion

was indicated by MALDI-MS. Separation by column chromatography in PE/EtOAc gave the pure product **3.8b** in a yield of 38%.

Compound **3.8b** was then subjected to ring-closing metathesis reaction conditions to link the butenyl-chains together. The sample was dissolved in CH_2Cl_2 (10 mg compound in 50 mL solvent) and Grubb's catalyst (2nd generation) was added.[9],[10] The reaction was performed under highly diluted conditions in order to prevent polymerisation due to intermolecular reactions. After degassing, the reaction mixture was heated to 40 °C, but no product formation was observed. The starting material was consumed and could not be seen in the MALDI spectrum anymore. The catalyst bonded to the substrate, evident by the MALDI mass, but was not able to perform further metathesis due to too much steric strain on the molecule. Hence, it is likely that the butane-straps are too short to allow self-encapsulation.

To relieve the steric strain, the strap-length was increased by one carbon to pentene. The same conditions for the Williamson ether synthesis were applied to **3.9** using 5-bromo-1-pentene instead of 4-bromo-1-butene.[11] **3.8e** was prepared in 30%, comparable to the yield of **3.8b**. High dilution of **3.8e** in CH_2Cl_2 (10 mg compound in 50 mL solvent), addition of Grubb's catalyst (2nd generation, 1.2 eq.), degassing, and heating to 40 °C yielded full conversion to **3.10** within 1 h, as confirmed by MALDI-MS. [9]–[11] After purification by column chromatography, the desired product could be isolated in a yield of 96%. Due to the two double bonds in the straps, three stereoisomers appear in the NMR spectra: *cis*/*cis*, *cis*/*trans*, and *trans*/*trans*, in a ratio of 1:2:1 which could not be separated by chromatographic methods.

In order to prepare a pure compound, the double bonds were hydrogenated. The encapsulated derivative **3.10** was dissolved in CH_2Cl_2/MeOH and 10% Pd on C was added.

The reaction was deoxygenated by purging with H_2 and stirred for 30 min. MALDI-MS showed complete conversion after less than 1 h. In total, of the desired product **3.1** could be isolated in a yield of 77%. The ^{1}H-NMR spectrum of **3.1** (Figure 49) proves in addition to the mass spectrum that the target compound has been formed.

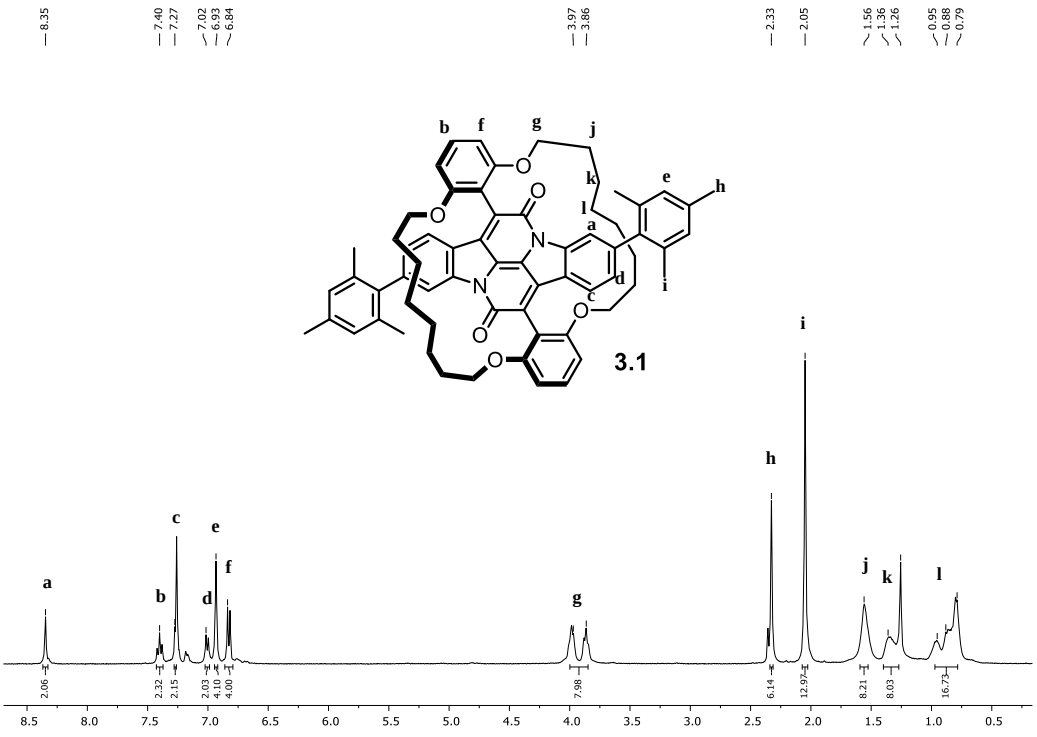

Figure 49: ^{1}H-NMR spectrum (400.2 MHz, $CDCl_3$) of the target compound 3.1.

In order to confirm whether the ring-closing reaction had occurred around the main body, a NOESY NMR spectrum (Figure 50) provided more information about interactions between the straps and the phenyl rings and bay-annulated main body. The only NOE between any atoms of the chains is between the protons resonating at about 4 ppm and the *m*-phenyl protons. However, no further interactions between the straps and any other aromatic protons can be seen. This suggests binding over the main body, since the chains are not in close proximity to any further protons. If the metathesis had happened between

straps on the same phenyl group, further NOEs to the *m*-phenyl as well as the *p*-phenyl protons might be expected.

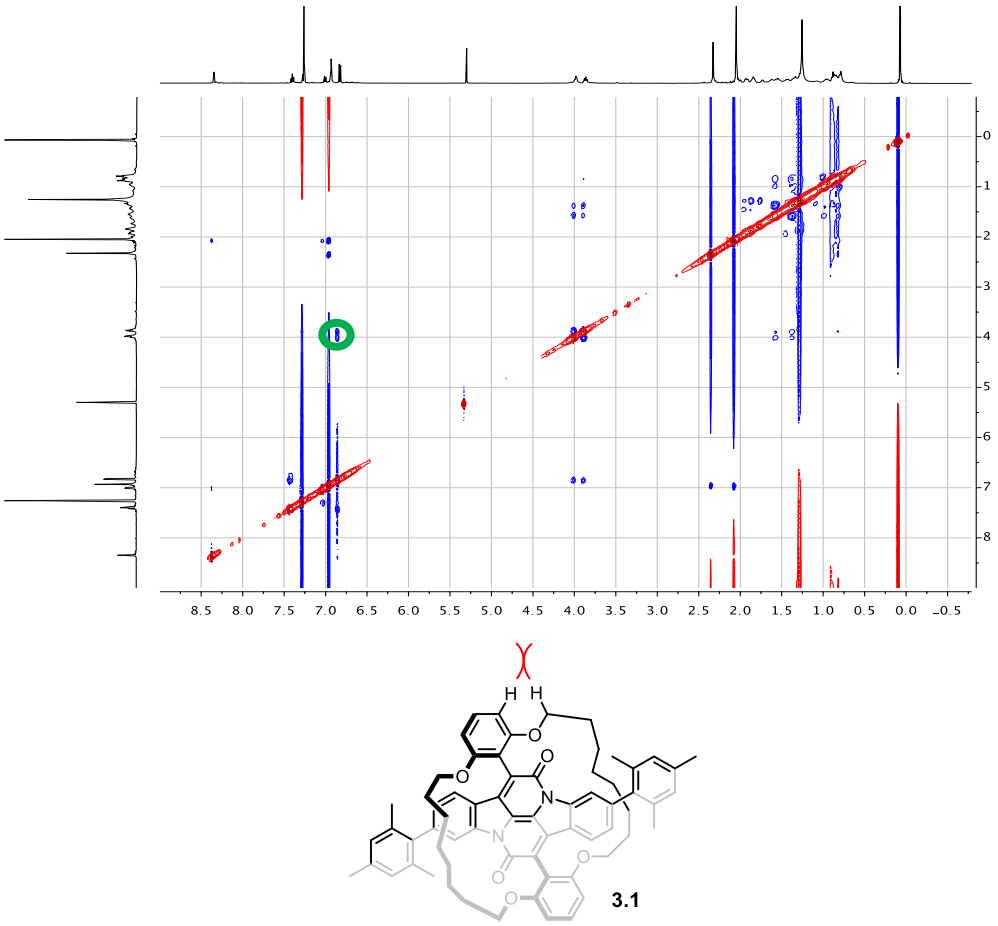

Figure 50: NOESY spectrum of the target compound 3.1. The molecular structure below represents where the interaction occurs.

3.3 Crystal Structure of a Bay-Annulated Self-Encapsulated Indigo

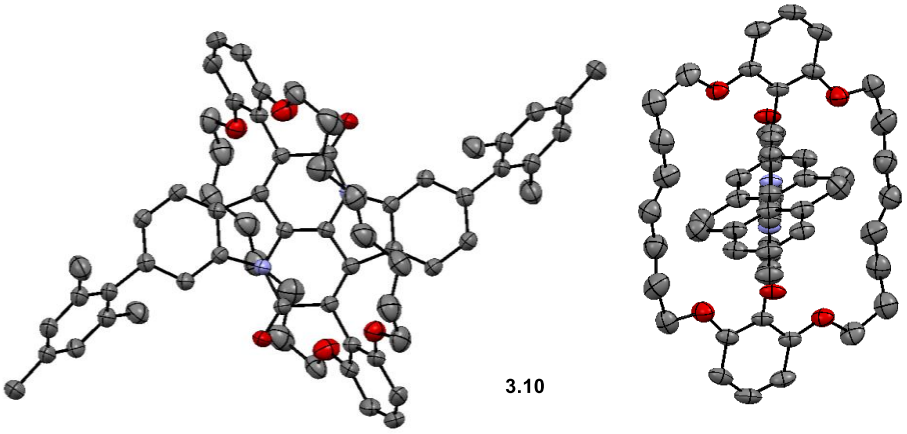

Figure 51: Crystal structure of the bay-annulated self-encapsulated indigo 3.10 before hydrogenation.

Crystals of **3.10** were obtained by slow evaporation of a $CDCl_3$ solution and measured by Yaoyao Xiong. Figure 51 displays the crystal structure of the compound and proves that encapsulation took place around the bay-annulated core. With *R* values of less than 10%, the structure is well defined and verifies the quality of the grown crystals (all crystal data are presented in the Appendix in Table 13). The only disorder in the crystal structure appears around the straps, due to the mixture of the *cis*/*cis*, *cis*/*trans*, and *trans*/*trans* isomers in the crystal (Figure 52). However the amount of residual electron density around the strap is very low and most of the electron density is actually located in the *trans*-position on both sides suggesting some preference for the trans-isomer to crystallise.

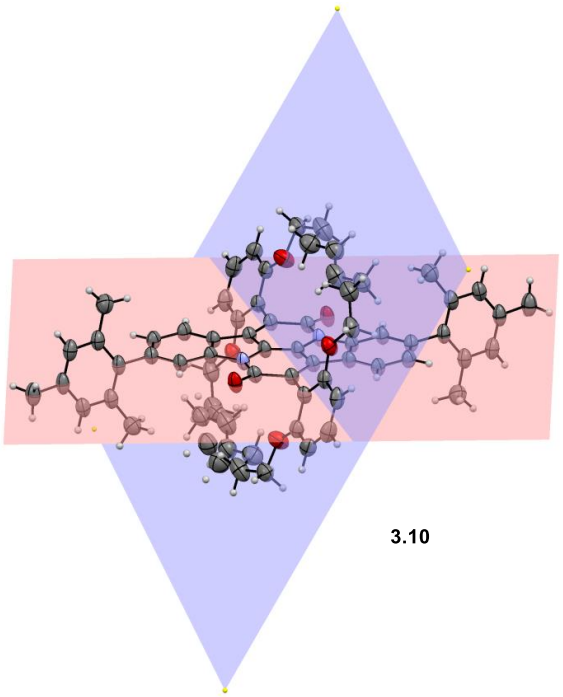

Figure 52: Display of the planes through the bay-anulated main body (red) and the attached phenyl rings (blue).

The torsion angle between the bay-annulated core and the encapsulating *ortho*-substituted phenyl moiety is 63°, deviating by 27° from the ideal angle of 90° (inserted planes in Figure 52). This torsion angle of **3.10** could not be smaller due to the distance between the core carbonyl moiety and the oxygen atom on the phenoxy rings (2.94 Å in the crystal); a shorter distance would lead to steric repulsion which is energetically unfavourable. The same outcome is seen in the self-encapsulated DPP-monomers from Bronstein *et al.* with a torsion angle of 71.38° and a strap-plane distance of 3.21 Å.[11] The packing in the crystal also reveals that no π-interactions between the bay-annulated core and other molecules are present (Figure 53). Solely, hydrogen-π-interactions, in which the aromatic rings are located perpendicular to the respective hydrogen atoms, emerge between the mesityl groups and hydrogen atoms of the chains with a length of 3.15 Å. This outcome confirms that encapsulation prevents any intermolecular π-π-interactions between the bay-annulated cores. These results can also be compared to the crystal structures of indigo derivatives

discussed in Chapter 2, for which intermolecular π-interactions are present allowing long-range ordering.

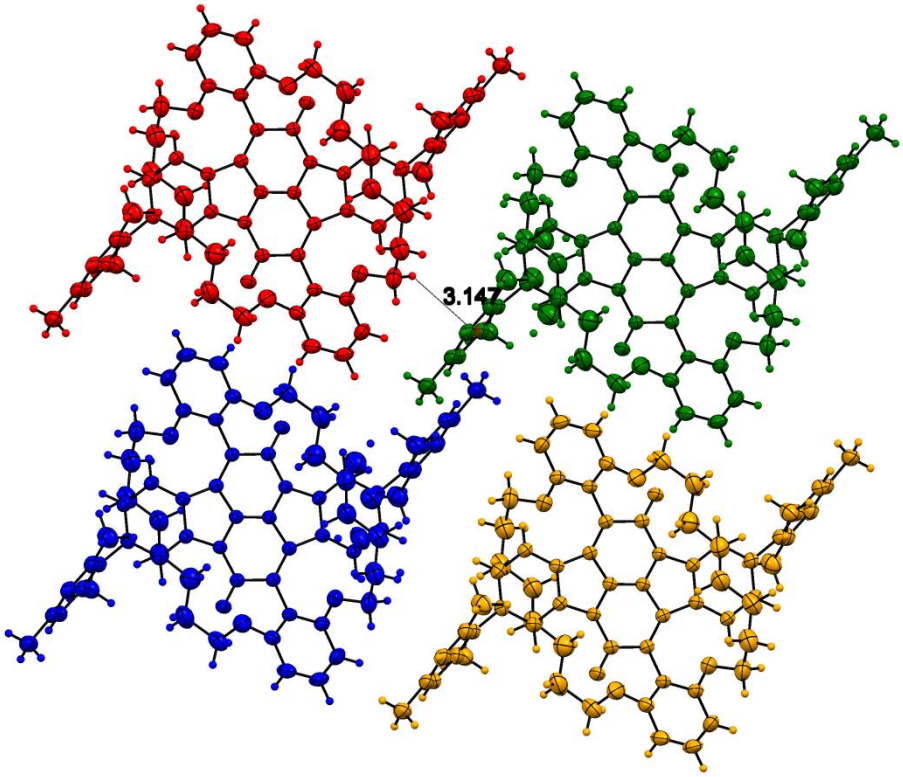

Figure 53: Crystal packing of 3.10 showing a H-*π* interaction between a strap CH and a mesityl group from the neighbouring molecule.

Crystals of the target structure were also obtained, but X-ray analysis showed a large degree of disorder, insufficient for refinement.

3.4 Photophysical Properties

The general procedures for the measurements can be found in Chapter 2. The photophysical measurements of the synthesised compounds **3.1**, **3.7**, **3.8a**, **3.8b**, **3.8d**, **3.9**, and **3.10** are described here. Bay-annulation and encapsulation to give **3.1** provide a unique way of tuning the properties of the indigo-derivative **3.7** by extending the chromophore. Figure 54 displays the absorption spectra of the respective derivatives and the influence of change in the indigo core; intermolecular hydrogen bonds shift the absorption in the region of 600 nm with a broad spectrum in which a shoulder at 550 nm can be seen. On the other hand, the bay-annulated, encapsulated species **3.1** shows a comparably blue-shifted absorption with a maximum at 531 nm and a three-finger pattern due to its rigidity.

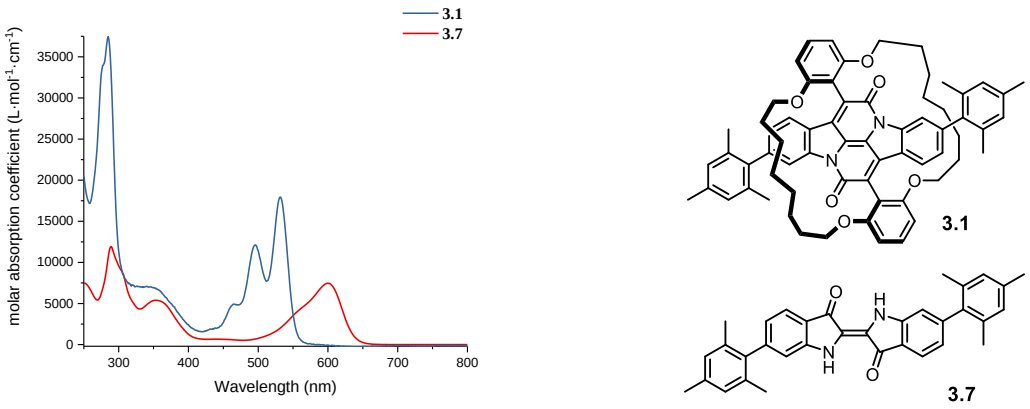

Figure 54: Absorption spectra of 3.1 and 3.7 in dichloromethane.

Between the bay-annulated dyes no large shifts in the absorption and emission wavelengths appear (Figure 55, **3.8a** and **3.1**); the absorption bands have the same pattern and overlap closely. The spectrum of the deprotected species **3.9** is not shown due to insolubility in dichloromethane. This also explains the low values for the fluorescence quantum yields of <1% due to its insolubility in dichloromethane (Table 3).

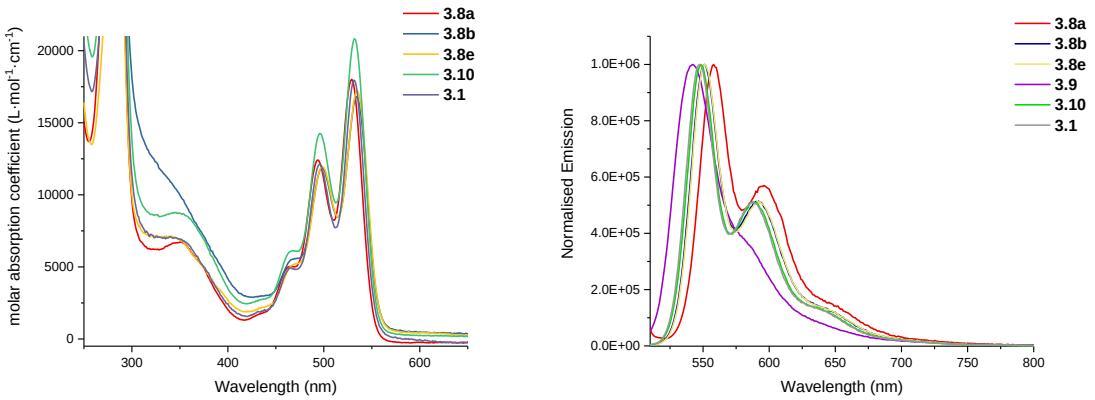

Figure 55: Absorption and emission spectra of the compounds 3.1, 3.8a, 3.8b, 3.8d, 3.9, and 3.10 in dichloromethane.

The emission and absorption parameters are listed in Table 3. In general, the molar absorption coefficients of the molecules are in a range of 10000 to 20000 and give fluorescence quantum yields between 42 and 53% with the exception of the free phenol **3.9** which revealed a smaller value of 0.6% due to its insolubility in CH_2Cl_2.

Table 10: Absorption and emission parameters in dichloromethane.

Compound	λ_{abs} [nm]	ε [L·mol^{-1}·cm^{-1}]	λ_{em} [nm]	QY [%]	τ [ns]
3.7	600	7468	-	-	-
3.8a	530	18010	548	42	3.55
	493	12594			
	465	5499			
3.9	538	959	542	0.6	3.33
	504	732			
	469	513			
3.8b	534	16811	551	53	4.19
	498	10864			

	464	5377			
3.8c	534	17201	551	51	4.09
	498	11906			
	465	5105			
3.10	531	20831	548	48	4.06
	495	14062			
	464	6066			
3.1	531	17941	547	44	4.13
	495	12356			
	464	5358			

For the comparison of the encapsulated species with the reference compound **3.8a**, measurements in different solvents were performed and the data are presented in Table 11.[6],[7],[11],[20],[21] In each solvent, the sample was prepared to have a maximum absorbance of less than 0.1, and the UV-vis absorption spectra were recorded. For emission spectra, the same sample was excited at 500 nm, and fluorescence emission between 510 and 850 nm was collected.

Table 11: Absorption and emission parameters of compound 3.8a and 3.1 in different solvents.

	3.8a					**3.1**				
Solvent	λ_{abs} **[nm]**	ε^a	λ_{em} **[nm]**[(1)]	**QY [%]**	τ **[ns]**[(2)]	λ_{abs} **[nm]**	ε^a	λ_{em} **[nm]**[1]	**QY [%]**	τ **[ns]**[(2)]
THF	535	19296	552	62	5.45	536	20054	552	71	6.08
	499	12908				500	11428			
	468	5358				469	4878			

MeOH	516	17279	538	19	1.59	520	17416	539	11	1.75
	483	13009				485	12733			
	453	6049				455	5597			
EtOAc	531	19649	548	51	5.35	533	21055	548	54	5.78
	495	13437				496	13790			
	465	5808				465	5788			
DMSO	530	18193	552	42	3.49	533	19440	550	39	3.60
	495	12841				496	13969			
	464	5541				464	6027			
Toluene	538	18747	557	68	5.64	535	21528	557	64	5.64
	501	12847				499	14080			
	471	5505				467	5788			
***n*-Hexane**	537	20948	551	64	6.38	536	23401	549	60	6.65
	500	13611				499	14699			
	469	5453				467	5725			
DCM	529	18010	558	42	3.55	532	17941	547	44	4.13
	494	12594				495	12356			
	465	5499				464	5358			

All measurements were performed at 25°C, [a] given in [$L \cdot mol^{-1} \cdot cm^{-1}$], [(1)]Excitation wavelength of 500 nm, [(2)] the results of the life-time measurements were estimated by reconvolution fits.

Figure 56 and Figure 57 display the absorption and emission spectra of **3.8a** and **3.1** in different solvents. The results show similar ε for the compounds in different solvents. The fluorescence quantum yields, the fluorescence lifetimes, and the absorption and emission wavelengths are not strongly impacted by the encapsulation of the compound. The largest

differences in the absorption and emission spectra are observed in methanol solutions. Differences for the spectra in methanol are caused by the insolubility of the dyes in the solvent. Larger deviations could be expected in the solid state, where aggregation is more likely and could have an impact on the fluorescence of the dyes.

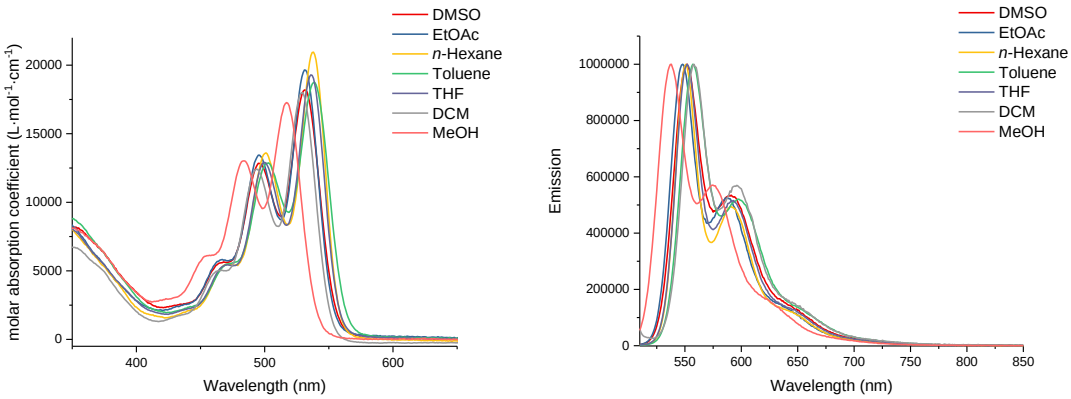

Figure 56: Influence of solvents on the absorption (left) and emission (right) spectra of 3.8a.

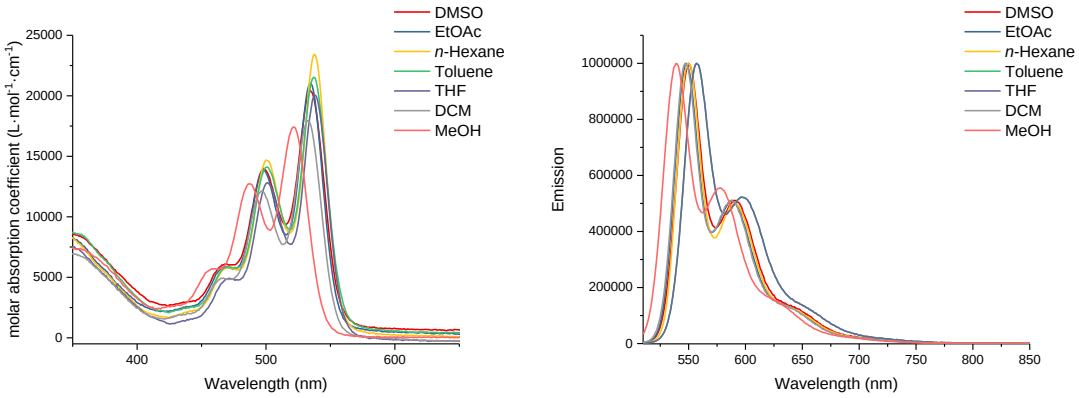

Figure 57: Influence of solvents on the absorption (left) and emission (right) spectra of 3.1.

The solid state behaviour was evaluated by measuring thin films of **3.8e** and **3.1**. Spin-coating of pure material led to an agglomeration rather than homogenous film formation. Therefore, a host material (*e.g.* PMMA, paraffin) was used to measure films/solid state spectra of the methoxy-species **3.8a** and the encapsulated dye **3.1**.

The dyes were dissolved in dichloromethane at a concentration of 2.30 mM for **3.8a** and **3.1**, and mixed with a stock solution of 10 wt% PMMA in toluene in different ratios to make films. The samples were spin-coated for 1 min at 1000 rpm and afterwards baked on a heating plate covered with aluminium foil at around 100 °C for 1 min. In addition to film preparation, a known amount of compound (77.0 nmol of each dye) was ground to a fine crystalline powder with 500 µL paraffin in a mortar to measure the photophysical properties of the crystalline materials. This paste was then transferred between two microscope slides. The results for the measurements of the spin-coated films and the coarse material in paraffin can be seen in Table 12. The fluorescence quantum yield results of the paraffin measurements are a mean value of three experiments for each compound.

Table 12: Fluoresence quantum yields in solid state of the methoxy and encapsulated derivatives.

	Dye	**Host Material**	**Weight Ratio Dye:Hostmaterial**	**QY [%]**
3.8a	25 µL	25 µL PMMA (10 wt%)	1 : 0.3	22
3.8a	10 µL	50 µL PMMA (10 wt%)	1 : 1.6	24
3.1	25 µL	25 µL PMMA (10 wt%)	1 : 0.3	26
3.1	10 µL	50 µL PMMA (10 wt%)	1 : 1.6	22
3.8a	0.63 mg	500 µL paraffin	1 : 900	27 ± 9
3.1	0.63 mg	500 µL paraffin	1 : 900	27 ± 7

Both experimental methods gave the same results within error, and fluorescence quantum yields around 25% for each of the dyes were measured. The molecular variation between the methoxy **3.8a** and the fully encapsulated compound **3.1** is not observed in monomeric structures. This suggests that the methoxy groups are already encapsulating the dye core enough to prevent aggregation and interactions with other molecules. Larger differences in

the quantum yield were expected in polymeric structures, assuming less long-range ordering. The absorption and emission spectra are shown in Figure 58 with excitation and emission maxima of 539 and 554 nm for **3.8a** and 543 and 556 nm for **3.1**.

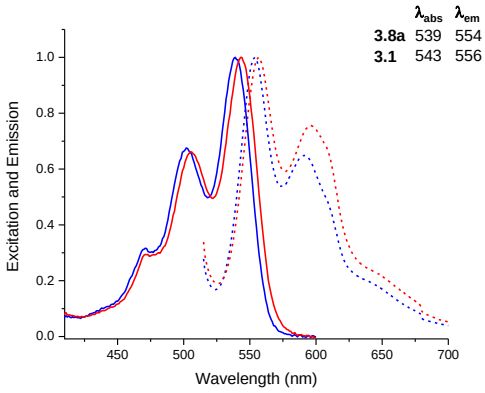

Figure 58: Normalised absorption and emission spectra (solid state, in paraffin) of the methoxy 3.8a (blue) and encapsulated 3.1 (red) indigoids in paraffin.

Fluorescence lifetime measurements of the paraffin mixtures have also been performed. The results can be compared to measurements in solution. For the methoxy derivative **3.8a** a mono-exponential decay constant of 3.55 ns was measured, and for the encapsulated dye **3.1** a mono-exponential decay constant of 4.31 ns. Since the fluorescence quantum yields in solid state decrease, shorter fluorescence lifetimes are to be expected. Measurements of the radiative decay constants gave values for these lifetimes of 2.69 ns for **3.8a** and 2.64 ns for **3.1**, being consistent with the lower quantum yields.

These results of the solution and solid state photophysical properties of the bay-annulated **3.8a** and encapsulated **3.1** derivatives do not show the expected behaviour of an increase in fluorescence quantum yields by encapsulation. In case of the bay-annulated indigo derivatives this means that introduction of *ortho*-substituted phenyl groups might already prevent intermolecular interactions which lead to quenching of the fluorescence. This most likely also applies for Bronstein's DPP derivative. In their report, a DPP derivative with

alkyl chains, in which π-interactions are promoted, is compared to the encapsulated version.[11] However, a comparison of the methoxy derivative and the final encapsulated compound was not investigated. Unfortunately, it is not possible to synthesise the indigo dye with alkyl chains, because the bay-annulation requires an aromatic acetyl chloride on the bridging unit. Therefore, we cannot compare the outcome for an alkylated derivative. However, we can state that for the bay-annulated indigoids enough steric hindrance is provided by methoxy groups (**3.8a**) to prevent intermolecular interactions in high concentrations, especially in the solid state.

3.5 Conclusion

In conclusion, a synthetic strategy for the bay-annulation and encapsulation of an indigo dye has been established. The starting material for the encapsulation, **3.8a**, is the first bay-annulated indigoid synthesised with *ortho*-substituted acid chlorides. Additionally, no similar bay-annulated, encapsulated indigo has been reported so far. The experimental challenges during the preparation of the compounds were overcome and we were able to demonstrate a reproducible route for the preparation of the target compound. With the crystal structure of the encapsulated species **3.10** it was shown that there are no intermolecular interactions between the bay-annulated cores in the solid state.

The analysis of the photophysics revealed that properties of the methoxy **3.8a** and encapsulated dye **3.1** concur and provide strong fluorescence in solution and solid state. The expected enhanced fluorescence quantum yields in solution and solid state by self-encapsulation could not be proven. It suggests that the methoxy groups in dye **3.8a** already have enough steric impact on the molecule to prevent intermolecular π-interactions.

However, measurements in neat films could not be performed, therefore improved properties for the encapsulated species are still possible.

Further investigation of the properties would be necessary to evaluate the use of these dyes in OLEDs or as fluorescent dyes in general.

3.6 Experimental Details

General Procedures

All reagents were purchased from commercial sources and used as received. Solvents were bought from Honeywell, formerly Sigma Aldrich. Column chromatography was carried out using SiO_2 60 (particle size 40-63 μm, Merck, UK) as stationary phase. NMR spectra were acquired on a Bruker AVII400, AVIII400, or AVII500 instrument. ^{1}H NMR chemical shifts are reported in ppm and were referenced internally to residual protons in the solvent (δ = 7.26 for $CDCl_3$; 2.50 for DMSO). $^{13}C\{^1H\}$ NMR chemical shifts are reported in ppm and were referenced internally with respect to the solvent signal (δ = 77.2 for $CDCl_3$; 39.52 for DMSO). Standard abbreviations indicating multiplicity were used as follows: s = *singlet*, d = *doublet*, dd = *doublet* of *doublets*, t = *triplet*, q = *quartet*, m = *multiplet*, br = broad signal. High-resolution mass spectra (HRMS) were obtained on a Bruker μTOF instrument or a Waters GCT.

Tert-butyl 2-(2,6-dimethoxyphenyl)acetate (**3.2a**)[13]

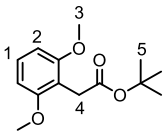

1,3-dimethoxybenzene (2.58 mL, 20.0 mmol, 1 eq.) was dissolved in dry THF (20 mL) at 20 °C under argon. To this solution *n*BuLi (16.5 mL, 26.0 mmol, 1.6 M in hexanes, 1.3 eq.) was added slowly, turning the solution yellow. This mixture was stirred for 2 h at 20 °C. CuI (4.20 g, 22.0 mmol, 1.1 eq.) was added to the solution, immediately turning the solution into a dark-brown slurry. After stirring at 20 °C for 1 h, the mixture was cooled to –78 °C. *Tert*-butyl bromoacetate (3.85 mL, 26.0 mmol, 1.3 eq.) was added over 30 min. The solution was slowly warmed to 20 °C and stirred overnight. The suspension was filtered through Celite and washed with Et_2O (20 mL). The organic phase was washed with water (2 × 100 mL). The aqueous phases were washed with Et_2O (2 × 100 mL). The organic phases were combined and washed with

an aqueous 10% Na_2CO_3 solution and brine. The organic phases were dried over $MgSO_4$ and the solvent evaporated. The product crystallised during evaporation yielding *tert*-butyl 2-(2,6-dimethoxyphenyl)acetate **3.2a** as a white solid (4.97 g, 19.7 mmol, 98%).

^{1}H NMR ($CDCl_3$, 400.2 MHz): δ 7.18 (t, J = 8.3 Hz, 1H, H1), 6.55 (d, J = 8.3 Hz, 2H, H2), 3.80 (s, 6H, H3), 3.60 (s, 2H, H4), 1.44 (s, 9H, H5).^{13}C NMR ($CDCl_3$, 100.6 MHz): δ 171.8, 158.5, 128.1, 112.5, 103.8, 80.1, 55.9, 30.1, 28.2. MS (ESI +ve) *m*/*z*: 275.0 ($[M+Na]^+$), ($C_{14}H_{20}O_4Na$ requires 274.31).

2-(2,6-dimethoxyphenyl)acetic acid (**3.3a**)

Tert-butyl 2-(2,6-dimethoxyphenyl)acetate (**3.2a**) (4.97 g, 19.7 mmol, 1 eq.) was dissolved in CH_2Cl_2 (15 mL) and trifluoroacetic acid (15.0 mL, 197 mmol, 10 eq.) and stirred at 20 °C for 1 h. Remaining acid and CH_2Cl_2 were removed *in vacuo* yielding the desired product **3.3a** as a white solid (3.84 g, 19.6 mmol, 99%).

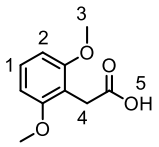

^{1}H NMR ($CDCl_3$, 400.2 MHz): δ 11.15 (br, 1H, H5), 7.23 (t, J = 8.4 Hz, 1H, H1), 6.58 (d, J = 8.4 Hz, 2H, H2), 3.82 (s, 6H, H3), 3.76 (s, 2H, H4). ^{13}C NMR ($CDCl_3$, 100.1 MHz): δ 176.2, 173.6, 158.4, 128.8 (C1), 103.9 (C2), 56.0 (C3), 28.7 (C4). MS (ESI +ve) *m*/*z*: 219.0 ($[M+Na]^+$, $C_{10}H_{12}O_4Na$ requires 218.2). HRMS (ESI) *m/z*: 219.0629 ($[M+Na]^+$, $C_{10}H_{12}O_4Na$ requires 219.0628).

2-(2,6-Dimethoxyphenyl)acetyl chloride (**3.4a**)

2-(2,6-dimethoxyphenyl)acetic acid (**3.3a**) (1.57 g, 8.00 mmol, 1 eq.) was dissolved in thionyl chloride (15.0 mL, 207 mmol, 25 eq.) and heated to 50 °C for 20 min. After cooling to 20 °C, the remaining thionyl chloride was removed *in vacuo* and the product dried under high vacuum yielding the acid chloride **3.4a**

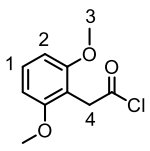

as brown oil (1.69 g, 7.87 mmol, 98%). The product was used immediately without further purification.

^{1}H NMR ($CDCl_3$, 400.2 MHz): δ 7.27 (t, J = 8.4 Hz, 1H, H1), 6.58 (d, J = 8.4 Hz, 2H, H2), 4.21 (s, 2H, H4), 3.82 (s, 6H, H3).

1,3-Bis(but-3-en-1-yloxy)benzene (**3.5b**)[17]

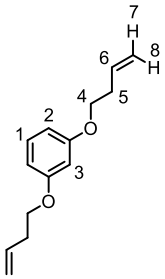

Recrystallised 1,3-dihydroxybenzene (1.00 g, 9.08 mmol, 1 eq.) and K_2CO_3 (10.0 g, 72.7 mmol, 8 eq.) were dissolved in anhydrous DMF (40 mL) and heated to 100 °C for 30 min. 4-Bromo-1-butene (4.00 mL, 39.4 mmol, 4 eq.) was slowly added and the mixture heated to 100 °C for 24 h. After cooling, EtOAc (50 mL) was added and the solution poured into ice water (500 mL). The aqueous phase was extracted with EtOAc (3 × 100 mL) and the organic phase washed with water (2 × 200 mL) and brine (2 × 100 mL). After drying over Na_2SO_4 and evaporation of the solvent, the crude product was purified via column chromatography (silica, PE 1:1 CH_2Cl_2) yielding product **3.5b** as a clear liquid (1.10 g, 5.04 mmol, 56%).

^{1}H NMR ($CDCl_3$, 400.2 MHz): δ 7.16 (t, J = 8.1 Hz, 1H, H1), 6.51 (d, J = 6.51 Hz, 1H, H2), 6.48 (m, 2H, H3), 5.91 (ddt, J = 17.0, 10.2, 6.7 Hz, 2H, H6), 5.17 (dq, J = 17.0, 1.7 Hz, 2H, H8), 5.11 (dt, J = 10.2, 1.7 Hz, 2H, H7), 4.00 (t, J = 6.7 Hz, 4H, H4), 2.54 (dt, J = 6.7, 1.7 Hz, 4H, H5). ^{13}C NMR ($CDCl_3$, 100.6 MHz): δ 160.3, 134.6 (C6), 130.0 (C1), 117.1 (C7), 107.0 (C2), 101.8 (C3), 67.3 (C4), 33.8 (C5). MS (ESI +ve) m/z: 219.2 ($[M+H]^+$, $C_{14}H_{19}O_2$ requires 219.30).

2-Bromo-1,3- bis(but-3-en-1-yloxy)benzene (**3.5b-Br**)

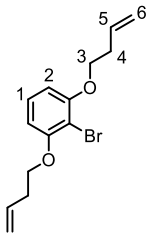

2-bromo-1,6-dihydroxybenzene (6.98 g, 36.9 mmol, 1 eq.) and K_2CO_3 (20.4 g, 141 mmol, 4 eq.) were dissolved in DMF (250 mL) and heated to 70 °C for 30 min. 4-Bromo-1-butene (30.0 mL, 299 mmol, 8 eq.) was slowly added and the mixture heated for 3 d. After cooling the reaction, K_2CO_3 was filtered off and EtOAc (250 mL) added to the filtrate. The solution was stirred with aqueous NaOH (3 M, 40 mL) for 30 min and the organic phase washed with water (3 × 250 mL) and brine (2 × 250 mL). After drying the organic phase over $MgSO_4$ and evaporation of the solvent, the product mixture was separated via column chromatography (PE 1:1 CH_2Cl_2) yielding product **3.5b-Br** as a clear liquid (9.35 g, 31.5 mmol, 85%).

^{1}H NMR ($CDCl_3$, 400.2 MHz): δ 7.17 (t, J = 8.3 Hz, 1H, H1), 6.55 (d, J = 8.3 Hz, 2H, H2), 5.95 (ddt, J = 17.1, 10.3, 6.8 Hz, 2H, H5), 5.21-5.11 (q, J = 1.7 Hz, 4H, H6), 4.07 (t, J = 6.8 Hz, 4H, H3), 2.60 (qt, J = 6.8, 1.7 Hz, 4H, H4) ppm. ^{13}C NMR (100.1 MHz, $CDCl_3$): δ 156.8, 134.3 (C5), 128.1 (C1), 117.3 (C6), 105.2 (C2), 102.5, 68.8 (C3), 33.7 (C4). MS (ESI +ve) m/z: 304.1 ([M(^{79}Br)+Li]$^+$, $C_{14}H_{17}{}^{79}BrO_2Li$ requires 304.13).

Tert-butyl 2-(2,6-bis(but-3-en-1-yloxy)phenyl)acetate (**3.2b**)

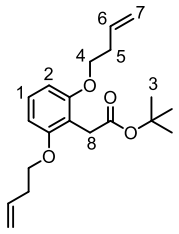

2-bromo-1,3-bis(but-3-en-1-yloxy)benzene (1.00 g, 3.36 mmol, 1 eq.) was dissolved in dry THF (6 mL). The solution was cooled down to –78 °C and *n*-BuLi (2.73 mL, 4.37 mmol, 1.3 eq., 1.6 M in hexane) was slowly added. The cooling bath was removed and the solution stirred for 1 h. CuI (833 mg, 4.37 mmol, 1.3 eq.) was added and the reaction was stirred for a further 1 h. *Tert*-butyl bromoacetate (650 μL, 4.37 mmol, 1.3 eq.) was added to the solution and the mixture stirred overnight. The mixture was then filtered through Celite and washed with Et_2O (100 mL). The organic phase was washed with brine (2 × 200 mL) then dried over

$MgSO_4$, and the solvent removed. Column chromatography with dichloromethane as eluent gave product **3.2b** as a white solid (809 mg, 2.43 mmol, 73%).

^{1}H NMR ($CDCl_3$, 400.2 MHz): δ 7.14 (t, J = 8.3 Hz, 1H, H1), 6.51 (d, J = 8.3 Hz, 2 H, H2), 5.90 (ddt, J = 17.0, 10.2, 6.8 Hz, 2 H, H6), 5.17–5.07 (m, 4 H, H7), 4.00 (t, J = 6.8 Hz, 4H, H4), 3.54 (s, 2H, H8), 2.53 (qt, J = 6.8, 1.4 Hz, 4 H, H5), 1.45 (s, 9 H, H3). ^{13}C NMR (100.1 MHz, $CDCl_3$): δ 194.6, 161.2, 138.5 (C6), 134.0 (C1), 117.8, 117.4 (C7), 109.9 (C2), 101.9, 67.8 (C4), 33.7 (C8), 33.6 (C5), 27.7 (C3). MS (ESI +ve) m/z: 355.2 ($[M+Na]^+$, $C_{20}H_{28}O_4Na$ requires 354.44).

2-(2,6-Bis(but-3-en-1-yloxy)phenyl)acetic acid (**3.3b**)

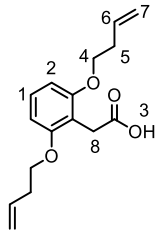

Tert-butyl 2-(2,6-bis(but-3-en-1-yloxy)phenyl)acetate (809 mg, 2.43 mmol, 1 eq.) was dissolved in a 1:1 mixture of CH_2Cl_2 and trifluoroacetic acid (6 mL) and stirred for 2 h. The remaining solvents were removed under vacuum. The product mixture was diluted with CH_2Cl_2 (50 mL) and washed with aq. HCl (1.0 M, 2 × 40 mL). The organic phase was dried over $MgSO_4$, and the solvent removed, yielding the desired product **3.3b** as a white solid (630 mg, 2.28 mmol, 94%).

^{1}H NMR ($CDCl_3$, 400.2 MHz): δ 10.73 (br, 1H, H3), 7.18 (t, J = 8.3 Hz, 1H, H1), 6.58 (d, J = 8.3 Hz, 2 H, H2), 5.89 (ddt, J = 17.0, 10.3, 6.8 Hz, 2 H, H6), 5.17–5.07 (m, 4 H, H7), 4.04 (t, J = 6.8 Hz, 4H, H4), 3.75 (s, 2H, H8), 2.53 (qt, J = 6.8, 1.4 Hz, 4 H, H5). ^{13}C NMR ($CDCl_3$, 100.1 MHz): δ 178.6, 157.7, 134.6 (C6), 128.6 (C1), 117.1 (C7), 111.5, 104.7 (C2), 67.8 (C4), 33.8 (C5), 28.9 (C8). MS (ESI +ve) m/z: 277.2 ($[M+H]^+$, $C_{34}H_{31}N_2O_2$ requires 277.2).

2-(2,6-Bis(but-3-en-1-yloxy)phenyl)acetyl chloride (**3.4b**)

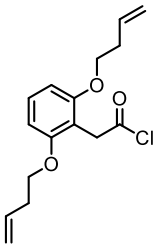

2-(2,6-Bis(but-3-en-1-yloxy)phenyl)acetic acid (150 mg, 0.50 mmol, 1 eq.) was dissolved in $SOCl_2$ (1.5 mL) and stirred for 2 h at 80 °C. The remaining $SOCl_2$ was removed under vacuum to yield the product **3.4b** in quantitative yield which was used without further purification and characterisation.

2-Bromo-1,3-dibutoxybenzene (**3.5c-Br**)

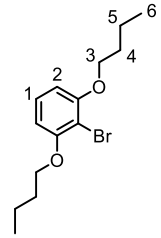

2-Bromo-1,3-dihydroxybenzene (3.00 g, 15.87 mmol, 1 eq.) and K_2CO_3 (8.77 g, 63.49, 4 eq.) was dissolved in dry DMF (150 mL) and heated to 70 °C. 1-Iodobutane (14.4 mL, 127 mmol, 8 eq.) was added and the solution stirred at 70 °C for 3 d. After cooling to 20 °C, the K_2CO_3 was filtered off and the solid washed with EtOAc. The organic mixture was washed with water (3 × 250 mL) and brine (2 × 250 mL), dried over $MgSO_4$, and the solvent removed. The desired product **3.5c-Br** was purified by column chromatography (2:1 PE/ CH_2Cl_2) giving **3.5c-B** as a white crystalline material (3.98 g, 14.7 mmol, 90%).

^{1}H NMR ($CDCl_3$, 400.2 MHz): δ 7.17 (t, J = 8.3 Hz, 1H, H1), 6.53 (d, J = 8.3 Hz, 2 H, H2), 4.02 (t, J = 6.7 Hz, 4 H, H3), 1.82 (ddt, J = 8.9, 7.9, 6.7 Hz, 4 H, H4), 1.53 (m, 4H, H5), 0.93 (dt, J = 17.4, 7.9 Hz, 6 H, H6). ^{13}C NMR (100.1 MHz, $CDCl_3$): δ 156.9, 128.0 (C1), 105.7 (C2), 102.2, 69.0 (C3), 31.3 (C4), 19.3 (C5), 13.8 (C6). MS (ESI +ve) m/z: 302.2 ($[M(^{79}Br)+H]^+$, $C_{14}H_{22}{}^{79}BrO_2$requires 302.1).

Tert-butyl 2-(2,6-dibutoxyphenyl)acetate (**3.2c**)

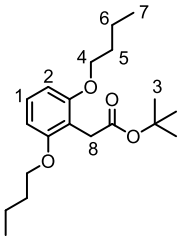

1-Bromo-2,6-bisbutoxybenzene (3.5 g, 11.6 mmol, 1 eq.) was diluted in THF and cooled to –70 °C. Over a syringe, *n*BuLi (9.44 mL, 1.6 M, 15.1 mmol, 1.3 eq.) was added to the solution and stirred for 1 h at 20 °C. CuI (2.88 g, 15.1 mmol, 1.3 eq.) was added and the emulsion stirred for another hour. *Tert*-butylbromoacetate (2.23 mL, 15.1 mmol, 1.3 eq.) was added to the solution and stirred for 3 h at 20 °C The mixture was filtered over celite and washed down with Et_2O (200 mL). The organic phase was extracted with brine (3 × 200 mL) and dried over $MgSO_4$. The crude product was separated with column chromatography (PE with increasing amount of CH_2Cl_2), giving the desired material **3.2c** in form of a white solid (1.91 g, 5.67 mmol, 50%).

^{1}H NMR ($CDCl_3$, 400.2 MHz): δ 7.13 (t, J = 8.3 Hz, 1H, H1), 6.52 (d, J = 8.3 Hz, 2 H, H2), 3.95 (t, J = 6.4 Hz, 4 H, H4), 3.62 (s, 2H, H8), 1.72 (m, 4 H, H6), 1.48 (m, 4H, H5), 1.44 (s, 12 H, H3), 0.96 (m, 6 H, H7) ppm. ^{13}C NMR ($CDCl_3$, 100.1 MHz): δ 171.5, 158.1, 128.0 (C1), 104.5 (C2), 68.2 (C4), 31.6 (C6), 30.1 (C8), 28.3 (C3), 19.4 (C5), 14.0 (C7) ppm. MS (ESI +ve) in methanol *m*/*z*: 337.2371 ($[M+H]^+$, $C_{34}H_{30}N_2O_2$ requires 337.2373)

1-(2,6-Dibutoxyphenyl) acetic acid (**3.3c**)

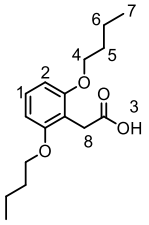

Tert-butyl 2-(2,6-dibutoxyphenyl)acetate (1.90 g, 5.65 mmol, 1 eq.) was diluted in a 1:1 mixture of CH_2Cl_2 and trifluoroacetic acid (10 mL, 23 eq.) and stirred for 2 h. The remaining solvents were removed under vacuum. The product mixture was dissolved in CH_2Cl_2 (50 mL) and extracted with aq. HCl (1.0 M, 2 × 40 mL). The organic phase was dried over $MgSO_4$, and the solvent removed, yielding the desired product **3.3c** as a white solid (1.35 mg, 4.80 mmol, 85%).

^{1}H NMR ($CDCl_3$, 400.2 MHz): δ 9.61 (br, 1H, H3), 7.18 (t, J = 8.3 Hz, 1H, H1), 6.52 (d, J = 8.3 Hz, 2 H, H2), 3.97 (t, J = 6.4 Hz, 4 H, H4), 3.75 (s, 2 H, H8), 1.75 (ddt, J = 8.8, 7.8, 6.3 Hz, 4H, H5), 1.46 (m, 4 H, H6), 0.95 (t, J = 7.8 Hz, 6 H, H7). ^{13}C NMR ($CDCl_3$, 100.1 MHz): δ 177.9, 157.9, 128.6 (C1), 111.2, 104.5 (C2), 68.3 (C4), 31.5 (C6), 29.0 (C8), 19.4 (C5), 14.0 (C7).

2-(2,6-Dibutoxyphenyl)acetyl chloride (**3.4c**)

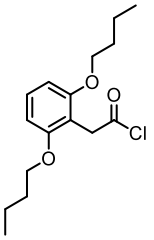

1-(2,6-Dibutoxyphenyl) acetic acid (150 mg, 0.50 mmol, 1 eq.) was dissolved in $SOCl_2$ (1.5 mL) and stirred for 2 h at 80 °C. The remaining $SOCl_2$ was removed under vacuum to yield the product **3.4d** in quantitative yield which was used without further purification and characterisation.

2',4',6'-Trimethyl-3-nitro-[1,1'-biphenyl]-4-carbaldehyde (**3.6**)

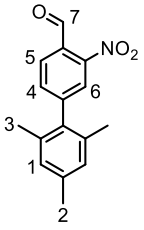

4-Bromo-2-nitrobenzoic acid (1.00 g, 4.35 mmol, 1.0 eq.), 2,4,6-trimethylphenylboronic acid (1.07 g, 6.52 mmol, 1.5 eq.), $Pd_2(dba)_3$ (49.9 mg, 0.09 mmol, 0.02 eq.), SPhos (71.4 mg, 0.18 mmol, 0.04 eq.), and K_2CO_3 (1.63 mL, 6.52 mmol, 4.0 M, 1.5 eq.) were dissolved in a 10:1 dioxane/H_2O (33 mL) mixture. The solution was degassed three times (freeze, pump, and thaw) and heated to 100 °C for 24 h under positive Ar pressure. The mixture was cooled to 20 °C and water (50 mL) was added. The aqueous phase was extracted with CH_2Cl_2 (3 × 50 mL) and the organic phases dried over $MgSO_4$. The solvent was removed *in vacuo*. The product was purified by column chromatography CH_2Cl_2/PE (1:1) yielding 4-mesityl-2nitrobenzoic acid **3.6** as a yellow solid (766 mg, 2.84 mmol, 65%).

^{1}H NMR ($CDCl_3$, 400.2 MHz): δ 10.47 (s, 1H, H7), 8.02 (d, 1 H, J = 7.8 Hz, H5), 7.91 (d, 1 H, J = 1.5 Hz, H6), 7.60 (dd, J = 7.8, 1.5 Hz, 1 H, H4), 6.98 (s, 2H, H1), 2.35 (s, 3 H,

H2), 2.00 (s, 6 H, H3). ^{13}C NMR ($CDCl_3$, 100.1 MHz): δ 188.1 (C7), 150.0, 148.2, 138.5, 135.4 (C5), 135.3, 129.9 (C4), 129.6, 128.7 (C1), 125.6 (C6), 67.1, 21.2 (C2), 20.8 (C3). MS (ESI +ve) *m*/*z*: 270.1 ($[M+H]^+$, $C_{34}H_{31}N_2O_2$ requires 269.1).

6,6'-Bismesityl indigo (**3.7**)

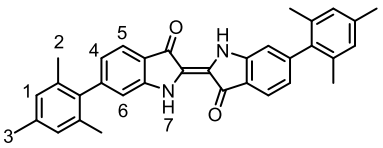

4-Mesityl-2-nitrobenzoic acid (500 mg, 1.86 mmol, 2 eq.) was dissolved in a 1:1 H_2O/acetone mixture (10 mL). Slowly NaOH (aq.) (2 M, 2.46 mL, 4.92 mmol) was added to the suspension. First, the clear solution turned green and after about 20 min a blue precipitate formed. The mixture was stirred overnight and the precipitate collected. The precipitate was washed with water (50 mL) and MeOH (20 mL). The product was washed into a separate flask with CH_2Cl_2 (100 mL). Evaporation of the solvent and drying under high vacuum yielded 6,6'-bismesityl indigo **3.7** as a blue solid (361 mg, 0.72 mmol, 78%).

^{1}H NMR ($CDCl_3$, 400.2 MHz): δ 8.95 (s, 2 H, H7), 7.79 (d, J = 7.8 Hz, 2 H, H5), 6.96 (s, 4 H, H1), 6.84 (t, J = 0.9 Hz, 2 H, H6), 6.78 (dd, J = 7.8 Hz, 2 H, H4), 2.35 (s, 6 H, H3), 2.06 (s, 12 H, H2). ^{13}C NMR ($CDCl_3$, 100.1 MHz): δ 188.4, 152.3, 150.4, 138.2, 137.4, 135.5 (C5), 128.4 (C1), 124.7 (C4), 122.7 (C6), 122.0, 118.8, 113.2, 21.2 (C3), 20.7 (C2). MS (ESI +ve) *m*/*z*: 499.2 ($[M+H]^+$, $C_{34}H_{31}N_2O_2$ requires 499.63). HRMS (ESI) *m/z*: 499.2384 ($[M+H]^+$, $C_{34}H_{31}N_2O_2$ requires 499.2380). UV/Vis (CH_2Cl_2): λ_{max}^{abs} (ε)= 599 (9513), 555, 354, 289.

7,14-Bis(2,6-dimethoxyphenyl)-3,10-dimesityldiindolo[3,2,1-de:3',2',1'-ij][1,5]naphthyridine-6,13-dione (**3.8a**)

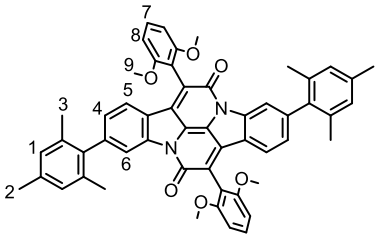

6,6'-Bismesityl indigo **3.7** (100 mg, 0.20 mmol, 1 eq.) was dried. A solution of **3.4a** (540 mg, 2.51 mmol, 13 eq.) in dry m-xylene (3.5 mL) was added, as well as 2,6-lutidine (22.0 μL, 0.20 mmol, 1 eq.), and degassed three times. The mixture was heated to 140 °C for 6 days and then cooled to 20 °C. The solvent was removed and the crude product purified via column chromatography, in petrol ether (1% Et_2O, increasing to 30%). The target compound **3.8a** was isolated as a red solid (58.4 mg, 0.07 mmol, 36%).

^{1}H NMR ($CDCl_3$, 400.2 MHz): δ 8.30 (dd, J = 1.5, 0.6 Hz, 2H, H6), 7.45 (t, J = 8.4 Hz, 2H, H7), 7.18 (dd, J = 7.9, 0.6 Hz, 4H, H5), 6.96 (dd, J = 7.9, 1.5 Hz, 2H, H4), 6.92 (s, 4H, H1), 6.76 (d, J = 8.4 Hz, 4H, H8), 3.78 (s, 12H, H9), 2.32 (s, 6H, H2), 2.03 (s, 12H, H3). ^{13}C NMR ($CDCl_3$, 100.1 MHz): 177.8, 159.0, 158.7, 145.5., 138.0, 137.1, 135.1, 134.5, 130.8 (C7), 128.3 (C1), 127.2 (C4), 125.1 (C5), 124.9, 124.6, 122.5, 118.8 (C6), 110.9, 103.8 (C8), 55.9 (C9), 21.2 (C2), 20.9 (C3). MS (MALDI, TOF LD+) *m/z*: 818.34 (100.0%), 819.34 (58.4%), 820.34 (16.7%), 821.35 (2.3%), found: 817.89). UV/Vis (CH_2Cl_2): λ_{max}^{abs} (ε)= 530 (18010), 494 (12594), 462 (5499) nm.

7,14-Bis(2,6-dibutoxyphenyl)-3,10-dimesityldiindolo[3,2,1-de:3',2',1'-ij][1,5]naphthyridine-6,13-dione (**3.8c**)

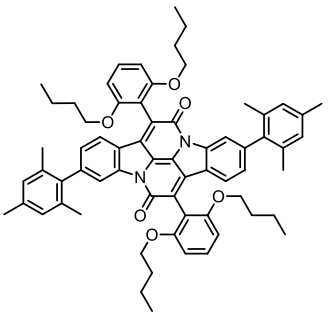

6,6'-Bismesityl indigo (10.0 mg, 0.02 mmol, 1 eq.) and 1-(2,6-bis(butoxy)phenyl)acid chloride (75.0 mg, 0.25 mmol, 12 eq.) were dissolved in m-xylene (5 mL) and 2,6-lutidine (2.2 μL, 0.02 mmol, 1 eq.) and degassed 3 times. The mixture was then heated to 140 °C for 6 d in a

closed flask. The solvent was then removed and the mixture purified with column chromatography (PE with 1–10% EtOAc), yielding less than 1 mg of product **3.8c** as a red solid. MS (MALDI, TOF LD+) *m/z*: 986.52 (100.0%), 987.53 (71.4%), 988.53 (25.1%), 989.53 (5.0%), 988.53 (1.2%), found: 986.8240).

7,14-Bis(2,6-dihydroxyphenyl)-3,10-dimesityldiindolo[3,2,1-de:3',2',1'-ij][1,5]naphthyridine-6,13-dione (**3.9**)

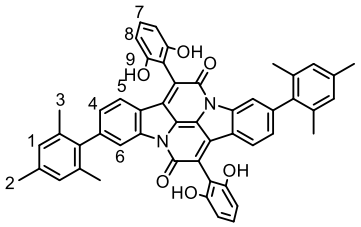

3.8a (117 mg, 571 μmol, 1 eq.) was dissolved in CH_2Cl_2 (5 mL) and cooled to –78 °C. BBr_3 in CH_2Cl_2 (75.0 μL, 73.3 μmol, 1 M, 12 eq.) was added dropwise to the solution and the mixture stirred for 6 h. Afterwards, MeOH (0.1 mL) was added and the solution diluted in EtOAc, which was then washed with water (3 × 25 mL). The organic layer was dried over $MgSO_4$ and the solvent evaporated. Column chromatography (PE with 1–10% EtOAc) gave product **3.9** as a red solid (2.00 mg, 2.62 μmol, 43%).

^{1}H NMR (DMSO-d_6, 400.2 MHz): δ 9.31 (s, 4H, H9), 7.99 (d, J = 1.4 Hz, 2H, H6), 7.24 (d, J = 7.9 Hz, 2H, H5), 7.11 (m, 4H, H4), 7.10 (m, 2H, H7), 6.94 (2, 4H, H1), 6.45 (d, J = 8.2 Hz, 4H, H8), 2.24 (s, 6H, H2), 1.95 (s, 12H, H3) ppm. ^{13}C NMR ($CDCl_3$, 125.8 MHz): δ 170.4, 158.4, 156.5, 144.7, 144.4, 137.5, 136.7, 134.8, 133.4, 130.0 (C4), 128.2 (C1), 127.2 (C7), 125.2 (C5), 124.3, 121.6, 117.0 (C6), 108.4, 106.7 (C8), 20.7 (C2), 20.4 (C3). MS (MALDI, TOF LD+) *m/z*: 762.27 (100.0%), 763.28 (54.1%), 764.28 (14.3%), 765.28 (1.7%), 764.28 (1.2%), found: 762.7169). HRMS (ESI) *m/z*: 763.2808 ($[M+H]^+$, $C_{50}H_{39}N_2O_6$ requires 763.2803). UV/Vis (CH_2Cl_2): λ_{max}^{abs} (ε)= 538 (959), 504 (732), 469 (513).

7,14-Bis(2,6-bis(but-3-en-1-yloxy)phenyl)-3,10-dimesityldiindolo[3,2,1-de:3',2',1'-ij][1,5]naphthyridine-6,13-dione (**3.8b**)

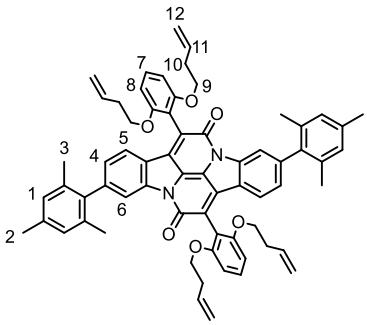

Compound **3.9** (31.3 mg, 41.0 μmol, 1 eq.), Cs_2CO_3 (668 mg, 2.05 mmol, 50 eq.), and 4-bromo-1-butene (208 μL, 2.05 mmol, 50 eq.) were dissolved in DMSO (0.5 mL). The mixture was heated to 100 °C for 3 h and then cooled to 20 °C. The mixture was then diluted in EtOAc (250 mL) and washed with brine (3 × 200 mL). The organic phase was dried over $MgSO_4$ and the solvent removed *in vacuo*. The desired compound was separated from impurities by column chromatography (PE/EtOAc 10%), yielding the desired molecule **3.8b** as a red solid (15.4 mg, 15.7 μmol, 38%).

^{1}H NMR ($CDCl_3$, 400.1 MHz): δ 8.32 (d, J = 1.5 Hz, 2H, H6), 7.39 (t, J = 8.4 Hz, 2H, H7), 7.29 (d, J = 8.0 Hz, 2H, H5), 6.96 (dd, J = 8.0, 1.5 Hz, 2H, H4), 6.93 (s, 4H, H1), 6.72 (d, J = 8.4 Hz, 4H, H8), 5.58 (ddt, J = 16.9, 10.1, 6.6 Hz, 4H, H11), 4.82 (dd, J = 16.9, 1.3 Hz, 4H, H12), 4.70 (dd, J = 10.1, 1.3 Hz 4H, H12), 4.03 (td, J = 6.6, 2.5 Hz, 8H, H9), 2.33 (s, 6H, H2), 2.28 (m, 8 H, H10), 2.04 (s, 12H, H3). ^{13}C NMR ($CDCl_3$, 125.8 MHz): δ 207.2, 158.1, 155.4, 138.9, 137.9, 135.7, 135.6, 131.9, 130.7, 128.3 (C1), 127.6, 125.7, 120.4, 118.5 (C6), 115.6 (C12), 105.6 (C8), 88.4, 68.2 (C11), 33.9, 32.1, 22.9 (C2), 20.8 (C3), 14.3. MS (MALDI, TOF LD+) *m/z*: 978.46 (100.0%), 979.46 (71.4%), 980.47 (25.1%), 981.47 (5.0%), 980.47 (1.2%), found: 979.361). HRMS (ESI) *m/z*: 979.4686 ($[M+H]^+$, $C_{66}H_{63}N_2O_6$ requires 979.4681). UV/Vis (CH_2Cl_2): λ_{max}^{abs} (ε)= 534 (16811), 498 (10864), 464 (5377).

7,14-Bis(2,6-bis(pent-4-en-1-yloxy)phenyl)-3,10-dimesityldiindolo[3,2,1-de:3',2',1'-ij][1,5]naphthyridine-6,13-dione (**3.8e**)

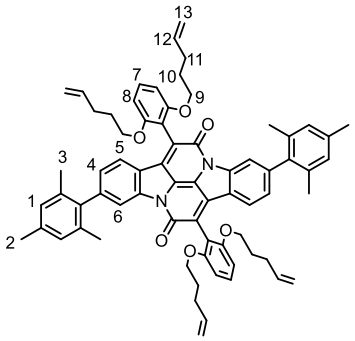

Compound **3.9** (30.0 mg, 39.3 μmol, 1 eq.), Cs_2CO_3 (128 mg, 393 μmol, 10 eq.), and 5-bromo-1-pentene (44.0 μL, 393 μmol, 10 eq.) were dissolved in DMSO (2 mL). The mixture was heated to 100 °C for 3 h and then cooled to 20 °C. EtOAc (250 mL) was added and the mixture extracted with brine (3 × 200 mL). The organic phase was dried over $MgSO_4$ and the solvent removed *in vacuo*. The final compound purified by comlumn chromatography (PE/ CH_2Cl_2 1:1), yielding the desired molecule **3.8e** as a red solid (12.4 mg, 12.0 μmol, 31%).

^{1}H NMR ($CDCl_3$, 400.1 MHz): δ 8.30 (d, J = 1.5 Hz, 2H, H6), 7.39 (t, J = 8.4 Hz, 2H, H7), 7.29 (d, J = 7.9 Hz, 2H, H5), 6.95 (dd, J = 7.9, 1.5 Hz, 2H, H4), 6.92 (s, 4H, H1), 6.71 (d, J = 8.4 Hz, 4H, H8), 5.59 (ddt, J = 16.9, 10.2, 6.6 Hz, 4H, H12), 4.48–4.74 (m, 8H, H13), 4.00 (t, J = 6.4 Hz, 8H, H9), 2.32 (s, 6H, H2), 2.01 (s, 12H, H3) 1.90 (m, 8 H, H11), 1.63 (q, J = 6.9 Hz, 8 H, H10). ^{13}C NMR ($CDCl_3$, 125.8 MHz): δ 158.9, 158.2, 155.4, 138.2, 137.9 (C12), 137.1, 135.7, 134.1, 131.9, 130.7 (C7), 128.3 (C1), 126.9 (C4), 125.7 (C5), 125.1, 124.7, 120.3, 118.5 (C6), 114.9 (C13), 112.4, 105.4 (C8), 68.2 (C9), 30.1 (C11), 28.5 (C10), 21.2 (C2), 20.8 (C3). MS (MALDI, TOF LD+) *m/z*: 1034.52 (100.0%), 1035.53 (75.7%), 1036.53 (28.3%), 1037.53 (6.1%), 1038.54 (1.3%), 1036.53 (1.2%), found: 1036.332). HRMS (ESI) *m/z*: 1035.5310 ($[M+H]^+$, $C_{70}H_{71}N_2O_6$ requires 1035.5307). UV/Vis (CH_2Cl_2): λ_{max}^{abs} (ε)= 534 (17201), 598 (11906), 465 (5105).

Self-encapsulated bay-annulated indigo (**3.10**)

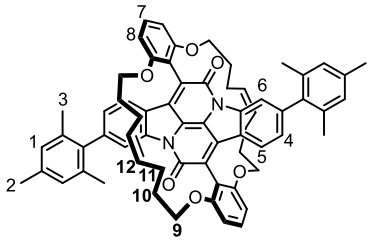

Compound **3.8e** (10.0 mg, 10.6 μmol, 1 eq.) was dissolved in CH_2Cl_2 (50 mL) and Grubbs' catalyst 2nd generation (10.4 mg, 12.2 μmol, 1.2 eq.) was added. The solution was degassed thoroughly and then heated to 40 °C for 1 h. The mixture was then filtered over a silica plug and washed down with EtOAc. The product was separated from impurities by column chromatography (PE/EtOAc 10%), yielding the target molecule **3.10** in a mixture of isomers as a red solid (9.94 mg, 10.2 μmol, 96%).

^{1}H NMR ($CDCl_3$, 400.1 MHz): δ 8.31 (m, 2H, H6), 7.42 (m, 2H, H7), 7.28 (m, 2H, H5), 7.00-6.97 (m, 2H, H4), 6.92 (s, 4H, H1), 6.86–6.81 (m, 4H, H8), 4.90–4.83 (m, 4H, H12), 4.07–3.86 (m, 8H, H9), 2.32 (s, 12H, H3), 2.05 (s, 6H, H2) 2.01 –1.84 (m, 8 H, H10/11), 1.70 –1.39 (m, 8 H, H10/11). ^{13}C NMR ($CDCl_3$, 125.8 MHz): δ 158.7, 158.5, 135.6, 130.9 (C7), 130.2 (C12), 129.3, 128.3 (C1), 127.6 (C8), 125.6 (C4), 118.8 (C6), 113.0, 112.4 (C5), 110.3, 109.9, 72.3 (C9), 30.4, 29.9 (C10/11), 27.1, 27.0 (C10/11), 26.5, 26.3, 24.4, 21.2 (C3), 20.8 (C2). MS (MALDI, TOF LD+) *m/z*: 978.46 (100.0%), 979.46 (71.4%), 980.47 (25.1%), 981.47 (5.0%), 980.47 (1.2%), found: 979.669). HRMS (ESI) *m/z*: 979.4685 ($[M+H]^+$, $C_{66}H_{63}N_2O_6$ requires 979.4681). UV/Vis (CH_2Cl_2): λ_{max}^{abs} (ε)= 531 (20831), 495 (14062), 464 (6066).

Hydrogenated self-encapsulated bay-annulated indigo (**3.1**)

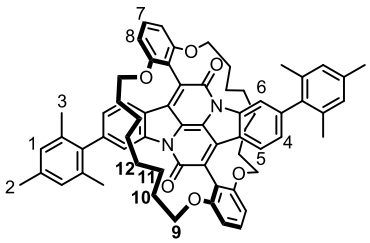

In a round-bottom flask, compound **3.10** (8.81 mg, 9.00 μmol, 1 eq.) and 10% Pd on C (17.0 mg, 144 μmol, 16 eq.) were dissolved in CH_2Cl_2/MeOH (5 mL/ 500 μL). A balloon of H_2 was then used to bubble through the mixture for 10 min and the

reaction then stirred under H_2 atmosphere for 30 min at 20 °C. The mixture was filtered through Celite and the filtrate concentrated giving **3.1** as a red solid (6.80 mg, 6.92 μmol, 77%).

^{1}H NMR ($CDCl_3$, 500.3 MHz): δ 8.35 (m, 2H, H6), 7.40 (t, J = 8.2 Hz, 2H, H7), 7.27 (m, 2H, H4), 7.00 (d, J = 8.0 Hz, 2H, H5), 6.93 (s, 4H, H1), 6.84 (d, J = 8.4 Hz, 4H, H8), 3.89 (m, 8H, H9), 2.33 (s, 6H, H2), 2.05 (s, 12H, H3), 1.56 (m, 8H, H10/11/12), 1.36 (m, 8H, H10/11/12), 0.95-0.88 (m, 8H, H10/11/12). ^{13}C NMR ($CDCl_3$, 125.8 MHz): δ 158.9, 158.6, 145.7, 145.3, 138.0, 137.2, 135.6, 133.9, 130.9 (C7), 128.3 (C1), 127.4 (C4), 125.8, 125.6 (C5), 124.9, 121.7, 118.7 (C6), 116.5, 110.1 (C8), 71.7 (C9), 31.5 (C10), 30.7 (C11), 27.4 (C12), 21.2 (C2), 20.9 (C3). MS (MALDI, TOF LD+) *m/z*: 982.49 (100.0%), 983.50 (71.4%), 984.50 (25.1%), 985.50 (5.0%), 984.50 (1.2%), found: 983.037). HRMS (ESI) *m/z*: 983.4994 ($[M+H]^+$, $C_{66}H_{67}N_2O_6$ requires 983.4994). UV/Vis (CH_2Cl_2): λ_{max}^{abs} (ε)= 531 (17941), 495 (12365), 464 (5358).

3.7 Appendix

Table 13: Properties of the Crystal Structure of 3.20.

	3.20
Empirical Formula	$C_{66}H_{62}N_2O_6$
Molecular Mass (g × mol^{-1})	979.23
Measurement Temperature [K]	150
Wavelength [Å]	1.54184
Crystal System	triclinic
Space Group	*P*-1
***a, b, c*[Å]**	7.5486(6), 12.2708(8), 14.3990(7)
***α, β, γ*[°]**	96.204(5), 105.174(6), 96.528(6)
V[Å^3]	1265.61
Z	1
d_{cal}[g×cm^3]	1.285
F(000)	520
Crystal Size [mm^3]	0.030×0.076×0.120
θ[°]	3.664 to 73.090
h, k, l	-9 to 9, -14 to 15, -10 to 17
Measured reflexes	11734
Independent reflexes	5201
R_{int}	0.042
Absorption Correction	multi-scan
Structure Solving	Full-matrix least-squares on F^2

Refined Parameters	362
***R* (I≥2σ(I))**	R=0.1030; wR_2=0.2353
***R* (all data)**	R=0.0724; wR_2=0.1953
GooF on F^2	0.9943
Rest Electron Density [e×Å^{-3}]	0.58, -0.35

Single crystal X-ray diffraction data were collected at 150 K using an Oxford Diffraction/Agilent SuperNovae A (Cu) X-ray source. The raw frame data were integrated and reduced using CrysAlisPro (Agilent Technologies, 2010). The structure was solved using charge flipping[24],[25] with SuperFlip method.[26] It was refined by full-matrix least-squares on F^2 in CRYSTALS.[27]–[29]

3.8 References

[1] Engi, G. *Zeitschrift für Angew. Chem.* **1914**, *27*, 144–148.

[2] Seixas de Melo, J.; Moura, A. P.; Melo, M. J. *J. Phys. Chem. A* **2004**, *108*, 6975–6981.

[3] Haucke, G.; Paetzold, R. *J. für Prakt. Chemie* **1979**, *917*, 978–986.

[4] Fallon, K. J.; Wijeyasinghe, N.; Yaacobi-Gross, N.; Ashraf, R. S.; Freeman, D. M. E.; Palgrave, R. G.; Al-Hashimi, M.; Marks, T. J.; McCulloch, I.; Anthopoulos, T. D.; Bronstein, H. *Macromolecules* **2015**, *48*, 5148–5154.

[5] He, B.; Pun, A. B.; Zherebetskyy, D.; Liu, Y.; Liu, F.; Klivansky, L. M.; McGough, A. M.; Zhang, B. A.; Lo, K.; Russell, T. P.; Wang, L.; Liu, Y. *J. Am. Chem. Soc.* **2014**, *136*, 15093–15101.

[6] Seixas de Melo, J.; Rondão, R.; Burrows, H. D.; Melo, M. J.; Navaratnam, S.; Edge, R.; Voss, G. *J. Phys. Chem. A* **2006**, *110*, 13653–13661.

[7] Kolaczkowski, M. A.; He, B.; Liu, Y. *Org. Lett.* **2016**, *18*, 5224–5227.

[8] Dou, L.; You, J.; Hong, Z.; Xu, Z.; Li, G.; Street, R. A.; Yang, Y. *Adv. Mater.* **2013**, *25*, 6642–6671.

[9] Sugiyasu, K.; Honsho, Y.; Harrison, R. M.; Sato, A.; Yasuda, T.; Seki, S.; Takeuchi, M. *J. Am. Chem. Soc.* **2010**, *132*, 14754–14756.

[10] Pan, C.; Sugiyasu, K.; Wakayama, Y.; Sato, A.; Takeuchi, M. *Angew. Chem. Int. Ed.* **2013**, *52*, 10775–10779.

[11] Leventis, A.; Royakkers, J.; Rapidis, A. G.; Goodeal, N.; Corpinot, M. K.; Frost, J.

M.; Bučar, D. K.; Blunt, M. O.; Cacialli, F.; Bronstein, H. *J. Am. Chem. Soc.* **2018**, *140*, 1622–1626.

[12] Arndt, F.; Eistert, B. *Berichte der Dtsch. Chem. Gesellschaft* **1935**, *68*, 200–208.

[13] Oestreich, M.; Sempere-Culler, F.; Machotta, A. *Synlett* **2006**, *2006*, 2965–2968.

[14] Clayden, J.; Clayden, L. O. C. J.; Baldwin, J. E.; Williams, R. M. *Organolithiums: Selectivity for Synthesis*; Organic chemistry series; Elsevier Science & Technology Books, 2002.

[15] Snieckus, V. *Chem. Rev.* **1990**, *90*, 879–933.

[16] Velkov, J.; Mincheva, Z.; Bary, J.; Boireau, G.; Fujier, C. *Synth. Commun.* **1997**, *27*, 375–378.

[17] Matsuda, T.; Okuda, A.; Watanabe, Y.; Miura, T.; Ozawa, H.; Tosaka, A.; Yamazaki, K.; Yamaguchi, Y.; Kurobuchi, S.; Koura, M.; Shibuya, K. *Bioorg. Med. Chem. Lett.* **2015**, *25*, 1274–1278.

[18] Barder, T. E.; Walker, S. D.; Martinelli, J. R.; Buchwald, S. L. *J. Am. Chem. Soc.* **2005**, *127*, 4685–4696.

[19] Baeyer, A.; Drewsen, V. *Berichte der Dtsch. Chem. Gesellschaft* **1882**, *15*, 2856–2864.

[20] He, B.; Pun, A. B.; Zherebetskyy, D.; Liu, Y.; Liu, F.; Klivansky, L. M.; McGough, A. M.; Zhang, B. A.; Lo, K.; Russell, T. P.; Wang, L.; Liu, Y. *J. Am. Chem. Soc.* **2014**, *136*, 15093–15101.

[21] Fallon, K. J.; Wijeyasinghe, N.; Yaacobi-Gross, N.; Ashraf, R. S.; Freeman, D. M. E.; Palgrave, R. G.; Al-Hashimi, M.; Marks, T. J.; McCulloch, I.; Anthopoulos, T.

D.; Bronstein, H. *Macromolecules* **2015**, *48*, 5148–5154.

[22] Ryu, I.; Matsubara, H.; Yasuda, S.; Nakamura, H.; Curran, D. P. *J. Am. Chem. Soc.* **2002**, *124*, 12946–12947.

[23] Kulkarni, P. P.; Kadam, A. J.; Mane, R. B.; Desai, U. V.; Wadgaonkar, P. P. *J. Chem. Res.* **1999**, 394–395.

[24] Palatinus, L.; Van Der Lee, A. *J. Appl. Crystallogr.* **2008**, *41*, 975–984.

[25] Palatinus, L. *Acta Crystallogr. Sect. B Struct. Sci. Cryst. Eng. Mater.* **2013**, *69*, 1–16.

[26] Palatinus, L.; Chapuis, G. *J. Appl. Crystallogr.* **2007**, *40*, 786–790.

[27] Betteridge, P. W.; Carruthers, J. R.; Cooper, R. I.; Prout, K.; Watkin, D. J. *J. Appl. Crystallogr.* **2003**, *36*, 1487–1487.

[28] Cooper, R. I.; Thompson, A. L.; Watkin, D. J. *J. Appl. Crystallogr.* **2010**, *43*, 1100–1107.

[29] Parois, P.; Cooper, R. I.; Thompson, A. L. *Chem. Cent. J.* **2015**, *9*, 30.

4

Evaluation of Electrochemical Binding

4.1 Introduction

The polarised binding interactions between tetralactam macrocycles and guest molecules based on hydrogen bonds have been introduced in Chapter 1. However, in partly reduced systems, the polarisation of these bonds is enhanced and leads to stronger hydrogen bonds between guest and host. This phenomenon has been used in molecular shuttles by Leigh and co-workers. Introduction of a photoreducible stopper provided a light-driven shuttle system. The tetralactam macrocycle (TLM, blue) is considered the shuttle which is bound to the succinamide moiety (red) in the neutral state. Photoinduced reduction by an external donor of the naphthalimide unit (green) enhanced its hydrogen bond acceptor strength inducing the shuttling process (Figure 59).[1]

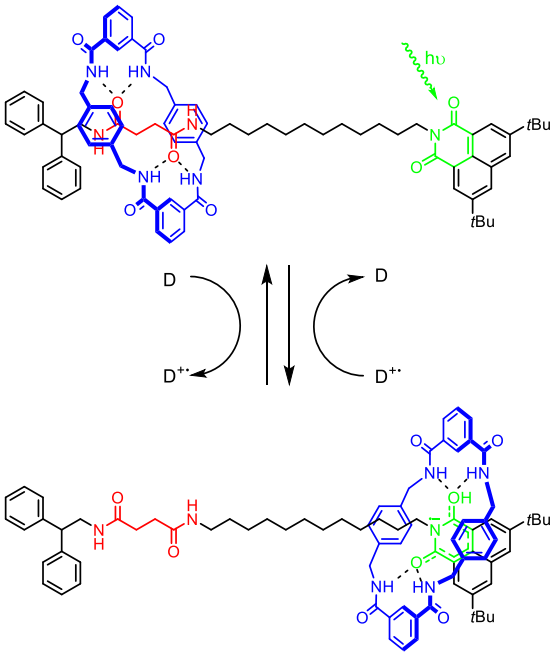

Figure 59: Molecular shuttle designed by Leigh and co-workers.[1]

Another example for polarised supramolecular hydrogen bonds can be found in encapsulated squaraine dyes. The use of squaraine dyes is limited due to their reactivity with nucleophiles (Figure 60).[2]–[6]

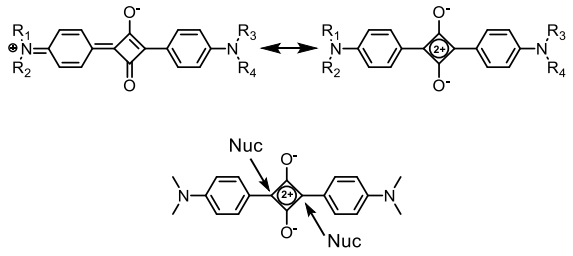

Figure 60: Molecular donor-acceptor structure of squaraine dyes.[2]–[4]

To improve the chemical stability and the photophysical properties, Smith and co-workers developed a method to implement squaraines into TLMs.[7] The encapsulation provides steric protection and was demonstrated by photobleaching experiments. In aqueous solution, a neutral squaraine dye loses its colour within a couple of days whereas the colour of the rotaxane remains for many weeks.[4]

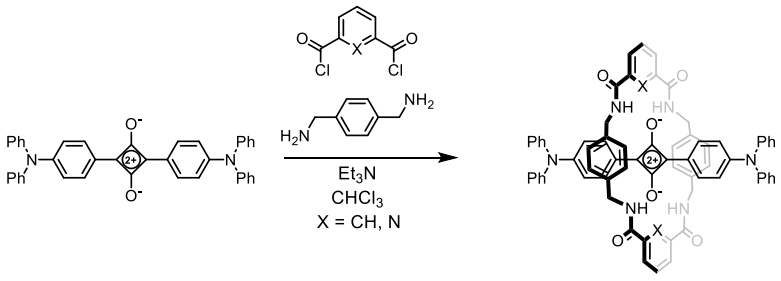

Figure 61: Squaraine rotaxanes prepared after the Leigh-method.[4]

The ‘naked’ dye aggregates in aqueous solution leading to broad absorption bands similar to its solid state. However, the absorption bands of the corresponding rotaxanes are sharp which suggests, when aggregated, the rotaxanes are prevented from getting close to engage in effective chromophore exciton coupling. The high binding affinity of the TLM with the squaraine keeps the macrocycle in place representing the desired shielding effect to prevent aggregation processes of the dyes.[4],[8]–[12]

Tetralactam macrocycles are also known to bind less polarised guests as explained in Chapter 1. In 1991 C. Hunter used a TLM as a macrocyclic host which is able to recognise *p*-benzoquinone (Figure 62).[13] The macrocycle acts as a hydrogen-bond donor, binding

the carbonyl groups of the quinone. The hydrogen atoms on the *p*-benzoquinone double bonds build edge-to-face π-interactions (green in Figure 62) with the phenyl walls of the macrocycle, strengthening the interaction between host and guest.[14] This experiment was also tested with other guests, *i.e.* tetramethylbenzoquinone, tetrachlorobenzoquinone, and anthraquinone, but the binding constants were less than 1 $dm^3 \cdot mol^{-1}$ for these complexes, suggesting that no binding under these conditions appeared. Changing one of the head-units in the macrocycle from isophthaloyl to pyridine leads to an increase in the binding constant between host and guest from 1200 to 1800 $dm^3 \cdot mol^{-1}$. The amide moieties in case of the pyridine head group are directed towards the inner centre of the macrocycle, strengthening their position due to intramolecular hydrogen bonds between the NH-moiety and the pyridine N-atom.[15]

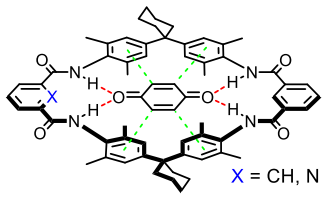

	K ($dm^3 \cdot mol^{-1}$)
X = CH	1200
X = N	1800

Figure 62: Molecular recognition of *p*-benzoquinone by a tetralactam macrocycle. Hydrogen bonds (red) and π-π interactions (green) hold the molecule in place.

An interesting outcome was shown when the host-guest complex of a TLM and *p*-benzoquinone was tested in electrochemical experiments.[16] Reduction of quinone increased the charge located on the oxygen atoms leading to an increased binding strength between the TLM and quinone. The reduction potential in the presence of a TLM is shifted to higher potentials of 390 mV relative to naked *p*-benzoquinone. With these results, Hunter and co-workers were able to demonstrate that stronger H-bonds perturb the electronic structure of a non-covalently bound host-guest complex.

This kind of electrochemically controlled H-bonding has already been explored before.[17] The requirements for these experiments are (1) having a reversible redox couple and (2) its ability to perturb the strength of the binding interactions holding the complex together in its reduced or oxidised state. There are two ways to increase the binding strength between the host and guest by electron transfer. The first is to enhance the acceptor strength of the H-acceptor by increasing the negative charge on the H-accepting atom (Figure 63, a). The second is to enhance the donor strength of the H-donor by oxidation, giving an increased positive charge on the H-donating group (Figure 63, b).

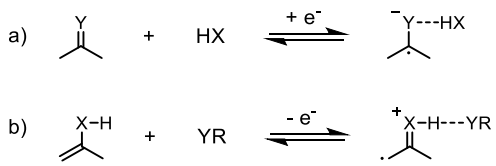

Figure 63: Increasing the H-bond strength by reduction (a) or oxidation (b).

Experimentally, changes in the reduction or oxidation potentials of the redox active species result in presence of a binding partner.[18] If a host binds more strongly to the oxidised partner, the oxidised guest will be stabilised and reduction of the complex will be harder, leading to a negative shift of the electrochemical potential E_{HG} compared to the potential E_G. However, if the host binds stronger to the reduced form, reduction will be easier, resulting in a positive shift of E_{HG} compared to E_G. The reduction and complex formations as well as their equilibria are depicted in Figure 64.

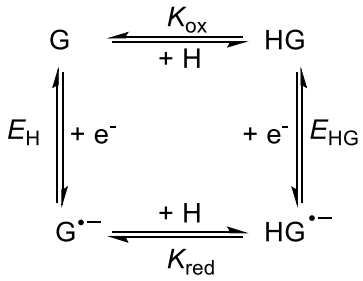

Figure 64: Scheme of squares showing the equilibria for electron transfer as well as the complex formation with their association constants.

When the electron transfer and the binding process are fast and reversible, the scheme of squares (Figure 64) represents the process as a one-electron redox couple, giving the following relationship between the potentials and the binding constants.

$$E_{HG} = E_G + \frac{RT}{nF} \cdot ln\left(\frac{1 + K_{ox}[\mathrm{H}]}{1 + K_{red}[\mathrm{H}]}\right) \quad (1)$$

If the concentration of the guest [H] or $K_{ox/red}$ is very large, equation 1 is reduced to the ratio of K_{red}/K_{ox}, also known as the binding enhancement factor, giving the following equation at 25 °C, corresponding to a 10-fold difference in the binding constants between the oxidation states.

$$10^{(E_{HG}-E_G)F/RT} = \frac{K_{red}}{K_{ox}} \quad (2)$$

For redox-dependent systems, two types of changes in the voltammetric behaviour are known.[19] If binding is strong in both oxidation states, resulting in large K_{red} and K_{ox}, addition of guest results in a small decrease of the redox wave and appearance of a new wave at higher potentials. In this 1:1 binding complex, addition of 1 equivalent guest leads to vanishing of the redox wave of the neutral complex and the appearance on a new redox wave at equal height as the free host redox wave. If on the other hand the binding constants are small or only one of the binding constants is large, the height of the CV wave does not

change, solely a shift of the half-wave potential is observed. Determination of the binding in this process can be performed by a binding titration. When no change in the wave shapes appears, both binding constants can be calculated by plotting the half-wave potential $E_{1/2}$ against the guest concentration [G] and fitting the curves to equation 1. In other cases, where the binding behaviour and the CVs are more complicated, binding constants are usually determined by CV simulation software to fit the experimental results to the scheme of squares (Figure 64).[17]

Square-wave voltammetry (SWV) is another common tool to measure electrochemical processes. Its advantages are that experiments can be performed much faster than CV or other differential pulse techniques which use scan rates of 1 to 10 mV/s compared to 1 V/s or faster. It is a form of linear potential sweep voltammetry combining square wave and staircase potentials applied to an electrode. In this method, the current is measured while the potential between the working and reference electrode is swept linearly. During each cycle the current is measured twice, at the end of the forward pulse and at the end of the reverse pulse. The difference between those two measurements is plotted against the potential staircase. SWV gives peaks for faradaic processes, for which the peak height is proportional to the concentration of the species in solution. A typical square-wave voltammogram is shown in Figure 65.[20]

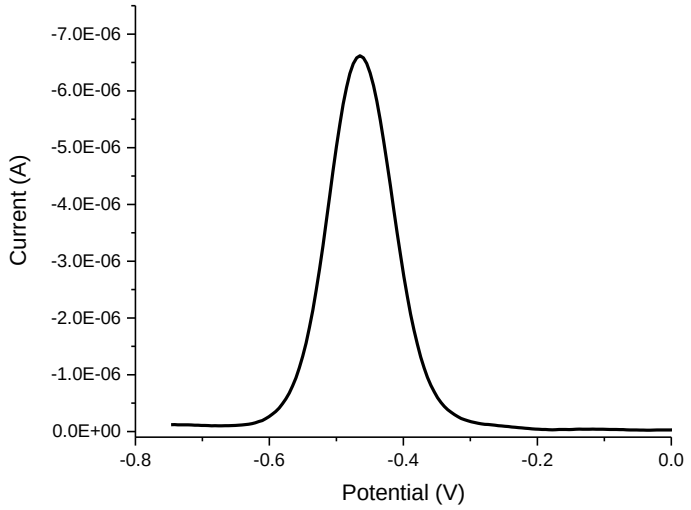

Figure 65: Typical square-wave voltammogram of a reversible compound in TBAP supporting electrolyte.

In this chapter, we describe the neutral and electrochemical binding in the singly reduced state between model compounds and indigoids in presence of tetralactam macrocycles. We wanted to find a method to encapsulate molecules like indigo into hydrogen binding macrocycles to prevent the aggregation of monomers over intermolecular hydrogen bonds and π-interactions. It will be shown that the binding strengths are enhanced by reducing the guests leading to more polarised hydrogen bonds. For the electrochemical measurements, a qualitative way for the evaluation of the reduced binding had to be found. With the published example of benzoquinone binding a tetralactam macrocycle in the reduced state,[16] a way for measuring the binding behaviour in these pseudorotaxanes was established. Also, simulations of the electrochemical binding behaviour to fit the experimental results to this model are shown.

4.2 Structural Similarity to Squaraine in the Reduced State

In the doubly reduced form, the negative charge density is further located on the oxygen atoms compared to the neutral form. This means that in theory tetralactam macrocycles should be able to build up hydrogen bonds to these carbonyl groups and should be especially enhanced in the reduced versions. Figure 66 shows how reduction of **2.8** leads to similar increased charge localisation on the oxygen atoms as seen in squaraines.

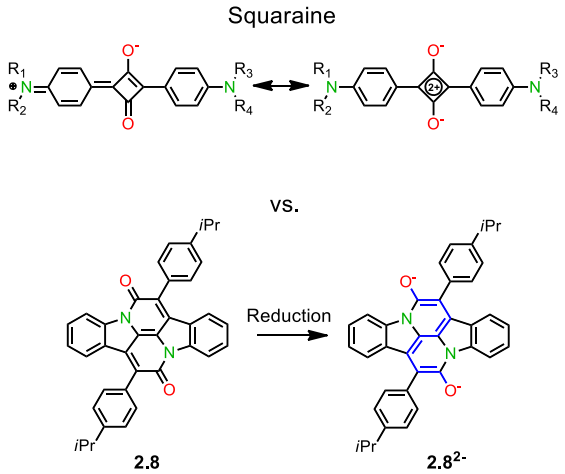

Figure 66: Squaraine in comparison to the indigo-derived dye 2.8 and its doubly reduced derivative with enhanced conjugation.

4.3 Synthesis

The synthesis of tetralactam macrocycles has been discussed in Chapter 1. Modification of the conditions led to the successful formation of the Vögtle-type macrocycles in moderate yields (Figure 67).[21],[22] The soluble diamine **4.1a** was synthesised by heating cyclohexanone and 2,6-dimethylaniline in HCl giving the target compound in a yield of 23%. To form the half cycle **4.1b**, the soluble diamine **4.1a** was reacted with **4.2** in dichloromethane using NEt_3 as base, leading to the formation of **4.1b** in 10% yield. A second addition of **4.2** under high dilution led to ring closure, obtaining **4.1c** in 74% yield.

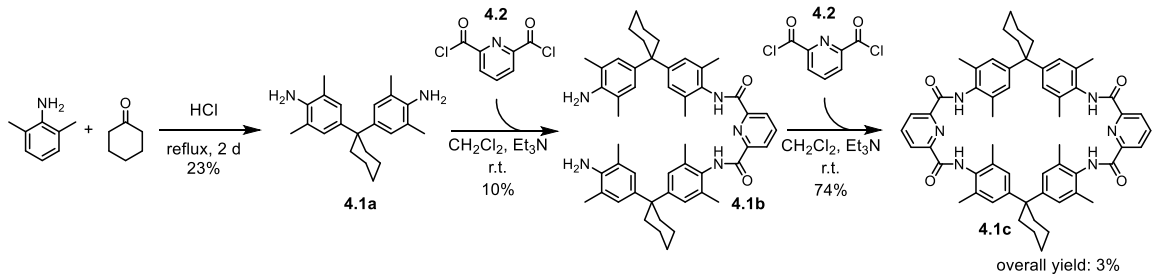

Figure 67: Synthesis of the Vögtle-type tetralactam macrocycle.

To compare different macrocycles, the synthesis of a TLM with naphthalene side walls was attempted (Figure 68). Solubility is a limiting factor for most tetralactam macrocycles.[21],[22] Therefore, *tert*-butyl groups were introduced on the pyridine unit **4.3a**. Oxidation and treatment with $SOCl_2$ gave the acid chloride **4.3c** needed for the macrocycle formation in an overall yield of 14%.[23] For the synthesis of the naphthalene subunit, the dicarboxylic acid **4.4a** underwent treatment with $SOCl_2$ followed by amination to give **4.4b** in 38%. Reduction with $LiAlH_4$ led to the poorly soluble species **4.4c** in a yield of 44%. The reaction of the acid chloride **4.3c** with the naphthalene spacer **4.4c** was tested under the known conditions for the formation of TLMs. Unfortunately, the synthesis of the half-cycle was unsuccessful. It was decided to focus on the binding studies between the Vögtle-type macrocycle **4.1c** and different guests.

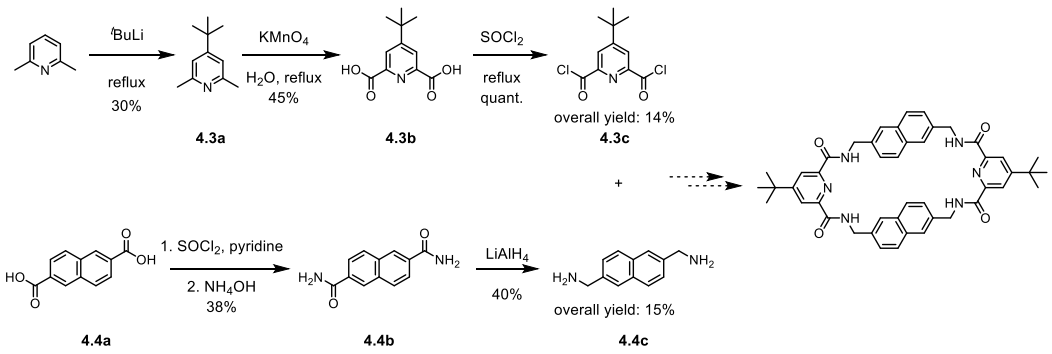

Figure 68: Synthetic scheme for the formation of a tetralactam macrocycle with naphthalene sidewalls.

4.4 Results

For the analysis of the electrochemistry, cyclic voltammetry and square-wave voltammetry were performed. Figure 69 shows a typical cyclic voltammogram of a reversible reaction. For the electrochemical measurements it was necessary that the electrochemical active species shows complete reversibility in the cell. This refers to the electron transfer kinetics between the electrode and the analyte. If the barrier for the electron transfer is low, the Nernstian equilibrium appears immediately after any change in applied potential. It is used to denote whether the analyte is stable upon reduction and can subsequently be reoxidised. The ideal value for the difference in the forward and backward peak potential is 60 mV.[24] In dichloromethane, however, the difference in forward and reverse potentials is usually larger than 60 mV due to the uncompensated resistance effect (Ohmic drop) which results in a slower electron transfer.[25]

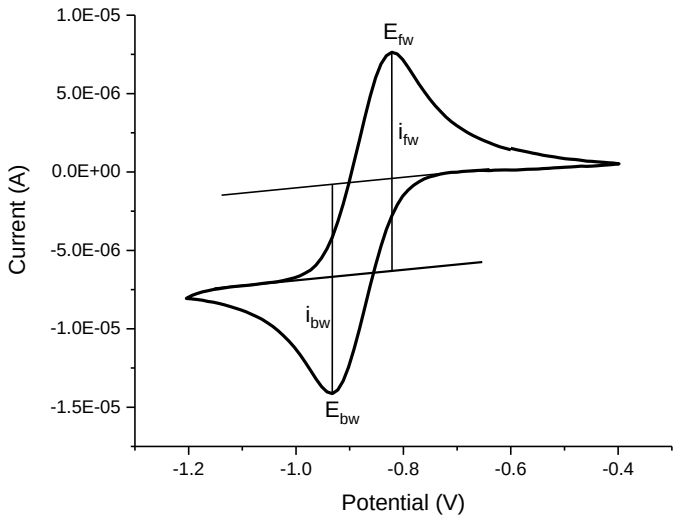

Figure 69: Typical cyclic voltammogram with i_{fw} and i_{bw} showing the forward and backward current, and E_{fw} and E_{bw} the forward and backward potential of a reversible reaction.

This can also be seen in the measurements of the reduction potentials of benzoquinone in presence of ferrocene (Figure 70). The reduction potential at around –1.5 V belongs to the

dianion of benzoquinone, the peak at –1.0 V to the radical anion of benzoquinone, and the potential at 0.0 V to the oxidation potential of ferrocene.

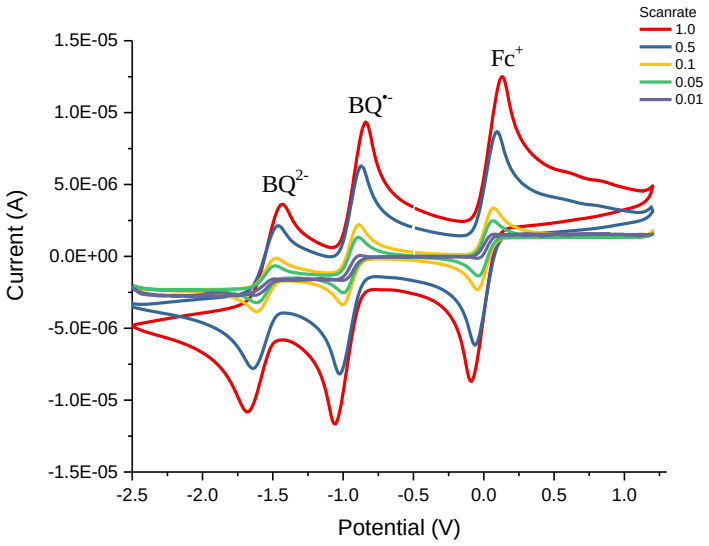

Figure 70: Scan rate dependence of cyclic voltammograms of benzoquinone (1 mM) in the presence of ferrocene (1 mM) and tert-butyl ammonium hexafluorophosphate (0.1 M in dichloromethane) as supporting electrolyte at different scan rates.

Measurements at different scan rates were performed to optimise the conditions to get reversible scan rates. The increase of the scan rate to 1.0 V/s leads to potential values of up to 252 mV, resulting in decreased reversibility compared to the ideal value of 60 mV. When measuring at slower scan rates, smaller differences can be achieved. The results show that the experiments should ideally be performed at a scan rate of 0.05 V/s since it shows the smallest difference in forward and reverse potential, indicating better reversibility than at higher scan rates. This is also visible when the scan rate is plotted against the potential difference (Figure 71).

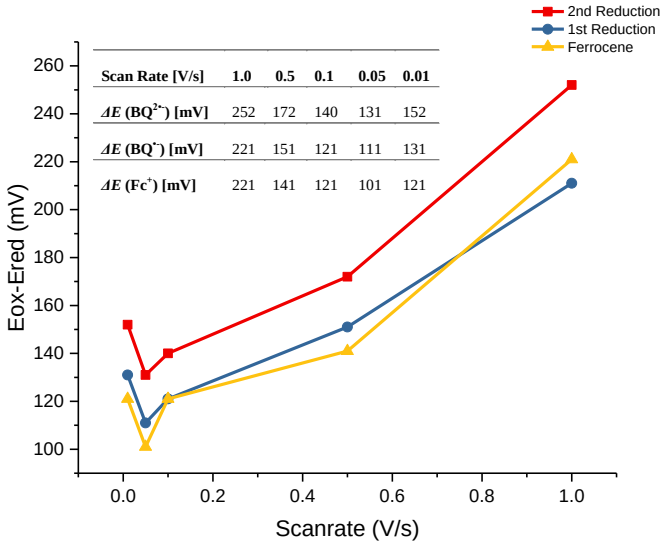

Figure 71: Differences in the forward and backward potentials of BQ and ferrocene.

In measurements of the reversibility of ferrocene in dichloromethane smaller energy differences between the forward and backward potential compared to the experiment in presence of benzoquinone were seen. These measurements were performed in a solution of TBAP in dichloromethane (0.1 M) with freshly cleaned electrodes. A one day old buffer solution was used to prepare the $AgNO_3$ solution for the $Ag/AgNO_3$ reference electrode and the ferrocene stock solution (1 mM). In Table 14 a summary of experimental changes leading to a decrease in the half-wave potentials of benzoquinone can be found. Entries 7-12 show how much influence the scan rate and the step rate have on the reversibility of the ferrocene cation. The values of the differences in the forward and backward potential ΔE during this experiment showed a decrease of over 100 mV depending on the measurement conditions.

Table 14: Measurement conditions for the reversibility test of ferrocene in the presence of TBAP as supporting electrolyte.

	Conditions	Scan Rate [mV/s]	Step [V]	ΔE [mV]
1	Degassing for 20 min	0.1	0.01	140
2	Degassing for 35 min	0.1	0.01	120
3	Degassing for 45 min	0.1	0.01	181
4	Freshly cleaned Pt electrode	0.1	0.01	150
5	Freshly cleaned carbonglass electrode	0.1	0.01	100
6	Freshly cleaned reference electrode with new $AgNO_3$ solution	0.1	0.01	100
7	Changed step rate to 0.002	0.1	0.002	85
8	Changed step rate to 0.01	0.1	0.01	100
9	Changed step rate to 0.001	0.1	0.001	77
10	Changed step rate to 0.0007	0.1	0.0007	77
11	Changed scan rate to 0.05 and step rate to 0.01	0.05	0.01	90
12	Changed scan rate to 0.05 and step rate to 0.05	0.05	0.005	85

Binding of benzoquinone with the macrocycle **4.1c** was tested with the optimised conditions (Table 14, entry 9). However, under these conditions the desired binding process between the macrocycle **4.1c** and *p*-benzoquinone did not occur. Addition of macrocycle **4.1c** to the guest solution led to a decrease in the current of the reduction peaks instead of the appearance of a second reduction wave at higher potentials. Measurements without ferrocene gave better reversibility. However, the binding behaviour of benzoquinone with the macrocycle **4.1c** still showed broadening of the oxidation and reduction waves and also irreversibility of the formed complex. It was expected to see a new reversible redox couple at higher potentials for the complex, but BQ was consumed during the reaction indicated by the decreasing signal during addition of guest. Experiments were performed to exclude factors that can impact the binding. These include: 1) switching to a carbonglass electrode

with a larger diameter, 2) using a silver wire instead of a reference electrode, 3) freshly sublimed BQ and with amylene stabilised CH_2Cl_2, 4) unstabilised CH_2Cl_2, 5) CH_2Cl_2 from a new bottle filtered over alumina, 6) CH_2Cl_2 filtered over alumina with the a carbonglass electrode with a wider diameter. In measurement 6) major improvements in the titration were visible. The reduction waves were reversible. However, the use of unstabilised CH_2Cl_2 filtered over alumina gave the best results. This might also be the reason since quinones are very pH sensitive in their reduced forms leading to irreversible redox waves, therefore any presence of acid during the titration would falsify the results. The measurements under the optimised is shown in Figure 72. The cyclic voltammetric and square-wave voltammetric curves show good quality of the data, but increasing the amount of macrocycle **4.1c** to higher than 2 eq. still led to a decrease in the current due to an increased substantial resistance.[26]

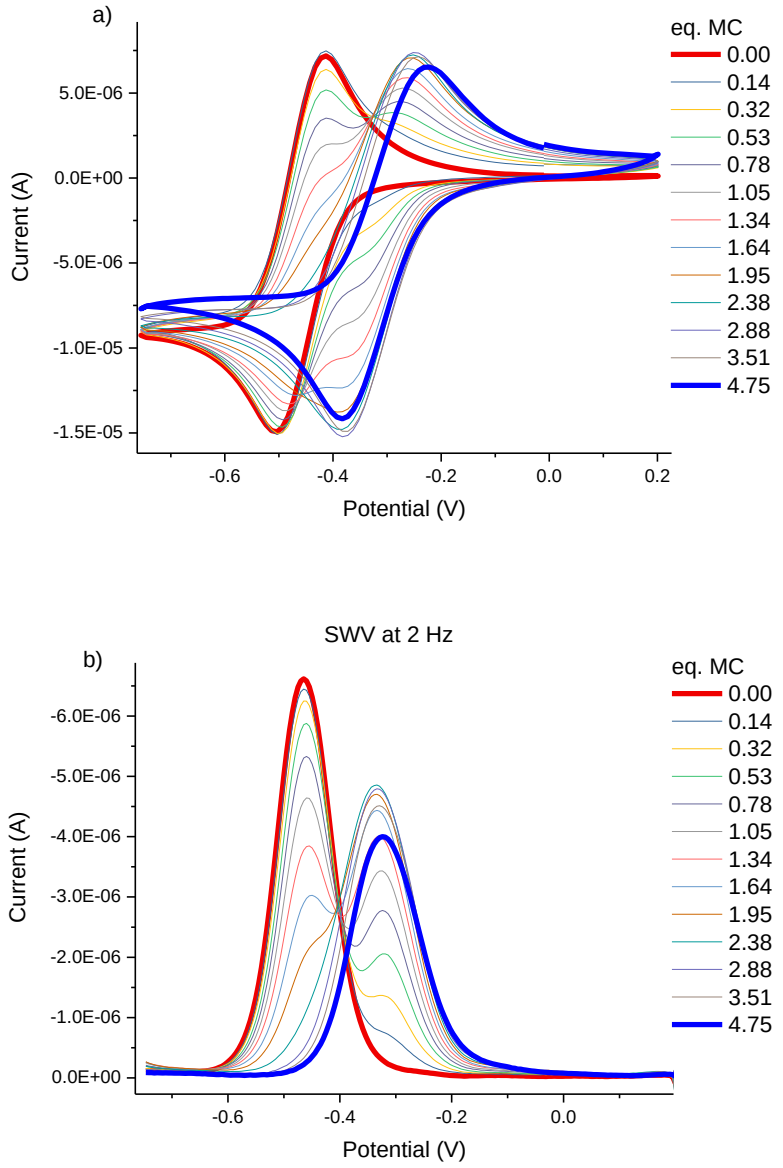

Figure 72: Cyclic voltammetry (a) and square-wave voltammetry (b) of a benzoquinone (1 mM) and macrocycle 4.1c titration in unstabilised CH_2Cl_2 from a fresh bottle filtered over alumina, with TBAP (0.1 M in dichloromethane) as supporting electrolyte.

The conditions for the titration of benzoquinone and **4.1c** were adapted for anthraquinone (Figure 74) and 6,6'-bismesityl indigo **3.7** (Figure 73). The binding between these compounds and the macrocycle only emerged with addition of more equivalents of host and no endpoints could be reached for either experiment. The concentration of 1.14×10^{-2} mol/L for the macrocycle **4.1c** corresponds to the saturated solution, therefore reverse

titrations were performed. The measurements were started from the saturated stock solution and diluted during the titration process. For 6,6'-bismesityl indigo **3.7**, a reaction similar to benzoquinone is visible (Figure 73). The more negative reduction potential decreases whereas another reduction potential for the bound complex appears. However, in the experiment not more than 9 eq. of MC **4.1c** could be added, due to restrictions of solubility of the MC **4.1c**, so the endpoint of the titration could not be reached.

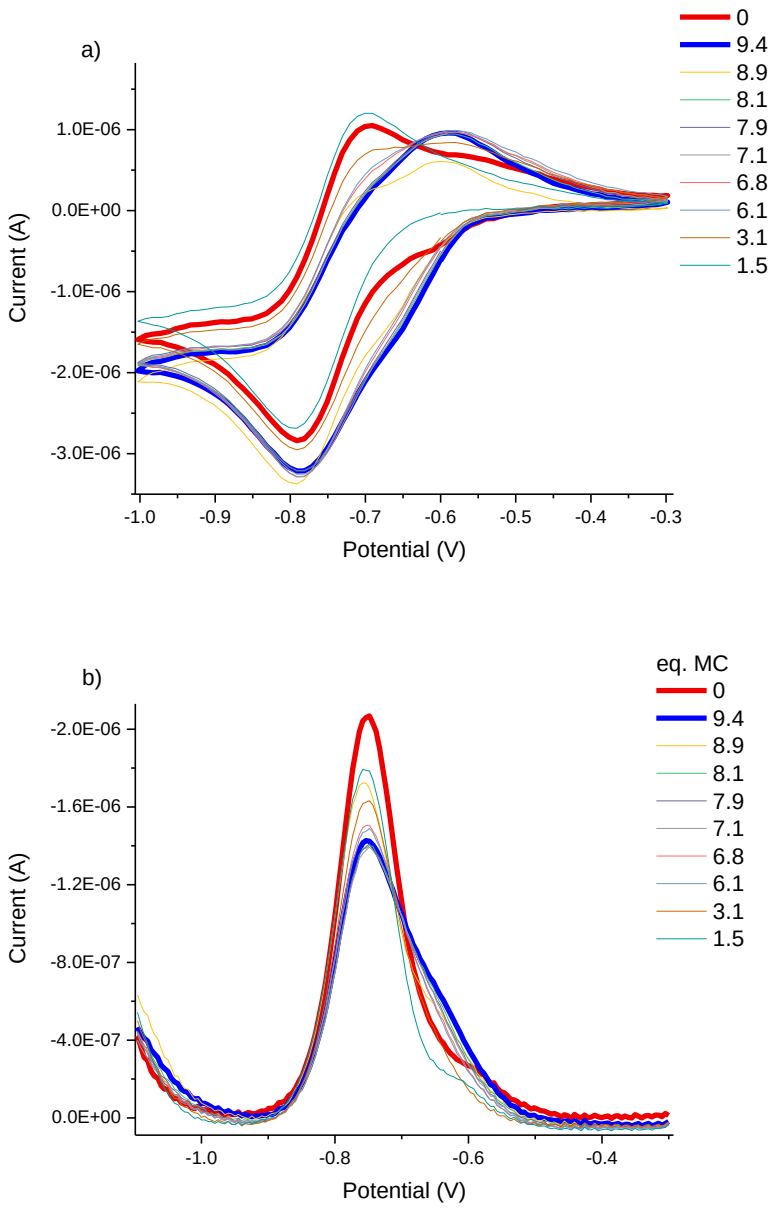

Figure 73: Cyclic voltammetry (a) and square-wave voltammetry (b) of a 6,6'-bismesityl indigo 3.7 (1 mM) and macrocycle 4.1c titration in stabilised CH_2Cl_2 from a fresh bottle filtered over alumina, with TBAP (0.1 M in dichloromethane) as supporting electrolyte.

Anthraquinone shows, in comparison to benzoquinone and 6,6'-bismesityl indigo **3.7**, a continuous shift to higher potentials when macrocycle **4.1c** is added. The system appears to be in fast exchange on a cyclic voltammetric timescale leading to the change in the shape of the voltammograms.

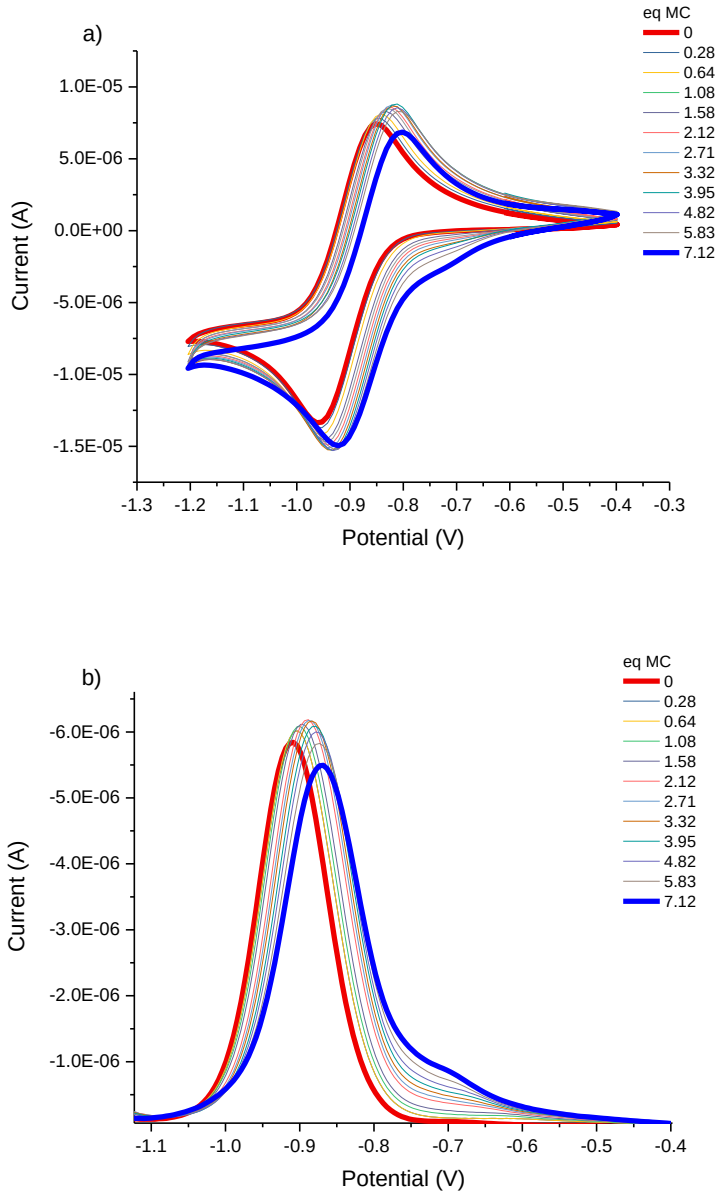

Figure 74: Cyclic voltammetry (a) and square-wave voltammetry (b) of an anthraquinone (1 mM) and macrocycle 4.1c titration in stabilised CH_2Cl_2 from a fresh bottle filtered over alumina, with TBAP (0.1 M in dichloromethane) as supporting electrolyte.

Also, experiments to incorporate dye **2.8** into the macrocycle **4.1c** were performed (Figure 75). The binding was first tested in the neutral state, but titrations at UV-vis and NMR concentrations both revealed no binding. Cyclic voltammetric experiments were also used to investigate binding between dye **2.8** and the macrocycle **4.1c**, but no shift in the reduction potentials was visible. Binding under any of these conditions did not occur. This is most

likely caused by the sterically demanding phenyl rings attached to the bay-annulated species which do not allow slippage of the dye into the cavity of the macrocycle.

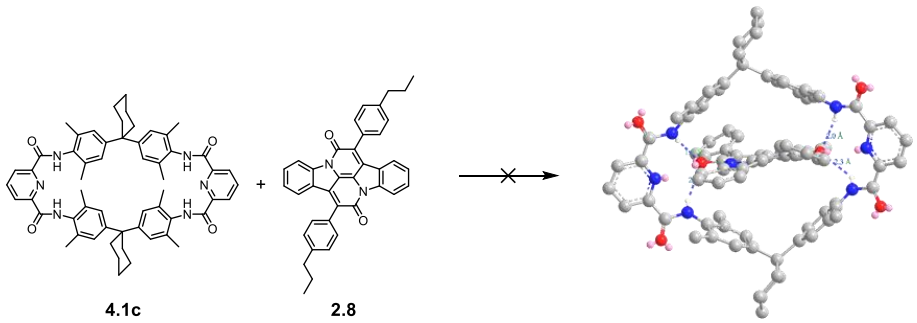

Figure 75: Desired complex formation of the bay-annulated indigo 2.8 and the macrocycle 4.1c.

4.5 Determination of the Binding Constants and Models to Explain the Electrochemical Observations

For a reversible redox couple that perturbs the binding strength in the reduced or oxidised state with a binding partner, the one-electron process can be described over a scheme of squares (Figure 76).[17] Here, the equilibria for the reduction of benzoquinone (Q) in presence of the macrocycle **4.1c** (M) are shown, where K_1 and K_2 are the binding constants of the complexes, and K_{e1} and K_{e2} are functions of the voltage.

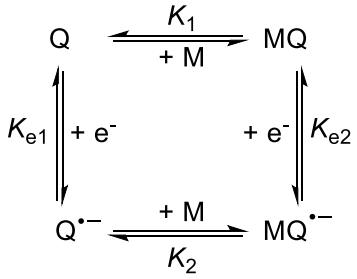

Figure 76: Scheme of squares showing the equilibria for electron transfer as well as the complex formation with their association constants.

[Q], [M] and [MQ] represent the concentrations of quinone, the macrocycle **4.1c**, and the complex, respectively. The electron transfers between quinone and its radical anion, as well as the complex and the respective radical anion can be expressed in Nernst equations with K_{e1} and K_{e2} as their stability constants (left and right equilibria in Figure 76).

$$K_{e1} = \frac{[\mathrm{Q}^{\cdot-}]}{[\mathrm{Q}]} \tag{3}$$

$$K_{e2} = \frac{[\mathrm{MQ}^{\cdot-}]}{[\mathrm{MQ}]} \tag{4}$$

$$E - E_{1/2}^{\mathrm{Q}} = \frac{RT}{nF} \cdot ln(K_{e1}) \tag{5}$$

$$E - E_{1/2}^{\mathrm{MQ}} = \frac{RT}{nF} \cdot ln(K_{e2}) \tag{6}$$

Equation (5) and (6) are can be subtracted to give:

$$E_{1/2}^{MQ} - E_{1/2}^{Q} = \frac{RT}{nF} \cdot ln\left(\frac{K_{e1}}{K_{e2}}\right) \tag{7}$$

The equilibrium constants for the complex formations are defined as K_1 and K_2 (top and bottom reactions in Figure 76) as follows:

$$K_1 = \frac{[\mathrm{MQ}]}{[\mathrm{Q}] \cdot [\mathrm{M}]} \tag{8}$$

$$K_2 = \frac{[\mathrm{MQ}^{\cdot -}]}{[\mathrm{Q}^{\cdot -}] \cdot [\mathrm{M}]} \tag{9}$$

Equation 3 can also be transformed to a term for the quinone concentration dependent on the concentration of the reduced quinone and the constant K_{e1},

$$[\mathrm{Q}] = \frac{[\mathrm{Q}^{\cdot -}]}{K_{e1}} \tag{10}$$

which can be inserted into equation (8) to get an expression for [MQ]:

$$K_1 = \frac{[\mathrm{MQ}]}{\frac{[\mathrm{Q}^{\cdot -}]}{K_{e1}} \cdot [\mathrm{M}]} \Rightarrow [\mathrm{MQ}] = \frac{K_1}{K_{e1}} \cdot [\mathrm{M}] \cdot [\mathrm{Q}^{\cdot -}] \tag{11}$$

With equation (8) a relation in dependency of [M] and the activity of the reduced quinone results by inserting the term for [MQ] from (11) into (4).

$$K_{e2} = \frac{[\mathrm{MQ}^{\cdot -}]}{[\mathrm{MQ}]} = \frac{[\mathrm{MQ}^{\cdot -}]}{\frac{K_1}{K_{e1}} \cdot [\mathrm{M}] \cdot [\mathrm{Q}^{\cdot -}]} \Rightarrow [\mathrm{MQ}^{\cdot -}] = \frac{K_1 \cdot K_{e2}}{K_{e1}} \cdot [\mathrm{M}] \cdot [\mathrm{Q}^{\cdot -}] \tag{12}$$

Equation (9) and (12) show the relationship between all association constants in the scheme.

$$K_2 = \frac{[\mathrm{MQ}^{\cdot-}]}{[\mathrm{Q}^{\cdot-}]\cdot[\mathrm{M}]} = \frac{\frac{K_1 \cdot K_{e2}}{K_{e1}}\cdot[\mathrm{M}]\cdot[\mathrm{Q}^{\cdot-}]}{[\mathrm{Q}^{\cdot-}]\cdot[\mathrm{M}]} = \frac{K_1 \cdot K_{e2}}{K_{e1}} = K_1 \cdot e^{\frac{nF(E_{1/2}^{\mathrm{MQ}} - E_{1/2}^{\mathrm{Q}})}{RT}} \quad (13)$$

Since the endpoint for the titration for the quinone system with the macrocycle **4.1c** is reached (Figure 72), the estimation of K_2 is straightforward. The half-wave potentials of quinone and the complex are measured with -0.46 V and -0.30 V, respectively. The ratio of K_{e1} and K_{e2}, also known as the binding enhancement factor, results from measurements, and K_1 is known from ^{1}H NMR titrations by Hunter *et al.* with a value of 230 M^{-1}.[27] The calculation of the ratio K_{e2}/K_{e1} is performed over the Nernst-equation (7):

$$E_{1/2}^{\mathrm{MQ}} - E_{1/2}^{\mathrm{Q}} = \frac{RT}{nF}\cdot ln\left(\frac{K_{e2}}{K_{e1}}\right) \Rightarrow -0.30 - (-0.46) = \frac{RT}{nF}\cdot ln\left(\frac{K_{e2}}{K_{e1}}\right) \quad (14)$$

$$\frac{K_{e2}}{K_{e1}} = 625$$

The value from equation (14) can be inserted in (13) to calculate the value of K_2:

$$K_2 = \frac{K_1 \cdot K_{e2}}{K_{e1}} \Rightarrow K_2 = 625 \cdot 230\ \mathrm{M}^{-1} = 1.44 \cdot 10^5\ \mathrm{M}^{-1} \quad (15)$$

In square-wave voltammetry, the current ΔI is measured by applying forward and backward potentials with a modulation amplitude. In the following, we assume equilibration of the electrochemical processes at each forward and backwards point, so that differences in concentration can be calculated from the Nernst equation. The difference in current can then be expressed as differences in concentration of reduced or oxidised species at the forward (V+DV) and backwards (V-DV) voltages according to equation 16.

$$\Delta I = ([\mathrm{Q}^{\cdot-}][\mathrm{MQ}^{\cdot-}](\mathrm{V} + \mathrm{dV}) - [\mathrm{Q}^{\cdot-}][\mathrm{MQ}^{\cdot-}](\mathrm{V} - \mathrm{dV}))\cdot \mathrm{A} \quad (16)$$

where ΔI is the current difference, V the voltage, and the pre-factor A which includes impacts of the electrode area, diffusion rate, scan rate, etc. This equation allows fitting of the data by plotting the applied potential as a function of the added concentration of the macrocycle and the current ΔI (Figure 77) with the function of equation (17), making use of the known values of the concentration and the binding constant in the neutral state. This formula includes the processes depicted in the scheme of squares (Figure 76). The binding constants K_{e1}, K_{e2}, and K_b are defined over the Nernst equations. The total concentration of [Q] is known and constant during the binding process, as well as the concentration of the macrocycle [M]. The binding process could then be simulated over the quadratic function 17.

$$\Delta I = \frac{-b(V) - \sqrt{b(V)^2 - 4 \cdot a(V) \cdot c(V)}}{2 \cdot a(V)} \tag{17}$$

$$c(V) = \frac{[\mathrm{Q}]_0[\mathrm{M}]_0}{1 + K_{e1}(V)}$$

$$b(V) = -\left(\frac{1}{K_a} + ([\mathrm{Q}]_0 + [\mathrm{M}]_0) \cdot \left(\frac{1 + K_{e2}(V)}{1 + K_{e1}(V)}\right)\right)$$

$$a(V) = (1 + K_{e2}(V)) \cdot \frac{2}{(1 + K_{e1}(V))}$$

$$K_{e2}(V) = e^{-(V - E^{\mathrm{MQ}^{\cdot -}}) \cdot \frac{nF}{RT}}$$

$$K_{e1}(V) = e^{-(V - E^{\mathrm{Q}^{\cdot -}}) \cdot \frac{nF}{RT}}$$

$$K_b = K_a \cdot e^{-(E^{\mathrm{Q}^{\cdot -}} - E^{\mathrm{MQ}^{\cdot -}}) \cdot \frac{nF}{RT}}$$

The application of this model requires the input of the guest concentration [Q], the changing concentration of host [M], the potentials V, the neutral binding constant K_b, and the

modulation amplitude. Aim is to fit this model to the experimental results. The goodness of the fit is strongly impacted by the data input. Fitting the data to this model gives a binding constant of $1.9 \times 10^5\ M^{-1}$ for the reduced quinone-macrocycle couple. This value is slightly higher than the value calculated from equation (16), but the error of the variables (*e.g.* concentrations, neutral binding constant) is relatively high and can explain this deviation. Small changes in the redox potentials result in large changes of the binding constant. Calculation of the constant with equation 15 requires the input of these reduction potentials resulting in a large error for the binding constant value.

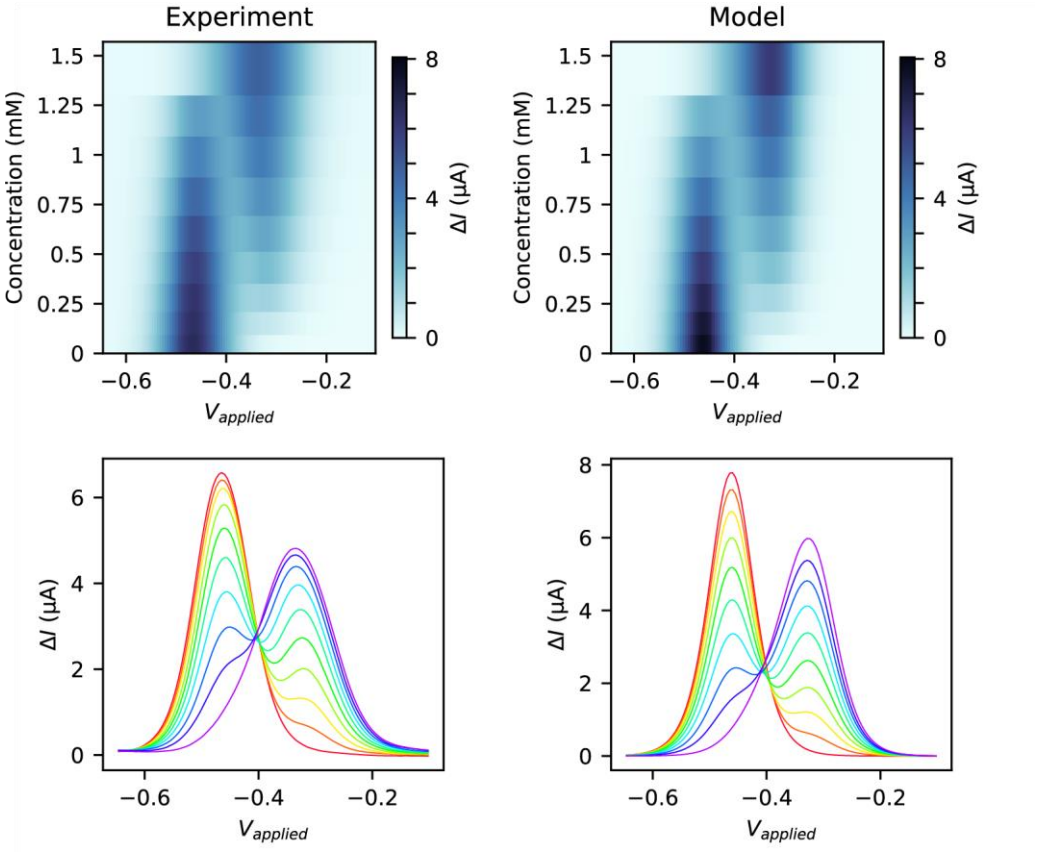

Figure 77: Fitting function of the benzoquinone and the macrocycle 4.1c titration by making use of the relationship in equation (17). The pre-factor is calculated as -27.04, and the standard potentials for $[Q^{\cdot -}]$ and $[MQ^{\cdot -}]$ are -0.4614 and -0.2857 V, respectively.

Since the electrochemical binding between benzoquinone and the macrocycle **4.1c** the electron transfer is slow, which led to the formation of two separate redox waves, we also

tried to determine the binding constant by a 1:1 binding isotherm as known in NMR- and UV-vis titrations.[28] The measured data points were fitted over the following function:

$$\Delta I = \frac{(K([\mathrm{G}] + [\mathrm{H}]_0) + 1) - \sqrt{(K([\mathrm{G}] + [\mathrm{H}]_0) + 1))^2 - (4K^2[\mathrm{H}]_0[\mathrm{G}])}}{2K[\mathrm{H}]_0} \qquad (18)$$

For which ΔI is the difference in current, K the binding constant, $[G]$ the guest concentration, and $[H]_0$ the initial host concentration. The definition of the binding constant K is here assumed to be K_1=K_2. Evaluation of the binding constant for the reaction of benzoquinone with the macrocycle **4.1c** gives a value of $4.7 \cdot 10^3$ M^{-1} for the appearing redox wave at -0.328 V which is much lower compared to the values estimated with equation (13) and (16) (Figure 78). In this model, however, not all parameters determining the binding in the reduced state are taken into account, and it is therefore not accurate for these electrochemical binding processes.

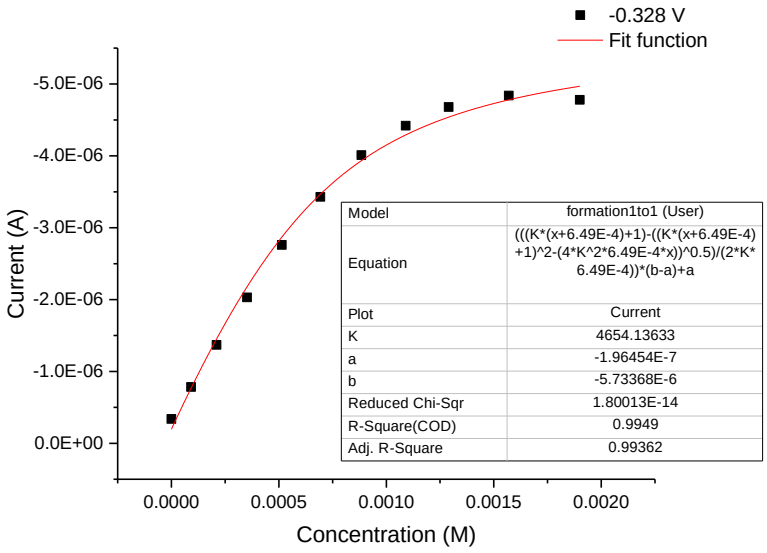

Figure 78: Binding isotherm for the titration of BQ with MC 4.1c (6.4 mM). The current values at a potential of -0.328 V were used for this plot.

Binding between 6,6'-bismesityl indigo **3.7** and the macrocycle **4.1c** was evaluated as shown for benzoquinone over the Nernst equations. The half-wave potentials are known from the measurements, and the binding constant K_1 for the neutral state is assumed to be 1 M^{-1} for this calculation. This value was assumed since no binding could be measured in the neutral state. Also, fits of the data with equation 17 did not converge at higher neutral binding constants.

$$E_{1/2}^{\mathrm{MQ}} - E_{1/2}^{\mathrm{Q}} = \frac{RT}{nF} \cdot ln\left(\frac{K_{e2}}{K_{e1}}\right) \Rightarrow -0.5795 - (-0.7601) = \frac{RT}{nF} \cdot ln\left(\frac{K_{e2}}{K_{e1}}\right)$$

$$\frac{K_{e2}}{K_{e1}} = 1133.2$$

The value for K_{e2}/K_{e1} can be inserted in (15) to calculate the value of K_2:

$$K_2 = \frac{K_1 \cdot K_{e2}}{K_{e1}} \Rightarrow K_2 = 1133.2 \cdot 1\ \mathrm{M}^{-1} = 1133.2\ \mathrm{M}^{-1}$$

Application of the binding model as shown for benzoquinone with equation (17), gives a value of 1050 M^{-1} for the binding constant in the reduced state. This shows that this fitting function is able to determine the binding behaviour between host and guest and give similar results as achieved from calculations. As mentioned, for neutral binding constants higher than 1 M^{-1} the fits did not converge, suggesting that our estimated value for the neutral binding constant is realistic.

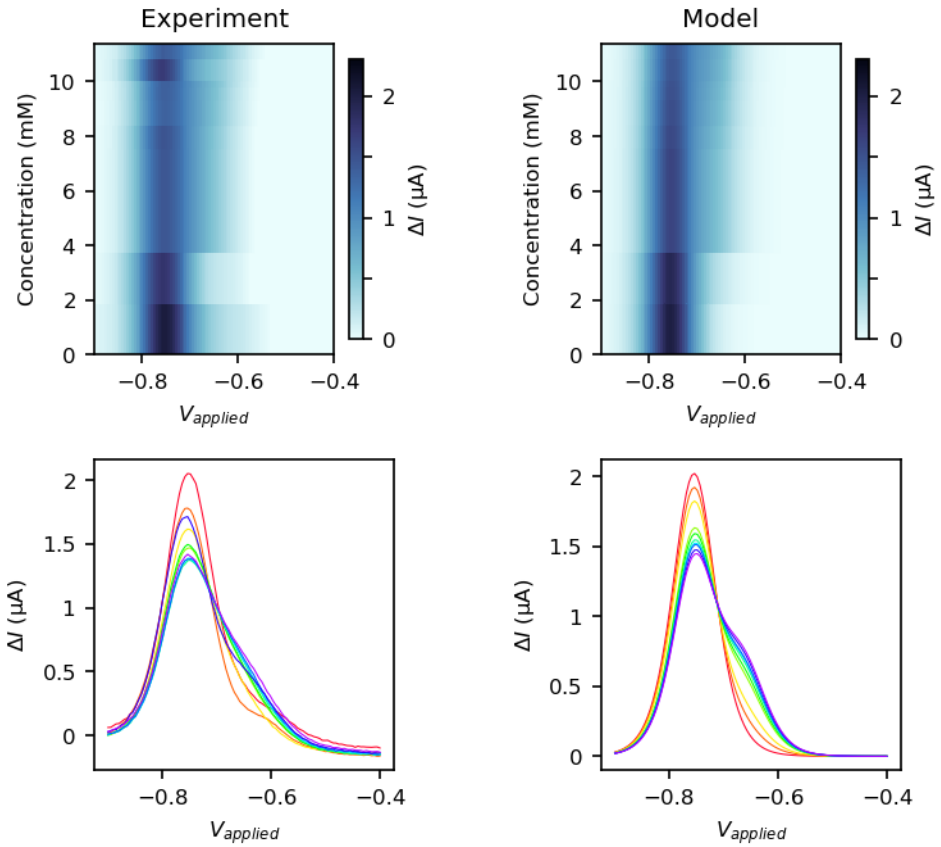

Figure 79: Fitting function of the 6,6'-bismesityl indigo 3.7 and the macrocycle 4.1c titration by making use of the relationship in equation (17). The pre-factor A is calculated as -311.92, and the standard potentials for $[I^{\cdot -}]$ and $[MI^{\cdot -}]$ are -0.7541 and -0.5136 V, respectively. Also, a neutral binding constant of 0.05 M^{-1} was used for this model.

If binding for the 6,6'-bismesityl indigo **3.7** -macrocycle **4.1c** complex (Figure 80) is evaluated over a 1:1 binding isotherm, the binding constant results with a value of only 260 M^{-1}. Evaluation over a 1:1 binding isotherm is again not possible because it does not take all processes during the electrochemical binding into account.

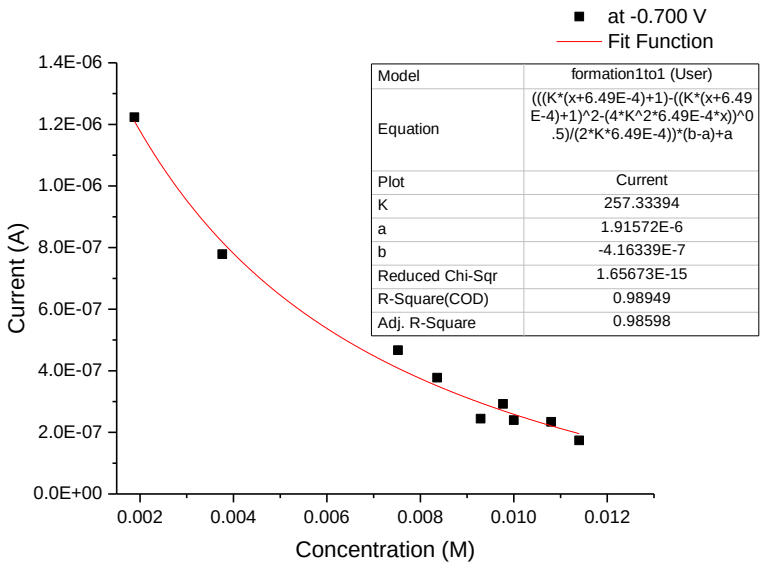

Figure 80: Binding isotherm for the titration of 6,6'-bismesitylindigo 3.7 with MC 4.1c (1.14×10^{-2} M). The current values at a potential of -0.700 V were used for this plot.

Binding for anthraquinone (A) with the macrocycle **4.1c** (M) shows compared to benzoquinone and 6,6'-bismesityl indigo **3.7** a continuous shift in the potentials during addition of guest. The binding constants K_1 and K_2 can be calculated over the following fitting function, as shown by Oliveira *et al.* assuming a fast electron transfer:[29]

$$E_{1/2}^{\mathrm{A}} - E_{1/2}^{\mathrm{MA}} = \frac{RT}{nF} \cdot ln\left(\frac{1 + K_1[\mathrm{M}]}{1 + K_2[\mathrm{M}]}\right) \tag{19}$$

In a system under dynamic equilibrium the chemical reactions are so fast that all binding steps are considered to be in equilibrium during the electrochemical reaction. Therefore, the system is considered as a single redox couple, defined over the Nernst equation. However, this model can only be applied to uncomplicated binding processes in which the half-wave potentials smoothly shift with no significant change in their shape, as seen in the titration of anthraquinone with the macrocycle **4.1c**.

$$E = E^0 + \frac{RT}{nF} \cdot ln\left(\frac{[\mathrm{A}] + [\mathrm{MA}]}{[\mathrm{A}^{\cdot-}] + [\mathrm{MA}^{\cdot-}]}\right) \tag{20}$$

Also, the binding constants are defined as:

$$K_1 = \frac{[\mathrm{MA}]}{[\mathrm{A}] \cdot [\mathrm{M}]} \tag{21}$$

$$K_2 = \frac{[\mathrm{MA}^{\cdot -}]}{[\mathrm{A}^{\cdot -}] \cdot [\mathrm{M}]} \tag{22}$$

Giving a relationship for (20), as follows:

$$E = E^0 + \frac{RT}{nF} \cdot ln\left(\frac{[\mathrm{A}](1 + K_1[\mathrm{M}]}{[\mathrm{A}^{\cdot -}](1 + K_2[\mathrm{M}]}\right) \tag{23}$$

The Nernst equation for the reduction process of [A] to $[\mathrm{A}^{\cdot -}]$

$$E = E^{\mathrm{A}}_{1/2} + \frac{RT}{nF} \cdot ln\left(\frac{[\mathrm{A}]}{[\mathrm{A}^{\cdot -}]}\right) \tag{24}$$

Subtraction of (24) from (23) gives (25):

$$\Delta E = E^{\mathrm{A}}_{1/2} - E^{\mathrm{MA}}_{1/2} = -\frac{RT}{nF} \cdot ln\left(\frac{(1 + K_1[\mathrm{M}]}{(1 + K_2[\mathrm{M}]}\right) \tag{25}$$

This equation shows the relationship of the Nernst equations as shown in equation (17) and [M] is used as the added concentration of the macrocycle.

Use of this fitting curve on the measured data points for the titration of anthraquinone with the macrocycle **4.1c** gives values for the neutral and reduced binding constants of 88.4 ± 30.2 M^{-1} and 1103 ± 111 M^{-1}, respectively (Figure 81). The binding for the reduced form is therefore enhanced by about two orders of magnitude, as also seen for the benzoquinone.

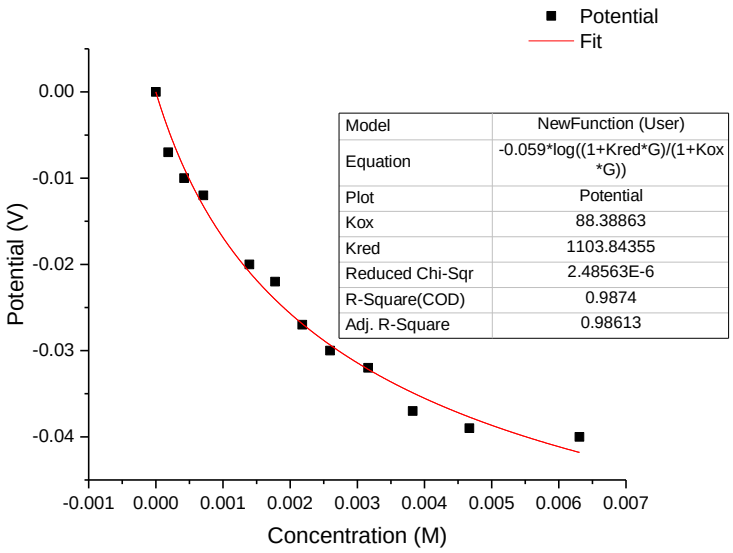

Figure 81: Binding isotherm for the titration of AQ with MC 4.1c.

Simulation of the binding process as shown for BQ and **3.7** (Figure 77 and Figure 79) gives a value of 1140 M^{-1} for the binding constant in the reduced state (Figure 82). This model also estimated a neutral binding constant of 88 M^{-1}, giving an almost equal binding constant for the reduced form. It shows that our binding model can estimate similar binding constants in the reduced state as from known methods if the neutral binding constant is known.[17],[29]

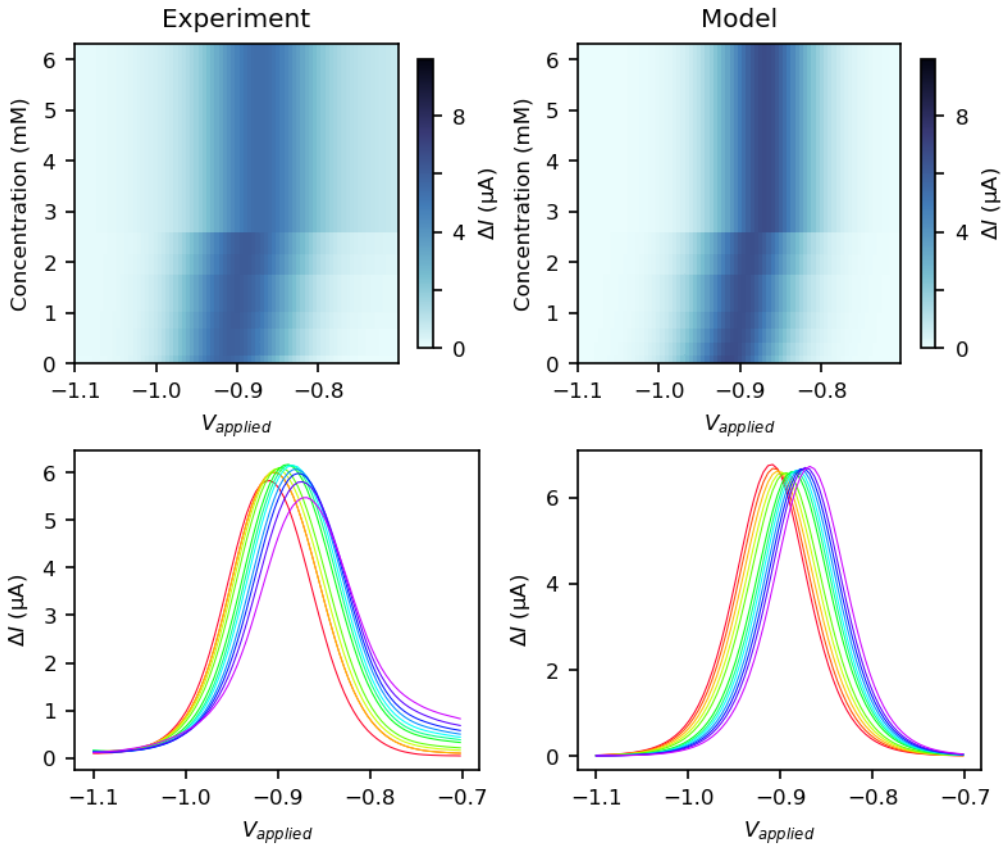

Figure 82: Fitting function of the anthraquinone and the macrocycle 4.1c titration by making use of the relationship in equation (17). The pre-factor is calculated as -53524.3, and the standard potentials for $[A^{\cdot -}]$ and $[MA^{\cdot -}]$ are -0.91 and -0.8443 V, respectively. Also, a neutral binding constant of 88 M^{-1} was used for this model.

The binding model in equation 25 solely shows dependence between the half-wave potentials and the guest concentration and can be adapted to processes like binding of anthraquinone with macrocycle **4.1c**. On the other hand, our simulation model also takes the changes in ΔI into account and therefore allows fitting of processes like binding of benzoquinone or 6,6'-bismesityl indigo **3.7** with TLM **4.1c** and can therefore be used for either of these binding processes.

4.6 Conclusions

In conclusion, we were able to successfully synthesise an altered Vögtle-type macrocycle with two pyridine head groups. These allow the formation of intermolecular hydrogen bonds of the NH-units with the pyridine-N, stabilising the conformation of the macrocycle. With this macrocycle binding experiments with quinones and a soluble indigo derivative were performed. The binding in the neutral state was known in most cases and compared to the changes in binding in their reduced forms, which was reached by electrochemical measurements. We were able to show that binding is largely enhanced between guest-host systems by up to two orders of magnitude. Molecules like anthraquinone or 6,6-bismesityl indigo, which are not able to bind tetralactam macrocycles in the neutral state, still show binding with the macrocycle in their reduced form. It was also shown, that depending on whether the binding is in slow or fast exchange on an electrochemical timescale, different fitting estimations can be applied to calculate the binding constants. However, our fitting model is the only one that can estimate both processes.

With these results, it should be possible to encapsulate molecules with low binding strengths in the neutral state by reduction. Also, it is possible to make a qualitative statement about the binding enhancement in the reduced state. Further on, these encapsulated monomers could be used for the formation of rotaxanes. This could be especially attractive for indigo, which is known to build up intermolecular hydrogen bonds and π-π interactions which would be prevented by this approach.

4.7 Experimental Details

General Procedures

All reagents were purchased from commercial sources and used as received. Solvents were bought from Honeywell, formerly Sigma Aldrich. Column chromatography was carried out using SiO_2 60 (particle size 40-63 μm, Merck, UK) as stationary phase. NMR spectra were acquired on a Bruker AVII400, AVIII400, or AVII500 instrument. ^{1}H NMR chemical shifts are reported in ppm and were referenced internally to residual protons in the solvent (δ = 7.26 for $CDCl_3$; 2.50 for DMSO). $^{13}C\{^1H\}$ NMR chemical shifts are reported in ppm and were referenced internally with respect to the solvent signal (δ = 77.2 for $CDCl_3$; 39.52 for DMSO). Standard abbreviations indicating multiplicity were used as follows: s = *singlet*, d = *doublet*, dd = *double* of *doublets*, t = *triplet*, q = *quartet*, m = *multiplet*, br = broad signal. High-resolution mass spectra (HRMS) were obtained on a Bruker μTOF instrument or a Waters GCT.

Voltammetric measurements were performed using an Autolab PGSTAT 12 with a glassy-carbon working electrode, platinum wire counter electrode and $Ag/AgNO_3$ quasi-reference electrode. Voltammograms were referenced to the Fc/Fc^+ couple as an internal reference after each measurement. Square wave voltammograms were acquired with a 5 mV step potential, 50 mV modulation amplitude and 2 Hz frequency. Exclusion of water was essential for the acquisition of clean voltammograms. The supporting electrolyte salt (tetra-*n*-butylammonium hexafluorophosphate, Bu_4NPF_6, TBAP) was dried by heating to the melting point under vacuum. Unstabilised CH_2Cl_2 (dried over alumina and stored over 4 Å molecular sieves) was added to the dry electrolyte to a concentration of 0.1 M electrolyte. Analyte solutions were prepared by addition of this electrolyte solution to the guest and macrocycle **4.1c**.

1,1-Bis(4-amino-3,5-dimethylphenyl)cyclohexane **4.1a**[22]

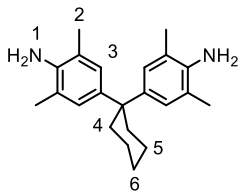

A mixture of 2,6-dimethylaniline (30.0 mL, 252 mmol), cyclohexanone (12.6 mL, 121 mmol), and concentrated aqu. HCl (33%, 30 mL) was refluxed for 2 d and cooled to 20 °C, whereby a yellow-brown solid is built. After dissolving the products in water (500 mL) and heating to boil, the solution was made basic by the addition of 1 M NaOH and extracted with chloroform (1 L). The organic phase was dried over $MgSO_4$ and concentrated in vacuo. The residue crystallised from pentane (500 mL) in form of yellow crystals to give **4.1a** (18.3 g, 56.1 mmol, 46%). ^{1}H NMR (400 MHz, $CDCl_3$): δ 6.84 (s, 4H, H3), 3.46 (br, 4H, H1), 2.17 (m, 4H, H4), 2.14 (s, 12H, H2), 1.53-1.46 (m, 6H, H5/6). ^{13}C NMR (100.1 MHz, $CDCl_3$): δ 139.7, 126.88, 121.2, 44.4, 37.33, 26.5, 23.0, 17.9. MS (ESI +ve) *m*/*z*: 323.2 ($[M+H]^+$, $C_{22}H_{31}N_2$ requires 323.2)

Half-cycle **4.1b**[22]

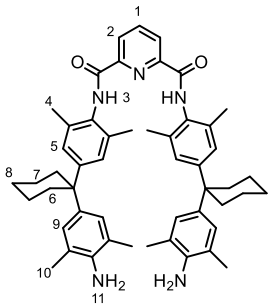

1,1-Bis(4-amino-3,5-dimethylphenyl)cyclohexane **4.1a** (10.0 g, 32.0 mmol) was dissolved in a solution of triethylamine (1.4 mL) in dichloromethane (50 mL). 2,6-Pyridinedicarbonyl chloride **4.2** (2.00 g, 9.70 mmol) was similarly dissolved in dichloromethane (100 mL), the solution transferred to a dropping funnel, and then added dropwise to the diamine solution over a period of 2 h at 20 °C. The mixture was stirred for further 12 h. The crude product was purified by column chromatography (15:1 $CHCl_3$:EtOAc, with increasing amount of EtOAc),yielding **4.1b** in form of a white solid (1.50 g, 1.93 mmol, 20%). ^{1}H NMR (400 MHz, CDCl3) δ 8.99 (s, 2H, H3), 8.50 (d, 2H, H2), 8.13 (m, 1H, H1), 7.03 (s, 4H, H5), 6.85 (2, 4H, H9), 3.45 (s, 4H, H11), 2.24 (s, 12H, H4), 2.21 (br, 8H, H6), 2.15 (s, 12H, H10), 1.55-1.46 (br, 12H, H7/8). ^{13}C NMR (100.1 MHz, $CDCl_3$): δ 171.22, 161.3,

148.3, 139.9, 139.1, 137.5, 134.2, 130.1, 126.7, 125.2, 121.2, 44.7, 36.9, 26.2, 22.8, 18.6, 17.9. MS (ESI +ve) *m/z*: 777.5 ($[M+H]^+$, $C_{51}H_{61}N_5O_2$ requires 777.08)

Full cycle **4.1c**[22]

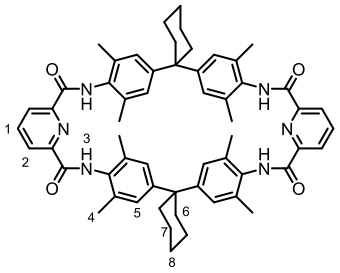

4.1b (481 mg, 620 µmol) was dissolved in a mixture of triethylamine (97.1 mg, 960 µmol) in dry CH_2Cl_2 (100 mL). In the same way, 2,6-pyridinedicarbonyl chloride **4.2** (131 mg, 620 µmol) was dissolved in dry CH_2Cl_2 (150 mL). At r.t. both solutions were simultaneously added to the same solvent (500 mL) over a period of 8 h. The crude product was purified by column chromatography (10:1 $CHCl_3$:EtOAc, R_f = 0.22), yielding **4.1c** as a white powder (418 mg, 461 µmol, 74 %). ^{1}H NMR (400 MHz, $CDCl_3$) δ 8.95 (s, 4H, H3), 8.49 (d, 4H, H2), 8.18 (m, 2H, H1), 6.99 (s, 8H, H5), 2.31–2.27 (br, 8H, H6), 2.20 (s, 24H, H4), 1.54 (br, 12H, H7/8).^{13}C NMR (100.1 MHz, $CDCl_3$): δ 172.1, 161.1, 148.7, 139.2, 134.8, 130.4, 126.9, 125.5, 60.6, 44.2, 36.2, 22.1, 19.2. MS (ESI +ve) *m/z*: 907.5 ($[M+H]^+$, $C_{58}H_{62}N_6O_4$ requires 907.17)

4-(tert-Butyl)-2,6-dimethylpyridine **4.3a**[32]

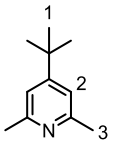

A solution of 2,6-lutidine (2.28 g, 21.3 mmol, 1 eq.) in dry heptane (17 mL) was slowly added to *t*-BuLi (25.0 mL, 1.7 M in pentane, 42.5 mmol, 2 eq.) at –78 °C and stirred for 1 h. After removing pentane *in vacuo*, the mixture was heated for 24 h to 40 °C. The suspension was then cooled to 10 °C and slowly treated with water (20 mL). After addition of 200 mL pentane, the organic phase was washed with water (250 mL) and dried over $MgSO_4$. Column chromatography in a 2:1 EtOAc and CH_2Cl_2 mixture gave the desired product **4.3a** in form of a clear liquid (1.04 g, 6.34 mmol, 30%). ^{1}H NMR ($CDCl_3$, 400 MHz) δ 6.94 (s, 2H, H2), 2.51 (2, 6H, H3), 1.28 ppm (s, 9H, H1). ^{13}C NMR

($CDCl_3$, 100 MHz) δ 160.4, 157.4 (C2), 117.2, 34.4 (C3), 30.6 (C1). MS (ESI +ve) *m*/*z*: 164.1 ($[M+H]^+$, $C_{11}H_{18}N$ requires 164.1).

4-(tert-Butyl)pyridine-2,6-dicarboxylic acid **4.3b**[30]

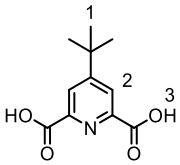

4-*tert*-butyl-2,6-dimethylpyridine **4.3a** (1.03 g, 6.31 mmol) and $KMnO_4$ (4.01 g, 25.4 mmol) were mixed in water (50 mL) and heated to reflux for 18 h. The mixture was filtered while hot to remove the brown MnO_2. The colourless solution was carefully neutralised with 4 M aqueous HCl until a pH of 5. The precipitated white solid was filtered off and purified by recrystallisation from hot water giving colourless needles. The remaining filtrate could be concentrated and left in the fridge over night to give more **4.3b** in form of a white solid (637 mg, 6.31 mmol, 45%). ^{1}H NMR (DMSO-d_6, 400 MHz) δ 8.12 (s, 2H, H2), 1.34 ppm (s, 9H, H1). ^{13}C NMR (DMSO-d_6, 100 MHz) δ 167.3, 167.1, 147.8 (C2), 126.1, 36.4, 30.5 (C1). MS (ESI +ve) *m*/*z*: 223.1 ($[M+H]^+$, $C_{11}H_{13}NO_4$ requires 223.23)

4-(tert-butyl)pyridine-2,6-dicarbonyl dichloride **4.3c**[32]

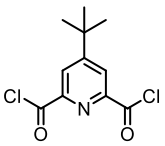

In a two-neck flask 4-*tert*-butyl-pyridyl-2,6-dicarboxylic acid **4.3b** (200 mg, 0.896 mmol) and thionyl chloride (5 mL, 68.85 mmol) were heated to reflux for 3 h. After cooling down to r.t., the remaining thionyl chloride was removed in vacuo and the product **4.3c** dried on high vacuum (220 mg, 0.846 mmol, 94%). The product was used immediately without further purification and characterisation.

2,6-naphthalenedicarboxamide **4.4b**[31]

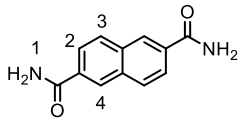

2,6-Naphthalenedicarboxylic acid **4.4a** (1.50 g, 9.25 mmol, 1.0 eq.), thionyl chloride (12.0 mL, 220 mmol, 23 eq.) and pyridine (1.50 mL, 24.8 mmol, 2.7 eq.) were stirred and heated to reflux for 2 h. After cooling to 20 °C all volatiles were removed. The remaining solid was dissolved in CH_2Cl_2 (19 mL) and NH_4OH (19 mL, 30%) was carefully added. The suspension was stirred for 30 min and sonicated a couple of times. After dilution in water (70 mL) the precipitate was filtered off and washed with water (140 mL). The remaining solid was dried under vacuum yielding 2,6-naphthalenedicarboxamide **4.4b** in form of a yellow solid (0.95 g, 4.44 mmol, 65%). ^{1}H NMR (400 MHz, DMSO-d_6): δ 8.53 (s, 2H, H1), 8.19 (s, 2H, H1), 8.06–8.00 (m, 4H, H2/3), 7.55 ppm (s, 2H, H4).^{13}C NMR (100.1 MHz, DMSO-d_6): δ 167.7, 133.3, 133.0, 128.8, 127.4, 125.9.,MS (ESI +ve) *m*/*z*: 215.0 ($[M+H]^+$, $C_{12}H_{11}N_2O_2$ requires 215.22)

Naphthalene-2,6-diyldimethanamine **4.4c**[23]

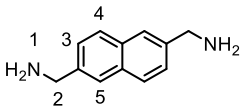

2,6-naphthalenedicarboxamide **4.4b** (250 mg, 1.17 mmol) was dissolved in dry THF (5 mL). A 1 M solution of $LiAlH_4$ in THF (5 mL) was added dropwise at 0 °C whereas the solution turned yellow-orange. The mixture was heated to reflux for 1 h, then cooled to 0 °C and treated with saturated aqueous KF solution. After extraction with 3 × 20 mL CH_2Cl_2, the organic phase was washed with brine, dried over $MgSO_4$, and the solvent removed *in vacuo*. The crude product was recrystallised from a $CHCl_3$ and HCl solution, yielding **4.4c** as a white solid of (83.0 mg, 446 µmol, 38%). ^{1}H NMR (DMSO-d_6, 400 MHz): δ 8.67 (br, 6H, H1), 8.04 (m, 2H, H5), 7.94 (m, 2H, H4), 7.70 (m, 2H, H3), 4.18 ppm (m, 4H, H2). ^{13}C NMR (DMSO-d_6, 100 MHz): δ 128.2 (C4), 127.8 (C5), 127.2 (C3), 40.43 ppm (C2). MS (ESI +ve) *m*/*z*: 187.0 ($[M+H]^+$, $C_{12}H_{15}N_2$ requires 187.3).

4.8 References

[1] Brouwer, A. M.; Frochot, C.; Gatti, F. G.; Leigh, D. A.; Mottier, L.; Paolucci, F.; Roffia, S.; Wurpel, G. W. H. *Science* **2001**, *291*, 2124–2128.

[2] Sprenger, H.-E.; Ziegenbein, W. *Angew. Chem. Int. Ed.* **1968**, *7*, 530–535.

[3] Schmidt, A. H. *Synthesis (Stuttg).* **1980**, *1980*, 961–994.

[4] Gassensmith, J. J.; Baumes, J. M.; Smith, B. D. *Chem. Commun.* **2009**, 6329.

[5] Ros-Lis, J. V.; García, B.; Jiménez, D.; Martínez-Máñez, R.; Sancenón, F.; Soto, J.; Gonzalvo, F.; Valldecabres, M. C. *J. Am. Chem. Soc.* **2004**, *126*, 4064–4065.

[6] Sancenón, F.; Martínez-Máñez, R.; Soto, J. *Angew. Chem. Int. Ed.* **2002**, *41*, 1416–1419.

[7] Arunkumar, E.; Forbes, C. C.; Noll, B. C.; Smith, B. D. *J. Am. Chem. Soc.* **2005**, *127*, 3288–3289.

[8] Gassensmith, J. J.; Arunkumar, E.; Barr, L.; Baumes, J. M.; DiVittorio, K. M.; Johnson, J. R.; Noll, B. C.; Smith, B. D. *J. Am. Chem. Soc.* **2007**, *129*, 15054–15059.

[9] Jacquemin, D.; Perpète, E. A.; Laurent, A. D.; Assfeld, X.; Adamo, C. *Phys. Chem. Chem. Phys.* **2009**, *11*, 1258.

[10] Chen, H.; Law, K.-Y.; Perlstein, J.; Whitten, D. G. *J. Am. Chem. Soc.* **1995**, *117*, 7257–7258.

[11] Johnston, A. G.; Leigh, D. A.; Murphy, A.; Smart, J. P.; Deegan, M. D. *J. Am. Chem. Soc.* **1996**, *118*, 10662–10663.

[12] Gassensmith, J. J.; Matthys, S.; Lee, J. J.; Wojcik, A.; Kamat, P. V.; Smith, B. D.

Chem. Eur. J. **2010**, *16*, 2916–2921.

[13] Hunter, C. A. *J. Chem. Soc. Chem. Commun.* **1991**, 749–751.

[14] Hunter, C. A.; Sanders, J. K. M. *J. Am. Chem. Soc.* **1990**, *112*, 5525–5534.

[15] Hunter, C. A.; Purvis, D. H. *Angew. Chem. Int. Ed.* **1992**, *31*, 792–795.

[16] Brooksby, P. A.; McQuillan, A. J.; Purvis, D. H.; Rowan, A. E.; Walsh, R.; Hunter, C. A.; Shannon, R. J. *Angew. Chem. Int. Ed.* **1995**, *33*, 2489–2491.

[17] *Electrochemistry of Functional Supramolecular Systems*; Paola, C., Alberto, C., Margherita, V., Eds.; John Wiley & Sons, Inc., 2010.

[18] Bu, J.; Lilienthal, N. D.; Woods, J. E.; Nohrden, C. E.; Hoang, K. T.; Truong, D.; Smith, D. K. *J. Am. Chem. Soc.* **2005**, *127*, 6423–6429.

[19] Miller, S. R.; Gustowski, D. A.; Chen, Z. hong; Gokel, G. W.; Echegoyen, L.; Kaifer, A. E. *Anal. Chem.* **1988**, *60*, 2021–2024.

[20] *Electroanalytical Methods*; Scholz, F., Ed.; Springer, 2005.

[21] Vögtle, F.; Meier, S.; Hoss, R. *Angew. Chem. Int. Ed. English* **1992**, *31*, 1619–1622.

[22] Hunter, C. A. *J. Am. Chem. Soc.* **1992**, *114*, 5303–5311.

[23] Furusho, Y.; Shoji, J.; Watanabe, N.; Kihara, N.; Adachi, T.; Takata, T. *Bull. Chem. Soc. Jpn.* **2001**, *74*, 139–147.

[24] Elgrishi, N.; Rountree, K. J.; McCarthy, B. D.; Rountree, E. S.; Eisenhart, T. T.; Dempsey, J. L. *J. Chem. Educ.* **2018**.

[25] Bond, A. M.; Oldham, K. B.; Snook, G. A. *Anal. Chem.* **2000**.

[26] Bernardo, A. R.; Stoddart, J. F.; Kaifer, A. E. *J. Am. Chem. Soc.* **1992**, *114*, 10624–10631.

[27] Adams, H.; Carver, F. J.; Hunter, C. A.; Osborne, N. J. *Chem. Commun.* **1996**, 2529–2530.

[28] Thordarson, P. *Chem. Soc. Rev.* **2011**, *40*, 1305–1323.

[29] Oliveira, R.; Groni, S.; Fave, C.; Branca, M.; Mavré, F.; Lorcy, D.; Fourmigué, M.; Schöllhorn, B. *Phys. Chem. Chem. Phys.* **2016**, *18*, 15867–15873.

[30] Zhang, J.; Khaskin, E.; Anderson, N. P.; Zavalij, P. Y.; Vedernikov, A. N. *Chem. Commun.* **2008**, 3625.

[31] Jeong, S.; Song, X.; Jeong, S.; Oh, M.; Liu, X.; Kim, D.; Moon, D.; Lah, M. S. *Inorg. Chem.* **2011**, *50*, 12133–12140.

[32] Agami, C.*; Bull. Soc. Chim. Fr.*, **1987**, *2*, 358-60.

5

Conclusions and Future Work

5.1 Conclusion

The synthesis and properties of encapsulated π-systems have been widely investigated. Several types of interaction between guest and host systems are known and utilised for the formation of rotaxanes.[1]–[5] Such systems are expected to shield guests from their surroundings to prevent stacking between the guests which would otherwise lead to a decrease in fluorescence quantum yields. Until now there have been no reports of encapsulating indigo or its derived materials in macrocyclic structures as an approach towards making them useful materials for OLEDs or other photonic applications.

The previous research regarding indigo and methods for the formation of rotaxanes have been reviewed in Chapter 1. Common strategies for encapsulation and its use as a tool to enhance the photophysical properties in the solid state were discussed. Additionally, focus was placed on examples of rotaxanes with hydrogen bonds [6] and self-encapsulation by metathesis reactions.[7],[8]

In Chapter 2 we investigated the substitution of indigo and the formation of bay-annulated indigo derivatives with fluorescence quantum yields of over 90% in solution. It was shown that acylation of the indigo-*N*-moiety led to structural changes, generating materials with improved emission.

The self-encapsulation of a bay-annulated indigo derivative was studied in Chapter 3. The challenging synthetic strategy gave a good emitter in solution and solid state (50% and 25% fluorescence quantum yields, respectively). The structural properties of the target molecule were investigated by X-ray crystallography and the photophysical properties analysed.

In Chapter 4 we quantified hydrogen bonding between tetralactam macrocycles, as H-donors, and reducible H-accepting hosts. The binding strength between the macrocycle and

the reduced form of the H-acceptor is increased by 3 orders of magnitude compared to the neutral binding, showing that this strategy can be used to enhance host-guest binding for the formation of rotaxanes. We found a way to simulate the data giving a fitting model, which showed similar results to the common methods to quantify the binding constants.

5.2 Future Work

For the self-encapsulated indigo derivatives it would be interesting to investigate the photophysical properties in polymeric structures. Immediate questions arising are whether the self-encapsulation leads to increased fluorescence quantum yields compared to the 'naked' species, but also how much influence the encapsulation has on the packing patterns. Also, substitution of indigo with bismethoxy phenyl groups would allow self-encapsulation over the indigoid subunit (Figure 48, right). Bay-annulation of this derivative could be performed by introduction of thienyl groups allowing bromination followed by polymerisation. Additionally, investigation of the photophysical behaviour of the unencapsulated monomer in comparison to the dye with mesityl groups can help to understand the influence of different substituents on indigo on the emissive properties.

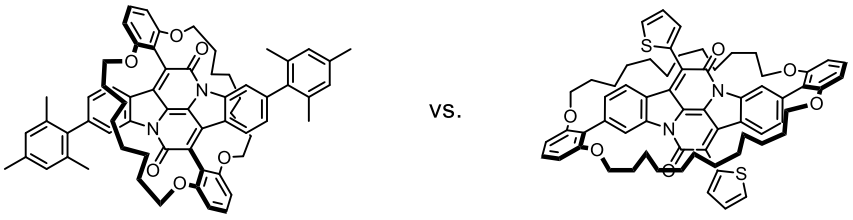

Figure 83: Self-encapsulation of bay-annulated indigo derivatives in two different ways.

The outcomes for synthesising rotaxanes with reduced species could also be very promising. If it is possible to polymerise the reduced indigo-tetralactam macrocycle complexes and/or to add large stopper groups, it would give indigo-based rotaxanes or pseudo-rotaxanes. The emissive properties would presumably be altered while maintaining

the planar structure of the indigo-host, which could lead to higher fluorescence quantum yields compared to the acylated species. This approach could be adapted also for DPP or similar dyes with H-bond accepting units.

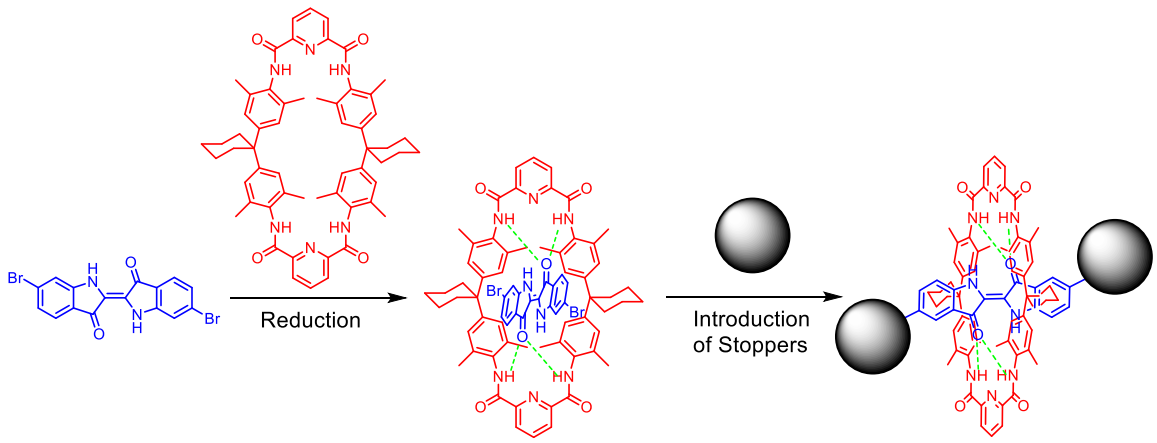

Figure 84: Synthetic strategy for the formation of pseudo-rotaxanes based on indigo, by partly reducing the dye to enhance the H-bond strength.

5.3 References

[1] Xue, M.; Yang, Y.; Chi, X.; Yan, X.; Huang, F. *Chem. Rev.* **2015**, *115*, 7398–7501.

[2] Michels, J. J.; O'Connell, M. J.; Taylor, P. N.; Wilson, J. S.; Cacialli, F.; Anderson, H. L. *Chem. Eur. J.* **2003**, *9*, 6167–6176.

[3] Taylor, P. N.; Hagan, A. J.; Anderson, H. L. *Org. Biomol. Chem.* **2003**, *1*, 3851–3856.

[4] Cacialli, F.; Wilson, J. S.; Michels, J. J.; Daniel, C.; Silva, C.; Friend, R. H.; Severin, N.; Samorì, P.; Rabe, J. P.; O'Connell, M. J.; Taylor, P. N.; Anderson, H. L. *Nat. Mater.* **2002**, *1*, 160–164.

[5] Brovelli, S.; Meinardi, F.; Winroth, G.; Fenwick, O.; Sforazzini, G.; Frampton, M. J.; Zalewski, L.; Levitt, J. a.; Marinello, F.; Schiavuta, P.; Suhling, K.; Anderson, H. L.; Cacialli, F. *Adv. Funct. Mater.* **2010**, *20*, 272–280.

[6] Seel, C.; Parham, A. H.; Safarowsky, O.; Hübner, G. M.; Vögtle, F. *J. Org. Chem.* **1999**, *64*, 7236–7242.

[7] Sugiyasu, K.; Honsho, Y.; Harrison, R. M.; Sato, A.; Yasuda, T.; Seki, S.; Takeuchi, M. *J. Am. Chem. Soc.* **2010**, *132*, 14754–14756.

[8] Ouchi, Y.; Sugiyasu, K.; Ogi, S.; Sato, A.; Takeuchi, M. *Chem. - An Asian J.* **2012**, *7*, 75–84.